DEVELOPMENT OF PERFECTLY MATCHED LAYER NUMERICAL BOUNDARY CONDITION IN A GENERALIZED COORDINATE SYSTEM

A Dissertation by

Srinivasa Perumal Velu

Master of Science, Wichita State University, 2010

Bachelor of Engineering, Bharathiar University, 2001

Submitted to the Department of Aerospace Engineering
and the faculty of the Graduate School of
Wichita State University
in partial fulfillment of
the requirements for the degree of
Doctor of Philosophy

December 2013

DEVELOPMENT OF PERFECTLY MATCHED LAYER
NUMERICAL BOUNDARY CONDITION IN
A GENERALIZED COORDINATE SYSTEM

The following faculty members have examined the final copy of this dissertation for form and content, and recommend that it be accepted in partial fulfillment of the requirement for the degree of Doctor of Philosophy with a major in Aerospace Engineering.

_____
Klaus A. Hoffmann, Committee Chair

_____
Kamran Rokhsaz, Committee Member

_____
Walter J. Horn, Committee Member

_____
Myose Y. Roy, Committee Member

_____
Victor Isakov, Committee Member

Accepted for the College of Engineering

_____
Vish Prasad, Interim Dean

Accepted for the Graduate School

_____
Abu S. M. Masud, Interim Dean

DEDICATION

To my beloved brother

Muthu Pattavarayan Velu

ACKNOWLEDGEMENTS

I would like to take this opportunity to thank the Department of Aerospace Engineering at Wichita State University for allowing me to carry out this research. I express profound gratitude to my advisor, Klaus A. Hoffmann, for his many years of thoughtful, patient guidance and suggestions throughout my studies, his undaunting encouragement, and his support in various ways, without which this dissertation effort would have remained only a distant dream of mine. I am very grateful for Jean-François Dietiker for providing me with resources to begin this work. I sincerely thank my committee members for their helpful comments and suggestions during all stages of this work, and I especially thank Kristie Ann Bixby for her assistance in editing my technical documents and conference publications.

I also acknowledge my family for their constant support and confidence in me. I sincerely thank my brother Muthu Pattavarayan Velu, who bore the great responsibility of taking care of my family and freed me from indispensable familial duties without which I would not have had peace of mind to dig deeper into my research so many miles away from my homeland. I express genuine gratefulness to my friends Lakshmi Narayanan Subramanian and Joshua Thomas for their magnanimous financial support during my journey through rough waters.

I extend deep gratitude to my most sincere friend Amy Haight and her children, who treated me like family on this foreign soil and offered me the opportunity to learn and appreciate the values of a Christian family unit. My earnest thanks go to Walter and Jean Walden for their generosity and moral support. I must acknowledge the enormous support and selfless help of a special friend, Debbie Wadman, who was always there for me with motherly care. And finally, I wish to thank all my friends and colleagues who directly or indirectly helped me throughout this process.

ABSTRACT

The research activity leading to this dissertation focused on the boundary treatment for computational fluid dynamics problems, especially those with unbounded domains. This involved a rigorous literature survey of boundary treatment techniques. The primary interest of this effort was on one of the emerging concepts of nonreflecting boundary treatment for numerical schemes, namely the perfectly matched layer (PML) absorbing technique. The need for an appropriate space-time transformation for a stable PML emphasized in previous efforts was the starting point for this developmental research activity. Based on this, unsplit PML equations were constructed for Euler equations linearized over a uniform mean flow with a proper space-time transformation. Dispersion analysis was carried out to demonstrate the effectiveness of the space-time transformation in terms of stability of the PML formulation. Numerous numerical simulations were carried out to investigate the stability of the PML formulation for long-term integration of various combinations of time-step size and PML parameters. The major focus of this research was to extend the construction of the PML for nonlinear Euler equations in a generalized coordinate system to widen its application in uniform and nonuniform grid structures. Emphasis was placed on the application of conventional numerical schemes without employing any form of artificial dissipation or numerical filtering. With this objective in mind, the split-form PML equations for nonlinear Euler equations were constructed. Various numerical simulations were carried out to validate the PML formulation and demonstrate its effectiveness as an absorbing boundary condition.

TABLE OF CONTENTS

TABLE OF CONTENTS (continued)

Chapter Page

LIST OF FIGURES

LIST OF FIGURES (continued)

Figure Page

LIST OF FIGURES (continued)

LIST OF FIGURES (continued)

Figure Page

LIST OF FIGURES (continued)

Figure Page

LIST OF FIGURES (continued)

LIST OF ABBREVIATIONS/NOMENCLATURE

Abbreviations

CAA	Computational aeroacoustics
CFD	Computational fluid dynamics
LEE	Linearized Euler equation
NPML	Number of PML layers
NRBC	Nonreflecting boundary condition
PDE	Partial differential equation
PML	Perfectly matched layer
TVD	Total variation diminishing

Roman Symbols

a	Speed of sound
A	Flux Jacobian
B	Flux Jacobian
d	Distance of grid point in PML layer from Euler-PML interface
D	Width of PML domain
e_t	Total energy per unit mass
e_i	Internal energy per unit mass
E	Flux vector in x-direction (physical space)
$\overline{E}$	Flux vector in ξ-direction (computational space)
$\overline{E}_p$	Flux vector of pseudo mean-flow in x-direction (physical space)

$\overline{\overline{E}}_p$	Flux vector of pseudo mean-flow in ξ-direction (physical space)
F	Flux vector in y-direction (physical space)
$\overline{F}$	Flux vector in η-direction (computational space)
$\overline{F}_p$	Flux vector of pseudo mean-flow in y-direction (physical space)
$\overline{\overline{F}}_p$	Flux vector of pseudo mean-flow in η-direction (computational space)
G	Flux vector in z-direction (physical space)
$\overline{G}$	Flux vector in ζ-direction (computational space)
h	Specific enthalpy
H	Damping term associated with PML in physical domain
$\overline{H}$	Damping term associated with PML in computational domain
i	Imaginary number
J	Jacobian of grid transformation
k	Wavenumber
L_{ref}	Reference length
M	Mach number
p	Fluid pressure
q	Auxiliary variable used in PML formulation
Q	Conservative variable
$\overline{Q}$	Generalized conservative variable
Q_0	Amplitude vector of plane wave

$Q^{'}$	Conservative fluctuation variable
$\bar{Q}_P$	Conservative pseudo mean-flow variable
$\tilde{Q}$	Conservative variable in frequency domain
t	Time
u	Cartesian velocity or velocity vector
U_0	Cartesian mean velocity
v	Cartesian velocity or velocity vector
V_0	Cartesian mean velocity
w	Cartesian velocity or velocity vector
x, y, z	Cartesian space variables

Greek Symbols

α	Damping rate inside PML layer
β	Parameter used in space-time transformation
Δ	Step-size
γ	Ratio of specific heats
ρ	Density
σ	Damping coefficient used in PML
σ_m	Maximum value of damping coefficient used in PML
τ	Generalized time variable

ω	Wave frequency
ξ,η,ζ	Generalized space variables

Subscripts

0	Signifying initial condition
p	Pseudo mean-flow
ref	Reference length
i	Index of a grid point in x- or ξ-direction
j	Index of a grid point in y- or η-direction

Superscripts

~	Signifying frequency domain variable
‾	Signifying generalized coordinate variable
1	Signifying sub-component
2	Signifying sub-component
'	Signifying fluctuating term or perturbation quantity

CHAPTER 1

INTRODUCTION

The potential of computational fluid dynamics (CFD) techniques has evolved into many dimensions in the past few decades, with tremendous technological growth in areas of numerical computing. It is well known that a numerical simulation usually requires truncation of the physical domain and introduction of an artificial boundary due to the limitation of a finite computational domain. Also, one must specify appropriate initial and boundary conditions to obtain a unique and accurate solution for a system of partial differential equations (PDE). This is a challenging and vital issue, since the imposed boundary conditions can seriously impact the computed solution. The boundary conditions implemented on artificial boundaries are very critical to successful numerical simulations. If these artificial boundaries are not transparent to the out-going disturbances, then reflections of large spurious waves from these artificial boundaries will contaminate the solution in the interior domain, which is certainly undesirable. Therefore, the truncated boundaries should be nonreflecting in order to obtain time-accurate solutions. A detailed discussion on spurious waves and the artifacts of numerical discretization can be found in the review of computational aeroacoustics (CAA) by Lele [1]. There is extensive literature on the nonreflecting boundary treatment, and a variety of methods has been proposed by several researchers in order to treat many computational problems [1-4]. These include out-flow boundary conditions based on characteristics, radiation boundary conditions based on far-field asymptotic solutions, and the absorbing zone or buffer layer technique.

Hoffmann and Chiang [5] group these boundary treatments into three major categories: simple extrapolation schemes, methods based on characteristics, and artificial/buffer zone techniques. The simple extrapolation scheme requires a larger computational domain for

reflection-free solutions, thus leading to increased computational effort and cost [6, 7]. Methods based on characteristics of multidimensional flow involve complicated procedures and make the boundary treatment difficult.

Tam [3] reviewed, in detail, the advances in numerical boundary conditions for CAA. Nizampatnam [6] and Nizampatnam et al. [8] carried out extensive investigation work on boundary conditions for computational aeroacoustics and development of the perfectly matched layer (PML) for aeroacoustic applications in time frequency domains. The development and application of the PML technique that falls into the category of an absorbing layer or buffer zone in a generalized coordinate system is the central focus of this research. The concept of PML was originally proposed by Berenger [9] for solving electromagnetic problems involving Maxwell equations in unbounded domains. The basic strategy of the PML absorbing technique is to introduce additional grid points, or layers, to surround the truncated physical domain so that the out-going disturbances are attenuated in the added zones. Inspired by the success of Berenger's PML method, Hu extended the PML technique to an aeroacoustic problem to solve linearized Euler equations (LEEs) for perturbation [10, 11]. A detailed literature review on the PML absorbing boundary condition has been provided in the work of Velu [7]. The originally proposed split-form PML equations was shown to be only weakly well-posed by Abarbanel and Gottlieb [12] through their detailed mathematical analysis of electromagnetic PML equations. Hesthaven [13], through his similarity transformation analysis, showed that both original unsplit and split-form equations proposed by Hu [10, 11] lost the symmetry and were weakly well-posed. A filtering technique was used by Hu [11] to overcome the instability. However, it is not an easy process to know a priori when one should apply filtering in a particular application. Tam and Auriault [14] extended the stability analysis through the dispersion relations of the PML

equations, and considered the role of phase signs and group velocities. They used artificial damping in order to obtain a stable solution. This is accomplished by absorbing only the short waves, which does not adversely affect the long waves. Subsequently, the concept of conserving the dispersion relation of the physical space equations was explored.

Several studies on the PML indicate that it can be viewed as a complex change of variables, and this idea was extended to Euler equations in constructing unsplit PML equations. Abarbanel et al. [15] used a coordinate transformation in such a way that the transformed coordinates preserved the dispersion relation. But their method can be applied in a situation where a rotation is used to align the mean flow with the computational grid. However, when the mean flow is not aligned to one of the axes, which is the case in general situations, an appropriate transformation will be required. Hu [16] attributed the exponential growth of the reflections to the angle of the wave-front normal vector and proposed the need of a proper space-time transformation to obtain a stable PML in order to align the group and phase velocities in the same direction. Following the concept of Abarbanel et al. [15], Hu [16] applied a complex change of variables for x and y, where the governing equations are expressed in frequency domain. Subsequently, he obtained the unsplit formulation in the time domain by introducing an auxiliary variable. This procedure produced a reflection-free solution, and a similar complex variable transformation with PML boundary treatment to Euler and Navier-Stokes equations was developed [17, 18]. The concept of PML is introduced in section 1.1.

1.1 Perfectly Matched Layer Boundary Condition

The PML is a nonreflecting boundary condition also called the absorbing boundary condition or buffer zone technique. It is a region with a width of a few grid points appended

adjacent to artificial boundaries called the PML domain. The common goal of the PML method is to dampen disturbances entering the PML domain in order to eliminate any physical or nonphysical reflections that contaminate the interior solution. A typical computational domain with a PML is shown in Figure 1.1. The governing equations in the PML domain are obtained in such a way that out-going waves are absorbed without reflection, when they impinge on the interface between the PML and the interior domain.

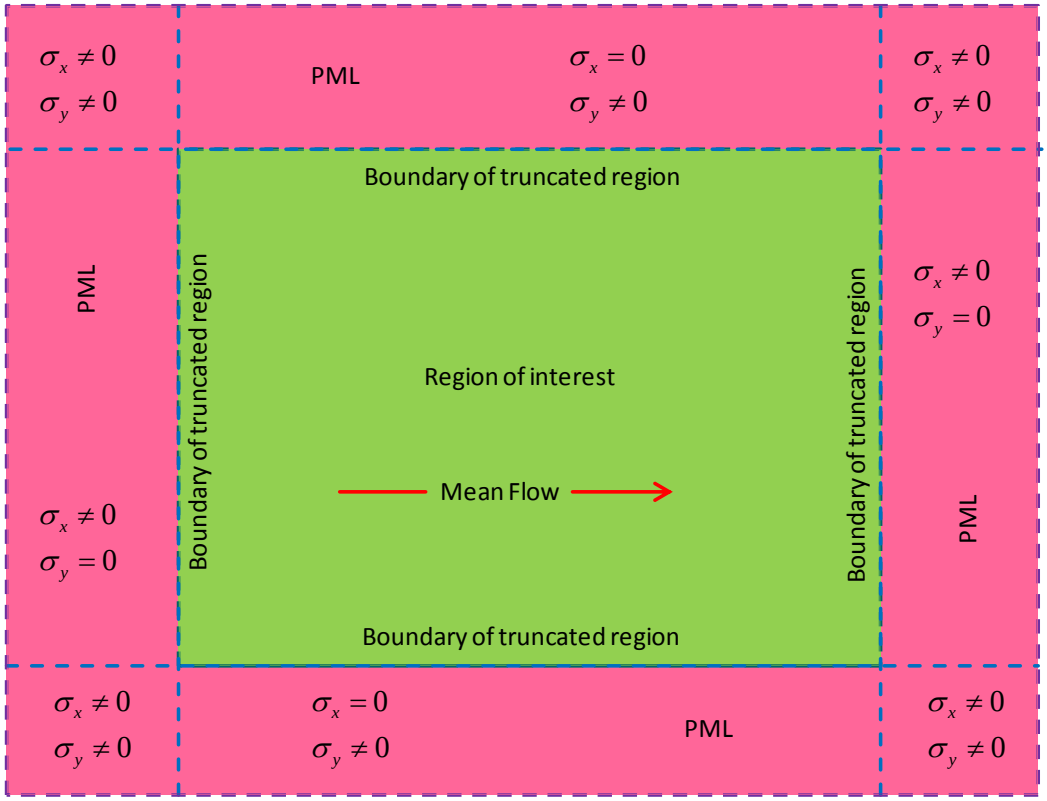

Figure 1.1. Schematic of computational domain showing interior domain and PML domain on boundary with absorption coefficients in the PML domain.

PML equations can be developed by splitting the dependent variables into sub-components [10] as well as in unsplit form [16], which does not involve splitting variables. The absorption coefficients, σ_x and σ_y, are introduced for the absorption of waves in the PML domain as complex change of variables [16]:

$$x \to x + \frac{i}{\omega}\int_{x_0}^{x} \sigma_x dx \quad , \quad y \to y + \frac{i}{\omega}\int_{y_0}^{y} \sigma_y dy \tag{1.1}$$

where $\sigma_x > 0$ and $\sigma_y > 0$ are the absorption coefficients, and x_0 and y_0 are the locations of the Euler PML interface. The absorption coefficients are varied across the layer in such a way that they are zero at the interface between the PML domain and the interior domain, and maximum at the outer boundary of the PML domain. The variation of σ_x and σ_y in the PML is governed by the following relation:

$$\sigma = \sigma_m \left(\frac{d}{D}\right)^{\alpha} \tag{1.2}$$

where D is the width of the PML domain, d is the distance from its interface with the interior domain, σ_m is the maximum value of σ, and α is the damping rate. Alternatively, the PML domain can also be viewed as consisting of layers with constant σ, which varies linearly [10]. The absorption coefficients, σ_x and σ_y, are assumed to be greater than or equal to zero. The coefficient σ_x is zero in a layer parallel to the x-direction, and the coefficient σ_y is zero in a layer parallel to the y-direction.

Both coefficients are greater than zero in the corner regions. Also, the larger the thickness, D, of the PML, the better the wave absorption. However, as thickness increases, the computational time and effort required also increase. At the end of a PML domain, certain boundary conditions, such as a solid-wall condition or other radiation boundary condition, can be applied. In numerical cases investigated in this research, extrapolation at the PML boundaries, i.e., the outer boundaries of the computational domain, is utilized. Parameters of the PML domains can be adjusted for desired absorption. They can also be determined independent of the size of the interior domain.

It has been shown that the theoretical reflection coefficients for incident linear waves at an interface between the interior domain and a PML domain are zero [11]. Thus, the amplitudes of waves that enter the PML domain decrease exponentially. In reality, the solution in the PML domain has no physical significance, since it only helps to prevent the contamination of the solution in the interior domain.

Up to the present time, research activities have shown that the PML technique is a powerful tool. The application of this scheme will greatly reduce the computational cost, since a small computational domain will suffice to solve the numerical problem.

This research effort focuses on the construction of a PML formulation based on the complex change of variables and space-time transformation for unbounded problems governed by linearized and nonlinear Euler equations in a generalized coordinate system. The split-form PML equations for linearized Euler equations over a uniform mean flow without and with space-time transformation and complex change of variables are constructed and investigated for their effectiveness in terms of stability. The main objective is to investigate the PML formulation for domains which are of a nonrectangular shape using generic/conventional numerical schemes for spatial discretization and temporal integration without employing any form of numerical filtering or artificial dissipation. For this purpose, the split formulation of a PML based on the complex variable transformation for unbounded problems governed by nonlinear Euler equations is constructed and applied in a generalized coordinate system. This enables the user to solve nonlinear Euler equations in physical domains that are nonrectangular in shape (x, y, z) or with nonuniform grid spacing by mapping the nonrectangular physical space or the physical space with nonuniform grid spacing, which is the case when grid clustering is used, to a rectangular uniform grid spacing (ξ, η, ζ) in the computational space [19]. A stability analysis on the PML

formulation can be carried out by analyzing the dispersion relation following the procedure used in the work of Velu and Hoffmann [20]. For nonuniform shear flows in the absence of an arbitrary mean-flow profile, a generalized procedure based on the spectral collocation method can be used for the stability analysis and the calculation of the PML parameter introduced in the space-time transformation [21].

This dissertation is organized as follows: Chapter 2 presents the governing equations in Cartesian and generalized coordinate systems. Chapter 3 describes the details of the numerical scheme and solver used for the numerical simulations. Chapters 4 and 5 are dedicated to the PML for linear and nonlinear Euler equations, respectively.

CHAPTER 2

GOVERNING EQUATIONS

2.1 3-D Euler Equations in Cartesian Coordinates

Euler equations in the physical space are given by

$$\frac{\partial Q}{\partial t}+\frac{\partial E}{\partial x}+\frac{\partial F}{\partial y}+\frac{\partial G}{\partial z}=0 \tag{2.1}$$

where

$$Q=\begin{bmatrix}\rho\\ \rho u\\ \rho v\\ \rho w\\ \rho e_t\end{bmatrix};\quad E=\begin{bmatrix}\rho u\\ \rho u^2+p\\ \rho uv\\ \rho uw\\ \rho hu\end{bmatrix};\quad F=\begin{bmatrix}\rho v\\ \rho vu\\ \rho v^2+p\\ \rho vw\\ \rho hv\end{bmatrix};\quad G=\begin{bmatrix}\rho w\\ \rho wu\\ \rho wv\\ \rho w^2+p\\ \rho hw\end{bmatrix} \tag{2.2}$$

and

$$h=e_t+\frac{p}{\rho};\quad e_t=e_i+\frac{u^2+v^2+w^2}{2};\quad p=\rho e_i(\gamma-1);\quad p=(\gamma-1)\rho\left(e_t-\frac{u^2+v^2+w^2}{2}\right) \tag{2.3}$$

in which u, v, and w are the velocity components in the x-, y-, and z-directions, respectively; p is the pressure; ρ is the density; h is the enthalpy; e_t is the total energy per unit mass; e_i is the internal energy per unit mass; and γ is the ratio of specific heats and equals 1.4.

2.2 3-D Euler Equations in Generalized Coordinates

If all CFD applications dealt with physical problems where a uniform, rectangular grid could be used in the physical plane, then the appropriate finite difference formulations of the governing partial difference equations could be applied in rectangular (x,y,z,t) space with

uniform values of Δx, Δy, Δz, and Δt. Unfortunately, the majority of physical domains of interest are nonrectangular in shape. To enhance the efficiency and accuracy of a numerical scheme and to simplify implementation of boundary conditions, a transformation from a curvilinear grid (x, y, z) in physical space to a rectangular grid in computational space (ξ, η, ζ) is performed. This requires the governing physical equations to be recast so as to apply them in the transformed, rectangular grid. This transformation is accomplished using the following relations [5]:

$$\tau = t \tag{2.4}$$

$$\xi = \xi(t, x, y, z) \tag{2.5}$$

$$\eta = (t, x, y, z) \tag{2.6}$$

$$\zeta = (t, x, y, z) \tag{2.7}$$

Using equations (2.4)–(2.7), partial derivatives in the physical space are related to the partial derivatives in the computational space by applying the chain rule of partial differentiation to obtain the following expressions:

$$\frac{\partial}{\partial t} = \frac{\partial}{\partial \tau} + \xi_t \frac{\partial}{\partial \xi} + \eta_t \frac{\partial}{\partial \eta} + \zeta_t \frac{\partial}{\partial \zeta} \tag{2.8}$$

$$\frac{\partial}{\partial x} = \xi_x \frac{\partial}{\partial \xi} + \eta_x \frac{\partial}{\partial \eta} + \zeta_x \frac{\partial}{\partial \zeta} \tag{2.9}$$

$$\frac{\partial}{\partial y} = \xi_y \frac{\partial}{\partial \xi} + \eta_y \frac{\partial}{\partial \eta} + \zeta_y \frac{\partial}{\partial \zeta} \tag{2.10}$$

$$\frac{\partial}{\partial t} = \xi_z \frac{\partial}{\partial \xi} + \eta_z \frac{\partial}{\partial \eta} + \zeta_z \frac{\partial}{\partial \zeta} \tag{2.11}$$

By applying equations (2.8)–(2.11) to equation (2.1), Euler equations in the physical space can be transformed to the computational space as

$$\frac{\partial \bar{Q}}{\partial \tau}+\frac{\partial \bar{E}}{\partial \xi}+\frac{\partial \bar{F}}{\partial \eta}+\frac{\partial \bar{G}}{\partial \zeta}=0 \tag{2.12}$$

where

$$\bar{Q}=\frac{Q}{J} \tag{2.13}$$

$$\bar{E}=\frac{1}{J}\left(\xi_t Q+\xi_x E+\xi_y F+\xi_z G\right) \tag{2.14}$$

$$\bar{F}=\frac{1}{J}\left(\eta_t Q+\eta_x E+\eta_y F+\eta_z G\right) \tag{2.15}$$

$$\bar{G}=\frac{1}{J}\left(\zeta_t Q+\zeta_x E+\zeta_y F+\zeta_z G\right) \tag{2.16}$$

where ξ_t, ξ_x, ξ_y, ξ_z, η_t, η_x, η_y, η_z, ζ_t, ζ_x, ζ_y, and ζ_z are the metrics of transformation, and J is the determinant of the Jacobian of the transformation. Equation (2.12) is solved in the computational domain with step-sizes of $\Delta\xi=\Delta\eta=\Delta\zeta=1.0$. A reverse transformation is carried out to compute the values in the original physical space. Only two-dimensional problems with subsonic flow are considered in this research.

2.3 2-D Euler Equations

In conservative form in Cartesian coordinates, two-dimensional Euler equations are written as

$$\frac{\partial Q}{\partial t}+\frac{\partial E}{\partial x}+\frac{\partial F}{\partial y}=0 \tag{2.17}$$

where

$$Q=\begin{bmatrix}\rho\\ \rho u\\ \rho v\\ \rho e_t\end{bmatrix};\quad E=\begin{bmatrix}\rho u\\ \rho u^2+p\\ \rho uv\\ \rho hu\end{bmatrix};\quad F=\begin{bmatrix}\rho v\\ \rho uv\\ \rho v^2+p\\ \rho hv\end{bmatrix} \tag{2.18}$$

and

$$h=e_t+\frac{p}{\rho};\quad e_t=e_i+\frac{u^2+v^2}{2};\quad p=\rho e_i\left(\gamma-1\right);\quad p=\left(\gamma-1\right)\rho\left(e_t-\frac{u^2+v^2}{2}\right) \tag{2.19}$$

in which u and v are the velocity components in the x- and y-directions, respectively; p is the pressure; ρ is the density; h is the enthalpy; e_t is the total energy per unit mass; e_i is the internal energy per unit mass; and γ is the ratio of specific heats and equals 1.4.

Euler equations, equation (2.17), in generalized coordinates are given by

$$\frac{\partial\bar{Q}}{\partial\tau}+\frac{\partial\bar{E}}{\partial\xi}+\frac{\partial\bar{F}}{\partial\eta}=0 \tag{2.20}$$

where

$$\bar{Q}=\frac{Q}{J};\ \bar{E}=\frac{1}{J}\left[\xi_t Q+\xi_x E+\xi_y F\right];\bar{F}=\frac{1}{J}\left[\eta_t Q+\eta_x E+\eta_y F\right] \tag{2.21}$$

2.3.1 Linearized Euler Equations over Uniform Mean Flow

By assuming that acoustic values are a small, linear, unsteady perturbation upon a steady mean flow, linearized Euler Equations, equations (2.22)–(2.25), are derived directly from Euler equations, equation (2.17). A detailed derivation is presented in Appendix I of the work of Velu [7].

$$\frac{\partial\rho'}{\partial t}+M_x\frac{\partial\rho'}{\partial x}+M_y\frac{\partial\rho'}{\partial y}+\left(\frac{\partial u'}{\partial x}+\frac{\partial v'}{\partial y}\right)=0 \tag{2.22}$$

$$\frac{\partial u'}{\partial t}+M_x\frac{\partial u'}{\partial x}+M_y\frac{\partial u'}{\partial y}+\frac{\partial p'}{\partial x}=0 \tag{2.23}$$

$$\frac{\partial v'}{\partial t} + M_x \frac{\partial v'}{\partial x} + M_y \frac{\partial v'}{\partial y} + \frac{\partial p'}{\partial y} = 0 \tag{2.24}$$

$$\frac{\partial p'}{\partial t} + M_x \frac{\partial p'}{\partial x} + M_y \frac{\partial p'}{\partial y} + \left(\frac{\partial u'}{\partial x} + \frac{\partial v'}{\partial y} \right) = 0 \tag{2.25}$$

in which u' and v' are the velocity perturbations in the x- and y-directions, respectively; p' is the perturbation pressure; ρ' is the perturbation density; and M_x and M_y are the mean flow velocity components in the x- and y-directions, respectively, normalized by the acoustic speed.

The LEE in conservative form in Cartesian coordinates is written as

$$\frac{\partial Q}{\partial t} + \frac{\partial E}{\partial x} + \frac{\partial F}{\partial y} = 0 \tag{2.26}$$

where

$$Q = \begin{bmatrix} \rho' \\ u' \\ v' \\ p' \end{bmatrix}; \quad E = \begin{bmatrix} M_x \rho' + u' \\ M_x u' + p' \\ M_x v' \\ M_x p' + u' \end{bmatrix}; \quad F = \begin{bmatrix} M_y \rho' + v' \\ M_y u' \\ M_y v' + p' \\ M_y p' + v' \end{bmatrix} \tag{2.27}$$

Here, Q, the solution vector, represents the aeroacoustic perturbation in density, velocity, and pressure. Using equation (2.20), the LEE, equation (2.26), in generalized coordinates is obtained and solved in the computational domain. As discussed in section 2.2, a reverse transformation is employed to calculate the values in the physical space.

CHAPTER 3

NUMERICAL SCHEME AND SOLVER DETAILS

3.1 Spatial Discretization

Recalling the 2-D Euler equations, equation (2.17), presented in Chapter 2.3, equation (2.17) is solved in the computational domain using equation (2.20). The convective terms in equation (2.20) are approximated by sixth order compact difference scheme [5, 7] for LEEs and second-order central difference expression [5], equation (3.1), for nonlinear Euler equations:

$$\left(\frac{\partial \bar{E}}{\partial \xi}\right)_{i,j} + \left(\frac{\partial \bar{F}}{\partial \eta}\right)_{i,j} = \frac{\bar{E}_{i+1,j} - \bar{E}_{i-1,j}}{2\Delta\xi} + \frac{\bar{F}_{i,j+1} - \bar{F}_{i,j-1}}{2\Delta\eta} \tag{3.1}$$

where i and j represent the indexes of a grid point in the ξ and η directions, respectively.

3.2 Time Integration

A modified fourth-order Runge-Kutta scheme is used for temporal integration as

$$\bar{Q}_{i,j}^{(1)} = \bar{Q}_{i,j}^{(n)} \tag{3.2}$$

$$\bar{Q}_{i,j}^{(2)} = \bar{Q}_{i,j}^{(n)} - \frac{\Delta\tau}{4}\left[\left(\frac{\partial \bar{E}}{\partial \xi}\right)_{i,j}^{(1)} + \left(\frac{\partial \bar{F}}{\partial \eta}\right)_{i,j}^{(1)} + \bar{H}_{i,j}^{(1)}\right] \tag{3.3}$$

$$\bar{Q}_{i,j}^{(3)} = \bar{Q}_{i,j}^{(n)} - \frac{\Delta\tau}{3}\left[\left(\frac{\partial \bar{E}}{\partial \xi}\right)_{i,j}^{(2)} + \left(\frac{\partial \bar{F}}{\partial \eta}\right)_{i,j}^{(2)} + \bar{H}_{i,j}^{(2)}\right] \tag{3.4}$$

$$\bar{Q}_{i,j}^{(4)} = \bar{Q}_{i,j}^{(n)} - \frac{\Delta\tau}{2}\left[\left(\frac{\partial \bar{E}}{\partial \xi}\right)_{i,j}^{(3)} + \left(\frac{\partial \bar{F}}{\partial \eta}\right)_{i,j}^{(3)} + \bar{H}_{i,j}^{(3)}\right] \tag{3.5}$$

$$\bar{Q}_{i,j}^{(n+1)} = \bar{Q}_{i,j}^{(n)} - \Delta\tau\left[\left(\frac{\partial \bar{E}}{\partial \xi}\right)_{i,j}^{(4)} + \left(\frac{\partial \bar{F}}{\partial \eta}\right)_{i,j}^{(4)} + \bar{H}_{i,j}^{(4)}\right] \tag{3.6}$$

where the superscripts n and $n+1$ refer to the time levels, and the superscripts within parentheses refer to the values at the intermediate stages. The term $\overline{H}$ is the damping term that appears in the PML formulation.

A method that is second-order accurate has a tendency to produce dispersion errors. A second-order central difference scheme used in this numerical solver is no exception, and in order to reduce the dispersion error, a total variation diminishing (TVD) scheme is employed by amending equation (3.6). Among the various available TVD schemes, the Davis-Yee symmetric TVD scheme [5], equation (3.7), is used in the numerical solver.

$$\begin{aligned}\overline{Q}_{i,j}^{(n+1)} = \overline{Q}_{i,j}^{(n)} &- \frac{1}{2}\frac{\Delta\tau}{\Delta\xi}\left[\left(X_A\right)_{i+\frac{1}{2},j}^{n}+\left(\Phi_\xi\right)_{i+\frac{1}{2},j}^{n}-\left(X_A\right)_{i-\frac{1}{2},j}^{n}+\left(\Phi_\xi\right)_{i-\frac{1}{2},j}^{n}\right] \\ &- \frac{1}{2}\frac{\Delta\tau}{\Delta\eta}\left[\left(X_B\right)_{i,j+\frac{1}{2}}^{n}+\left(\Phi_\eta\right)_{i,j+\frac{1}{2}}^{n}-\left(X_B\right)_{i,j-\frac{1}{2}}^{n}+\left(\Phi_\eta\right)_{i,j-\frac{1}{2}}^{n}\right]\end{aligned} \tag{3.7}$$

where X_A and X_B are the eigenvector matrices of the flux Jacobian matrices $\partial\overline{E}/\partial\overline{Q}$ and $\partial\overline{F}/\partial\overline{Q}$, respectively, and Φ_ξ and Φ_η are the flux limiter vectors given by equations (3.8)–(3.11).

$$\left(\Phi_\xi\right)_{i+\frac{1}{2},j}^{n} = -\left\{\frac{\Delta\tau}{\Delta\xi}\left[\left(\alpha_\xi\right)_{i+\frac{1}{2},j}\right]^2\left(G_\xi\right)_{i+\frac{1}{2},j}+\psi\left[\left(\alpha_\xi\right)_{i+\frac{1}{2},j}\right]\left[\left(\delta_\xi\right)_{i+\frac{1}{2},j}-\left(G_\xi\right)_{i+\frac{1}{2},j}\right]\right\} \tag{3.8}$$

$$\left(\Phi_\xi\right)_{i-\frac{1}{2},j}^{n} = -\left\{\frac{\Delta\tau}{\Delta\xi}\left[\left(\alpha_\xi\right)_{i-\frac{1}{2},j}\right]^2\left(G_\xi\right)_{i-\frac{1}{2},j}+\psi\left[\left(\alpha_\xi\right)_{i-\frac{1}{2},j}\right]\left[\left(\delta_\xi\right)_{i-\frac{1}{2},j}-\left(G_\xi\right)_{i-\frac{1}{2},j}\right]\right\} \tag{3.9}$$

$$\left(\Phi_\eta\right)_{i,j+\frac{1}{2}}^{n} = -\left\{\frac{\Delta\tau}{\Delta\eta}\left[\left(\alpha_\eta\right)_{i,j+\frac{1}{2}}\right]^2\left(G_\eta\right)_{i,j+\frac{1}{2}}+\psi\left[\left(\alpha_\eta\right)_{i,j+\frac{1}{2}}\right]\left[\left(\delta\eta\right)_{i,j+\frac{1}{2}}-\left(G_\eta\right)_{i,j+\frac{1}{2}}\right]\right\} \tag{3.10}$$

$$\left(\Phi_\eta\right)_{i,j-\frac{1}{2}}^{n} = -\left\{\frac{\Delta\tau}{\Delta\eta}\left[\left(\alpha_\eta\right)_{i,j-\frac{1}{2}}\right]^2\left(G_\eta\right)_{i,j-\frac{1}{2}}+\psi\left[\left(\alpha_\eta\right)_{i,j-\frac{1}{2}}\right]\left[\left(\delta\eta\right)_{i,j-\frac{1}{2}}-\left(G_\eta\right)_{i,j-\frac{1}{2}}\right]\right\} \tag{3.11}$$

where α_ξ and α_η are the eigenvalue vectors corresponding to X_A and X_B, respectively. In the expressions given by equations (3.8)–(3.11),

$$\left(\delta_\xi\right)_{i+\frac{1}{2},j} = \left(X_A\right)^{-1}_{i+\frac{1}{2},j}\left(J^{-1}_{i+\frac{1}{2},j}\right)\left(Q_{i+1,j} - Q_{i,j}\right) \quad , \quad J_{i+\frac{1}{2},j} = \frac{1}{2}\left(J_{i+1,j} + J_{i,j}\right) \tag{3.12}$$

$$\left(\delta_\xi\right)_{i-\frac{1}{2},j} = \left(X_A\right)^{-1}_{i-\frac{1}{2},j}\left(J^{-1}_{i-\frac{1}{2},j}\right)\left(Q_{i-1,j} - Q_{i,j}\right) \quad , \quad J_{i-\frac{1}{2},j} = \frac{1}{2}\left(J_{i-1,j} + J_{i,j}\right) \tag{3.13}$$

$$\left(\delta_\eta\right)_{i,j+\frac{1}{2}} = \left(X_B\right)^{-1}_{i,j+\frac{1}{2}}\left(J^{-1}_{i,j+\frac{1}{2}}\right)\left(Q_{i,j+1} - Q_{i,j}\right) \quad , \quad J_{i,j+\frac{1}{2}} = \frac{1}{2}\left(J_{i,j+1} + J_{i,j}\right) \tag{3.14}$$

$$\left(\delta_\eta\right)_{i,j-\frac{1}{2}} = \left(X_B\right)^{-1}_{i,j-\frac{1}{2}}\left(J^{-1}_{i,j-\frac{1}{2}}\right)\left(Q_{i,j-1} - Q_{i,j}\right) \quad , \quad J_{i,j-\frac{1}{2}} = \frac{1}{2}\left(J_{i,j-1} + J_{i,j}\right) \tag{3.15}$$

The limiters are given by equations (3.16)–(3.19),

$$\left(G_\xi\right)_{i+\frac{1}{2},j} = \min \operatorname{mod}\left\{2\left(\delta_\xi\right)_{i-\frac{1}{2},j},\ 2\left(\delta_\xi\right)_{i+\frac{1}{2},j},\ 2\left(\delta_\xi\right)_{i+\frac{3}{2},j},\ \frac{1}{2}\left[\left(\delta_\xi\right)_{i-\frac{1}{2},j} + \left(\delta_\xi\right)_{i+\frac{3}{2},j}\right]\right\} \tag{3.16}$$

$$\left(G_\xi\right)_{i-\frac{1}{2},j} = \min \operatorname{mod}\left\{2\left(\delta_\xi\right)_{i-\frac{1}{2},j},\ 2\left(\delta_\xi\right)_{i+\frac{1}{2},j},\ 2\left(\delta_\xi\right)_{i+\frac{3}{2},j},\ \frac{1}{2}\left[\left(\delta_\xi\right)_{i-\frac{1}{2},j} + \left(\delta_\xi\right)_{i+\frac{3}{2},j}\right]\right\} \tag{3.17}$$

$$\left(G_\eta\right)_{i,j+\frac{1}{2}} = \min \operatorname{mod}\left\{2\left(\delta_\eta\right)_{i,j-\frac{1}{2}},\ 2\left(\delta_\eta\right)_{i,j+\frac{1}{2}},\ 2\left(\delta_\eta\right)_{i,j+\frac{3}{2}},\ \frac{1}{2}\left[\left(\delta_\eta\right)_{i,j-\frac{1}{2}} + \left(\delta_\eta\right)_{i,j+\frac{3}{2}}\right]\right\} \tag{3.18}$$

$$\left(G_\eta\right)_{i,j-\frac{1}{2}} = \min \operatorname{mod}\left\{2\left(\delta_\eta\right)_{i,j-\frac{1}{2}},\ 2\left(\delta_\eta\right)_{i,j+\frac{1}{2}},\ 2\left(\delta_\eta\right)_{i,j+\frac{3}{2}},\ \frac{1}{2}\left[\left(\delta_\eta\right)_{i,j-\frac{1}{2}} + \left(\delta_\eta\right)_{i,j+\frac{3}{2}}\right]\right\} \tag{3.19}$$

In equations (3.8)–(3.11), the term ψ represents the entropy correction term which is given by

$$\psi = \begin{cases} \left|\alpha_\xi\right| & for \quad \left|\alpha_\xi\right| \geq \varepsilon \\ \dfrac{\alpha_\xi^2 + \varepsilon^2}{2\varepsilon} & for \quad \left|\alpha_\xi\right| < \varepsilon \end{cases} \tag{3.20}$$

The positive constant ε is selected within the range of $0.0 \leq \varepsilon \leq 0.125$. The numerical simulations shown in this research use a value of 0.0001. A global time-step size is used in all numerical simulations.

3.3 Nondimensionalization

Calculations in the computational domain are carried out in nondimensional form. Among the many choices available, L_{ref}, a_0, L_{ref} / a_0, ρ_0, and $\rho_0 a_0^2$ are used as length, velocity, time, density, and pressure scales, respectively, in this research effort, where L_{ref} is a reference length, a_0 is the speed of sound, and ρ_0 is the mean flow density.

3.4 Work Station Specifications

All simulations were run on the DELL Precision WorkStation T3400 powered with an Intel (R) Core (TM) 2 Extreme CPU Q6800 @ 2.93 GHz (4 CPUs). All calculations were made with double precision of accuracy.

CHAPTER 4

PML FOR LINEARIZED EULER EQUATIONS OVER UNIFORM MEAN FLOW

4.1 Linearized Euler Equations

The LEEs given by equations (2.22)–(2.25) are written in vector form as

$$\frac{\partial Q}{\partial t} + A\frac{\partial Q}{\partial x} + B\frac{\partial Q}{\partial y} = 0 \tag{4.1}$$

where

$$Q = \begin{bmatrix} \rho' \\ u' \\ v' \\ p' \end{bmatrix}; \quad A = \begin{bmatrix} M_x & 1 & 0 & 0 \\ 0 & M_x & 0 & 1 \\ 0 & 0 & M_x & 0 \\ 0 & 1 & 0 & M_x \end{bmatrix}; \quad B = \begin{bmatrix} M_y & 0 & 1 & 0 \\ 0 & M_y & 0 & 0 \\ 0 & 0 & M_y & 1 \\ 0 & 0 & 1 & M_y \end{bmatrix} \tag{4.2}$$

in which u' and v' are the velocity perturbations in the x- and y-directions, respectively; p' is the perturbation pressure; ρ' is the perturbation density; M_x and M_y are the mean flow velocity components in the x- and y-directions, respectively, normalized by the acoustic speed; and Q, the solution vector, represents the aeroacoustic perturbation in density, velocity, and pressure.

The LEE for a uniform mean flow in the x direction is

$$\frac{\partial Q}{\partial t} + A\frac{\partial Q}{\partial x} + B\frac{\partial Q}{\partial y} = 0 \tag{4.3}$$

where

$$Q = \begin{bmatrix} \rho' \\ u' \\ v' \\ p' \end{bmatrix}; \quad A = \begin{bmatrix} M_x & 1 & 0 & 0 \\ 0 & M_x & 0 & 1 \\ 0 & 0 & M_x & 0 \\ 0 & 1 & 0 & M_x \end{bmatrix}; \quad B = \begin{bmatrix} 0 & 0 & 1 & 0 \\ 0 & 0 & 0 & 0 \\ 0 & 0 & 0 & 1 \\ 0 & 0 & 1 & 0 \end{bmatrix} \tag{4.4}$$

Providing the mean flow Mach number (M_x), the perturbation quantities can be solved in a straight-forward manner from equation (4.3).

4.2 PML Equations Using Two-Component Splitting

For the implementation of the PML, ρ', u', v', and p' in equation (4.4) are split into subcomponents in coordinate directions as ρ_1, ρ_2, u_1, u_2, v_1, v_2, p_1, and p_2. Following the concept of Berenger's PML technique [9], the original system of four equations is rewritten into a system of eight equations, equations (4.5)–(4.12), with the introduction of absorption coefficients, σ_x and σ_y, in the coordinate directions [10]. Equations (4.5)–(4.12) are the governing perfectly matched layer equations of the linearized Euler equations, equation (4.3).

$$\frac{\partial \rho_1}{\partial t} + \sigma_x \rho_1 = -\frac{\partial (u_1 + u_2)}{\partial x} - M_x \frac{\partial (\rho_1 + \rho_2)}{\partial x} \tag{4.5}$$

$$\frac{\partial \rho_2}{\partial t} + \sigma_y \rho_2 = -\frac{\partial (v_1 + v_2)}{\partial y} \tag{4.6}$$

$$\frac{\partial u_1}{\partial t} + \sigma_x u_1 = -\frac{\partial (p_1 + p_1)}{\partial x} - M_x \frac{\partial (u_1 + u_2)}{\partial x} \tag{4.7}$$

$$\frac{\partial u_2}{\partial t} + \sigma_y u_2 = 0 \tag{4.8}$$

$$\frac{\partial v_1}{\partial t} + \sigma_y v_1 = -\frac{\partial (p_1 + p_1)}{\partial y} \tag{4.9}$$

$$\frac{\partial v_2}{\partial t} + \sigma_x v_2 = -M_x \frac{\partial (v_1 + v_2)}{\partial x} \tag{4.10}$$

$$\frac{\partial p_1}{\partial t} + \sigma_x p_1 = -\frac{\partial (u_1 + u_2)}{\partial x} - M_x \frac{\partial (p_1 + p_2)}{\partial x} \tag{4.11}$$

$$\frac{\partial p_2}{\partial t}+\sigma_y p_2=-\frac{\partial\left(v_1+v_2\right)}{\partial y} \tag{4.12}$$

The PML damping coefficients are zero in the interior domain (see Figure 1.1). It is to be noted that, when $\sigma_x=\sigma_y=0$ and $\rho^{'}=\rho_1+\rho_2$, $u^{'}=u_1+u_2$, $v^{'}=v_1+v_2$, and $p^{'}=p_1+p_2$, equations (4.5)–(4.12) are reduced to LEEs, i.e., equation (4.3).

In generalized coordinates, ξ and η, the conservative form of the PML equations for uniform mean flow, take the following form [7]:

$$\frac{\partial\overline{Q}}{\partial\tau}+\frac{\partial\overline{E}}{\partial\xi}+\frac{\partial\overline{F}}{\partial\eta}+\overline{H}=0 \tag{4.13}$$

where

$$\overline{Q}=\begin{bmatrix}\rho_1\\ \rho_2\\ u_1\\ u_2\\ v_1\\ v_2\\ p_1\\ p_2\end{bmatrix} \quad ; \quad \overline{E}=\frac{1}{J}\begin{bmatrix}\xi_x\left(M_x\rho^{'}+u^{'}\right)+\xi_y\left(v^{'}\right)\\ 0\\ \xi_x\left(M_x u^{'}+p^{'}\right)\\ 0\\ 0\\ \xi_x\left(M_x v^{'}\right)+\xi_y\left(p^{'}\right)\\ \xi_x\left(M_x p^{'}+u^{'}\right)+\xi_y\left(v^{'}\right)\\ 0\end{bmatrix} \quad ;$$

$$\overline{F}=\frac{1}{J}\begin{bmatrix}0\\ \eta_x\left(M_x\rho^{'}+u^{'}\right)+\eta_y\left(v^{'}\right)\\ 0\\ \eta_x\left(M_x u^{'}+p^{'}\right)\\ \eta_x\left(M_x v^{'}\right)+\eta_y\left(p^{'}\right)\\ 0\\ 0\\ \eta_x\left(M_x p^{'}+u^{'}\right)+\eta_y\left(v^{'}\right)\end{bmatrix} \quad ; \quad \overline{H}=\frac{1}{J}\begin{bmatrix}\sigma_\xi\rho_1\\ \sigma_\eta\rho_2\\ \sigma_\xi u_1\\ \sigma_\eta u_2\\ \sigma_\eta v_1\\ \sigma_\xi v_2\\ \sigma_\xi p_1\\ \sigma_\eta p_2\end{bmatrix} \tag{4.14}$$

The source term, $\overline{H}$, in equations (4.13) and (4.14) represents the damping term associated with the PML layers. Equation (4.13) is solved in the computational domain.

4.3 Three-Step PML Procedure

The procedure for the construction of a stable PML formulation with a space-time transformation essentially involves three steps [17, 18]:

- A proper space-time transformation is determined and applied to the governing equations. This is a crucial step in the construction of an effective PML equation. The main purpose of applying a space-time transformation is to ensure that in the transformed coordinates all linear waves supported by Euler equations have consistent phase and group velocities. Inconsistency in these two velocities inside the PML domain will result in amplification instead of damping of the waves. This will be demonstrated through a dispersion analysis for acoustic waves and numerical simulations in section 4.4.2 for the LEE.
- A PML complex change of variables is applied in the frequency domain as per equation (1.1). After writing the equations in the frequency domain, they are split in coordinate directions to obtain a split-form PML or retained as is to obtain the PML in an unsplit form, and then simplification and reorganization of the equations is performed.
- The time domain absorbing boundary condition is derived from the frequency domain equations. This is the last step in which the equation in the frequency domain is written back in the time domain in the transformed coordinates. Finally, the PML equation is obtained in the original coordinates through a reverse transformation.

4.3.1 PML Equations with Transformation in Unsplit Form

Now, by introducing new variables $\bar{x}$, $\bar{y}$, and $\bar{t}$ as used in the work of Hu [16],

$$\bar{x} = x, \quad \bar{y} = \sqrt{1-M^2}\,y, \quad \bar{t} = t + \frac{M}{1-M^2}x \tag{4.15}$$

the LEE, equation (4.3), with the new variables is found to be

$$\left(I + \frac{M}{1-M^2}A\right)\frac{\partial Q}{\partial \bar{t}} + A\frac{\partial Q}{\partial \bar{x}} + \sqrt{1-M^2}B\frac{\partial Q}{\partial \bar{y}} = 0 \tag{4.16}$$

where I is the identity matrix. Then, by applying the PML complex change of variables as per equation (1.1),

$$x' = \left(1 + \frac{i\sigma_x}{\omega}\right)\bar{x}, \quad y' = \left(1 + \frac{i\sigma_y}{\omega}\right)\bar{y} \tag{4.17}$$

in the frequency domain, the LEE, equation (4.16), takes the form of

$$-i\bar{\omega}\left(I + \frac{M}{1-M^2}A\right)Q + \frac{1}{\left(1 + \frac{i\sigma_x}{\bar{\omega}}\right)}A\frac{\partial Q}{\partial \bar{x}} + \frac{1}{\left(1 + \frac{i\sigma_y}{\bar{\omega}}\right)}\sqrt{1-M^2}B\frac{\partial Q}{\partial \bar{y}} = 0 \tag{4.18}$$

where $\bar{\omega}$ is the frequency in the transformed equation, which is equal to ω. Subsequent to multiplying equation (4.18) by $\left(1 + i\sigma_x/\bar{\omega}\right)\left(1 + i\sigma_y/\bar{\omega}\right)$, the LEE in the frequency domain is rewritten back in the time domain as

$$\begin{aligned}\left(I + \frac{M}{1-M^2}A\right)Q\left[\frac{\partial Q}{\partial \bar{t}} + \left(\sigma_x + \sigma_y\right)Q + \sigma_x\sigma_y q\right] + A\frac{\partial Q}{\partial \bar{x}} + \sigma_y A\frac{\partial q}{\partial \bar{x}} \\ + \sqrt{1-M^2}B\frac{\partial Q}{\partial \bar{y}} + \sigma_x\sqrt{1-M^2}B\frac{\partial q}{\partial \bar{y}} = 0\end{aligned} \tag{4.19}$$

where q is an auxiliary variable given by

$$\frac{\partial q}{\partial t} = Q \tag{4.20}$$

Finally, in terms of the original variables x, y, and t, the new formulation of the PML equations is expressed as

$$\frac{\partial Q}{\partial t}+A\frac{\partial Q}{\partial x}+B\frac{\partial Q}{\partial y}+\sigma_y A\frac{\partial q}{\partial x}+\sigma_x B\frac{\partial q}{\partial y}+\left(\sigma_x+\sigma_y\right)Q \\ +\sigma_x\sigma_y q+\sigma_x\frac{M}{\sqrt{1-M^2}}A\left(Q+\sigma_y q\right)=0 \tag{4.21}$$

Equations (4.21) and (4.20) are the governing PML equations of the LEE, equation (4.3), in unsplit form. The auxiliary variable q needs to be calculated only within the PML domain where σ_x or σ_y is a non-zero value. Thus, it is not necessary to calculate q within the interior domain, where the absorption coefficients are zero.

In generalized coordinates, ξ and η, the conservative form of the PML equations for uniform mean flow takes the following form:

$$\frac{\partial\overline{Q}}{\partial\tau}+\frac{\partial\overline{E}}{\partial\xi}+\frac{\partial\overline{F}}{\partial\eta}+\overline{H}=0 \tag{4.22}$$

where

$$\overline{Q}=\begin{bmatrix}\rho'\\ u'\\ v'\\ p'\end{bmatrix}\quad;\quad \overline{E}=\frac{1}{J}\begin{bmatrix}\xi_x\left(\left(M_x\rho'+u'\right)+\sigma_\eta\left(M_xq_\rho+q_u\right)\right)+\xi_y\left(v'+\sigma_\xi q_v\right)\\ \xi_x\left(\left(M_xu'+p'\right)+\sigma_\eta\left(M_xq_u+q_p\right)\right)\\ \xi_x\left(M_xv'+\sigma_\eta M_xq_v\right)+\xi_y\left(p'+\sigma_\xi q_p\right)\\ \xi_x\left(\left(M_xp'+u'\right)+\sigma_\eta\left(M_xq_p+q_u\right)\right)+\xi_y\left(v'+\sigma_\xi q_v\right)\end{bmatrix}\quad;$$

$$\overline{F}=\frac{1}{J}\begin{bmatrix}\eta_x\left(\left(M_x\rho'+u'\right)+\sigma_\eta\left(M_xq_\rho+q_u\right)\right)+\eta_y\left(v'+\sigma_\xi q_v\right)\\ \eta_x\left(\left(M_xu'+p'\right)+\sigma_\eta\left(M_xq_u+q_p\right)\right)\\ \eta_x\left(M_xv'+\sigma_\eta M_xq_v\right)+\eta_y\left(p'+\sigma_\xi q_p\right)\\ \eta_x\left(\left(M_xp'+u'\right)+\sigma_\eta\left(M_xq_p+q_u\right)\right)+\eta_y\left(v'+\sigma_\xi q_v\right)\end{bmatrix}\quad; \tag{4.23}$$

$$\overline{H} = \frac{1}{J}\begin{bmatrix} \left(\sigma_\xi + \sigma_\eta\right)\rho + \sigma_\xi\sigma_\eta q_\rho + \left(\left(M_x/\left(1-M_x^2\right)\right)\sigma_\xi\left(\left(M_x\rho' + u'\right) + \sigma_\eta\left(M_x q_\rho + q_u\right)\right)\right) \\ \left(\sigma_\xi + \sigma_\eta\right)u + \sigma_\xi\sigma_\eta q_u + \left(\left(M_x/\left(1-M_x^2\right)\right)\sigma_\xi\left(\left(M_x u' + p'\right) + \sigma_\eta\left(M_x q_u + q_p\right)\right)\right) \\ \left(\sigma_\xi + \sigma_\eta\right)v + \sigma_\xi\sigma_\eta q_v + \left(\left(M_x/\left(1-M_x^2\right)\right)\sigma_\xi\left(M_x v' + \sigma_\eta M_x q_v\right)\right) \\ \left(\sigma_\xi + \sigma_\eta\right)p + \sigma_\xi\sigma_\eta q_p + \left(\left(M_x/\left(1-M_x^2\right)\right)\sigma_\xi\left(\left(M_x p' + u'\right) + \sigma_\eta\left(M_x q_p + q_u\right)\right)\right) \end{bmatrix}$$

and

$$\frac{\partial \overline{q}}{\partial \tau} = \overline{Q} \tag{4.24}$$

In equation (4.23), the subscript of q represents the corresponding physical variable associated with the vector q. The source term, $\overline{H}$, in equations (4.22) and (4.23) represents the damping term associated with the PML layers. Equations (4.22) and (4.24) are solved in the computational domain.

4.4 Numerical Results

The split-form of PML formulation, equation (4.13), and the unsplit formulation, equations (4.22) and (4.24), are validated by considering an initial value problem with two-dimensional acoustic and vorticity disturbances, equations (4.25)–(4.28), as provided by category three of benchmark problems of computational aeroacoustics [22]. The mean flow is in the direction of the x-axis, with $M = M_x = 0.5$. The square physical domain, [-110, 110] x [-110, 110], is a uniform grid with spacing of $\Delta x = \Delta y = 1$ which includes a PML domain of ten grid points on the four sides, as shown in Figures 4.1(a) and (b). In the computational domain, $\Delta\xi = \Delta\eta = 1$. The values of $\sigma_m = \alpha = 2$ are selected.

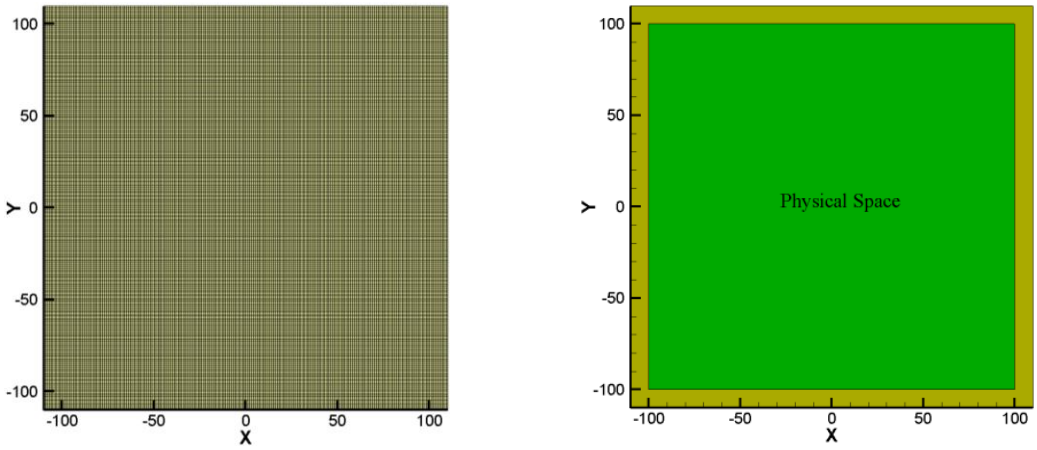

(a) (b)

Figure 4.1. Square physical domain for uniform grid: (a) grid structure, (b) PML domain (shaded region in olive green) and physical space. Number of PML layers (NPML) = 10.

$$\rho = A_0 \exp\left[-(\ln 2)\left(\frac{(x-x_a)^2+(y-y_a)^2}{9}\right)\right] + C_0 \exp\left[-(\ln 2)\left(\frac{(x-x_b)^2+(y-y_b)^2}{25}\right)\right] \quad (4.25)$$

$$p = A_0 \exp\left[-(\ln 2)\left(\frac{(x-x_a)^2+(y-y_a)^2}{9}\right)\right] \quad (4.26)$$

$$u = B_0 (y-y_b) \exp\left[-(\ln 2)\left(\frac{(x-x_b)^2+(y-y_b)^2}{25}\right)\right] \quad (4.27)$$

$$v = -B_0 (x-x_b) \exp\left[-(\ln 2)\left(\frac{(x-x_b)^2+(y-y_b)^2}{25}\right)\right] \quad (4.28)$$

These equations include an acoustic pulse centered at (x_a, y_a), and vorticity and entropy pulses both centered at (x_b, y_b), with amplitudes of $A_0 = 1$, $B_0 = 0.04$, and $C_0 = 0.1$. Initially, the acoustic pulse is located at the origin, $(x_a, y_a) = (0, 0)$, and the vorticity and entropy pulses are located at $(x_b, y_b) = (67, 0)$. A time-step size of 0.1 is used for time integration.

It is found that both split and unsplit formulations produced identical results, and the unsplit-formulation solution is presented here in this section. The u velocity contours obtained using the unsplit-PML formulation at various time levels are presented in Figure 4.2. It can be seen that the waves are absorbed in the PML domain with no reflection.

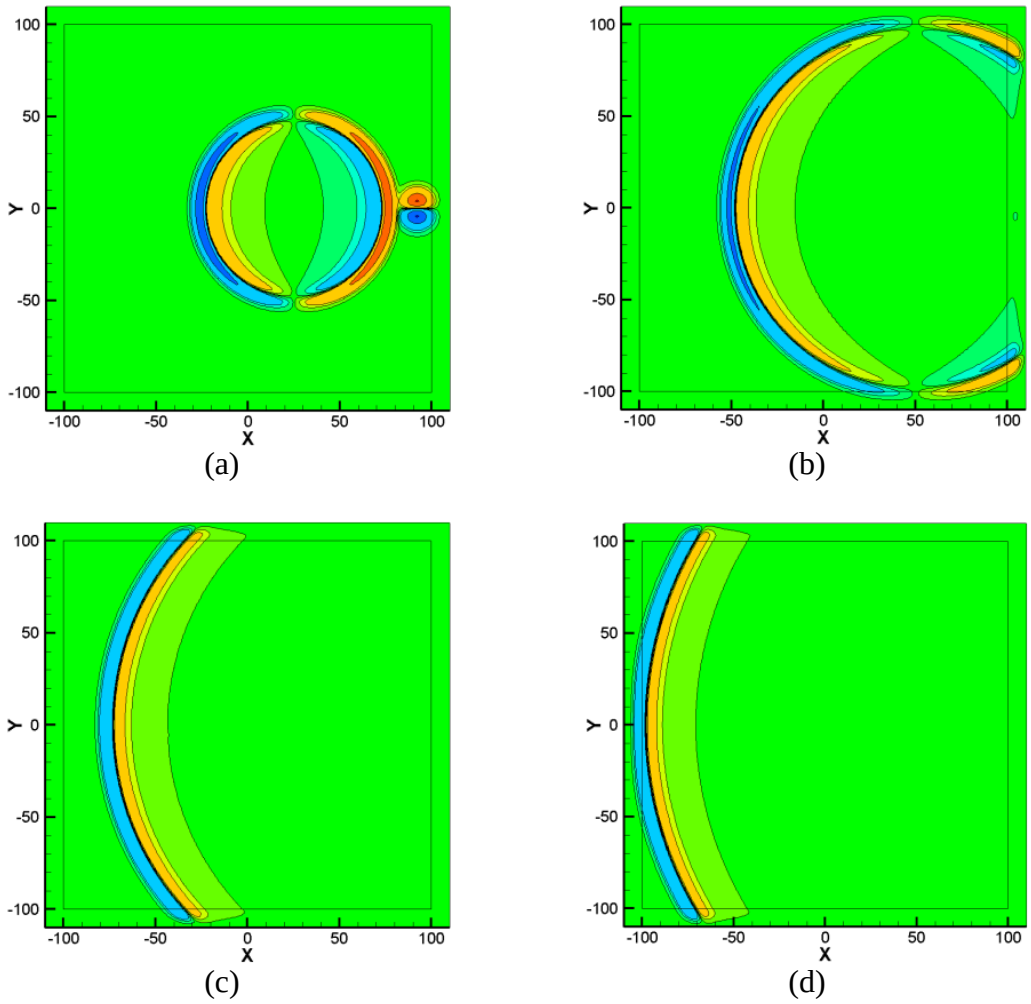

Figure 4.2 u-velocity contours at values of ±0.1, ±0.05, ±0.01, ±0.005, and ±0.001showing acoustic and vorticity pulses: M = 0.5 at (a) t = 50, (b) t = 100, (c) t = 150, and (d) t = 200, with $\sigma_m = \alpha = 2$ and NPML = 10.

The analytical solution [22] for this initial value problem with an acoustic pulse, vorticity and an entropy pulses is given by equations (4.29)–(4.32):

$$p = \frac{1}{2\alpha_1}\int_0^\infty e^{\frac{-\xi^2}{4\alpha_1}} \cos(\xi t)\, J_0(\xi\eta)\, \xi\, d\xi \tag{4.29}$$

$$\rho = p + 0.1\, e^{-\alpha_2\left[(x-67-Mt)^2+y^2\right]} \tag{4.30}$$

$$u = \frac{(x-Mt)}{2\alpha_1\eta}\int_0^\infty e^{\frac{-\xi^2}{4\alpha_1}} \sin(\xi t)\, J_1(\xi\eta)\, \xi\, d\xi \; + \; 0.04y\, e^{-\alpha_2\left[(x-67-Mt)^2+y^2\right]} \tag{4.31}$$

$$v = \frac{y}{2\alpha_1\eta}\int_0^\infty e^{\frac{-\xi^2}{4\alpha_1}} \sin(\xi t)\, J_1(\xi\eta)\, \xi\, d\xi \; - \; 0.04(x-67-Mt)\, e^{-\alpha_2\left[(x-67-Mt)^2+y^2\right]} \tag{4.32}$$

where

$J_0(\;)$ and $J_1(\;)$ are Bessel functions of order 0 and 1.

$$\alpha_1 = \frac{\ln(2)}{9}\,,\ \alpha_2 = \frac{\ln(2)}{25} \tag{4.33}$$

$$M = 0.5\,, \text{ and } \eta = \left[(x-Mt)^2 + y^2\right]^{\frac{1}{2}} \tag{4.34}$$

Figures 4.3 and 4.4 show a comparison of the PML solution with the analytical solution along line $y = 0$ at $t = 200$ for u velocity and pressure, respectively. Figures 4.5 and 4.6 show a similar comparison at $t = 600$ for u velocity and pressure, respectively. The u velocity as a function of time at a selected point (100, 0) on the Euler and PML domain interface is shown in Figure 4.7. The numerical solution compares very well with the analytical solution.

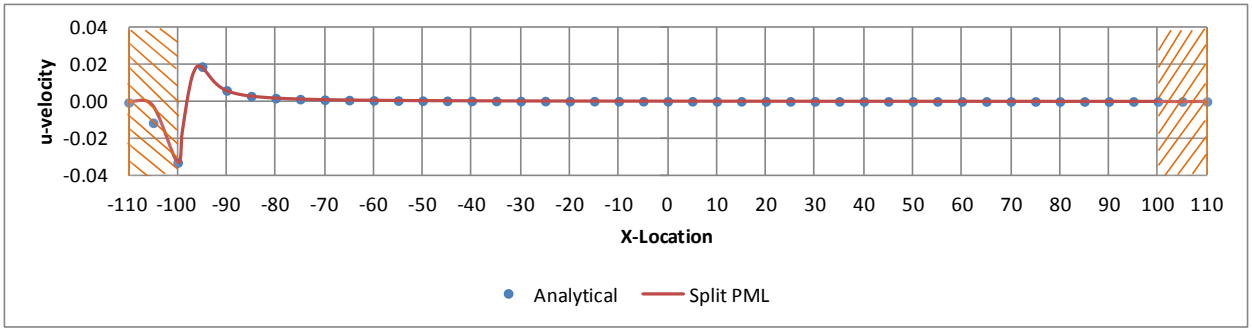

(a)

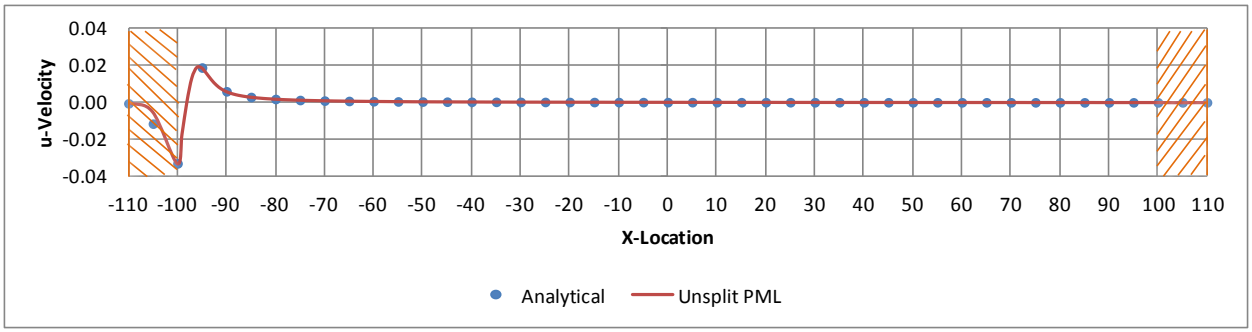

(b)

Figure 4.3. u-velocity along line y = 0 for M = 0.5 at t = 200: (a) analytical vs. split PML, (b) analytical vs. unsplit PML, with $\sigma_m = \alpha = 2$ and NPML = 10.

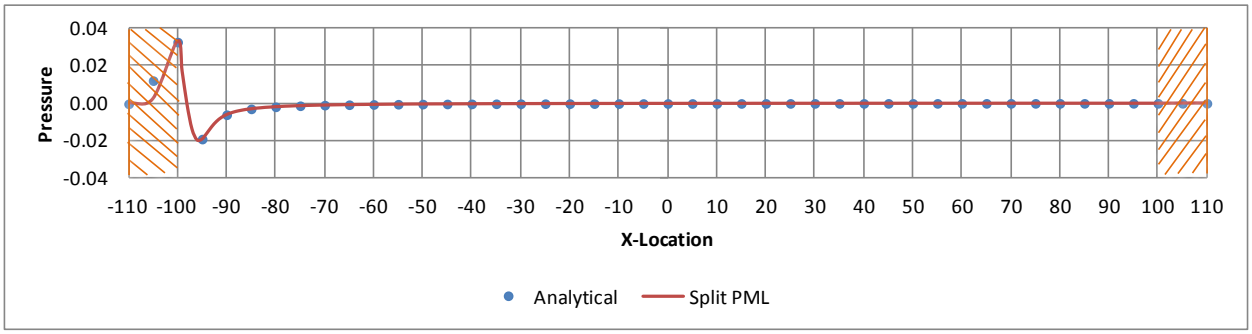

(a)

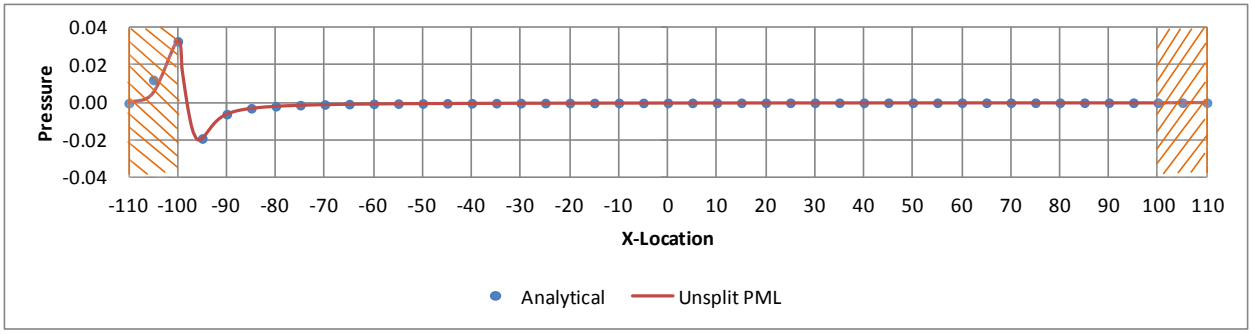

(b)

Figure 4.4. Pressure along line y = 0 for M = 0.5 at t = 200: (a) analytical vs. split PML, (b) analytical vs. unsplit PML, with $\sigma_m = \alpha = 2$ and NPML = 10.

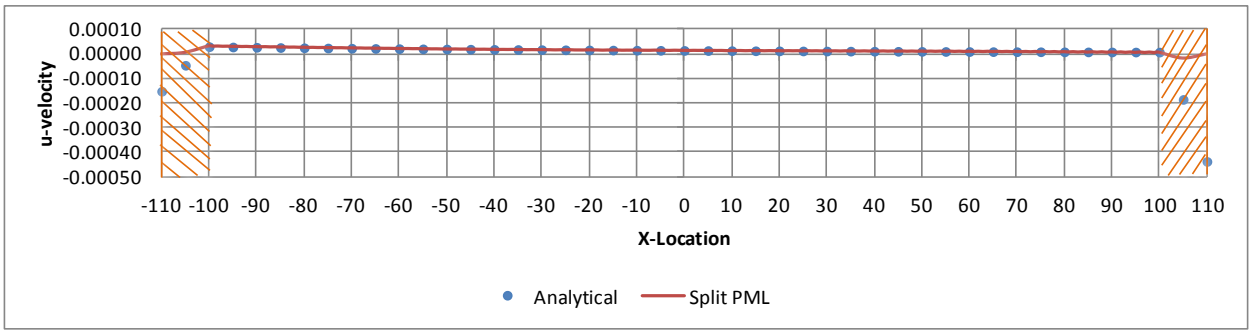

(a)

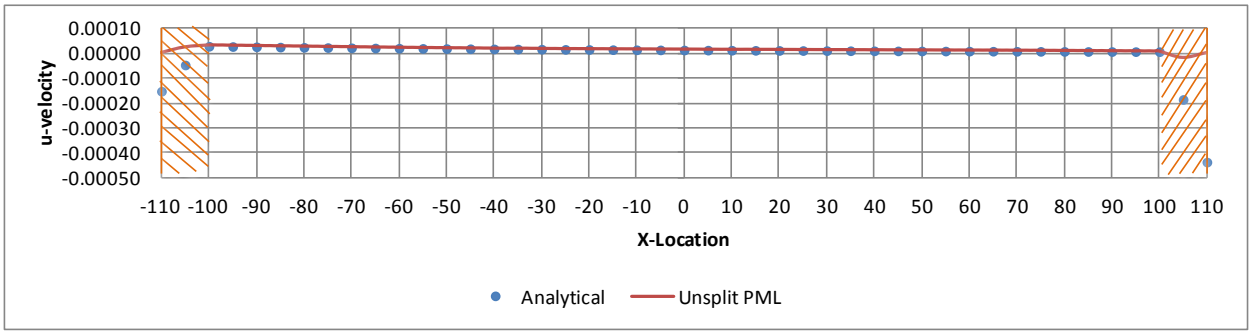

(b)

Figure 4.5. u-velocity along line y = 0 for M = 0.5 at t = 600: (a) analytical vs. split PML, (b) analytical vs. unsplit PML, with $\sigma_m = \alpha = 2$ and NPML = 10.

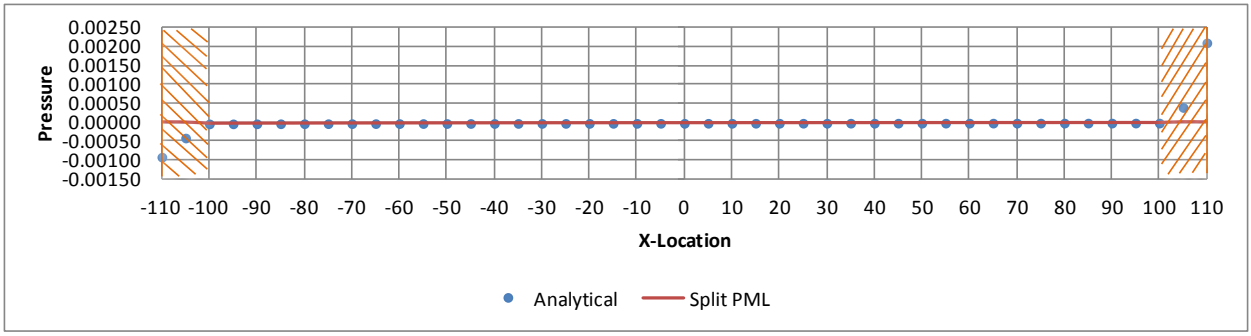

(a)

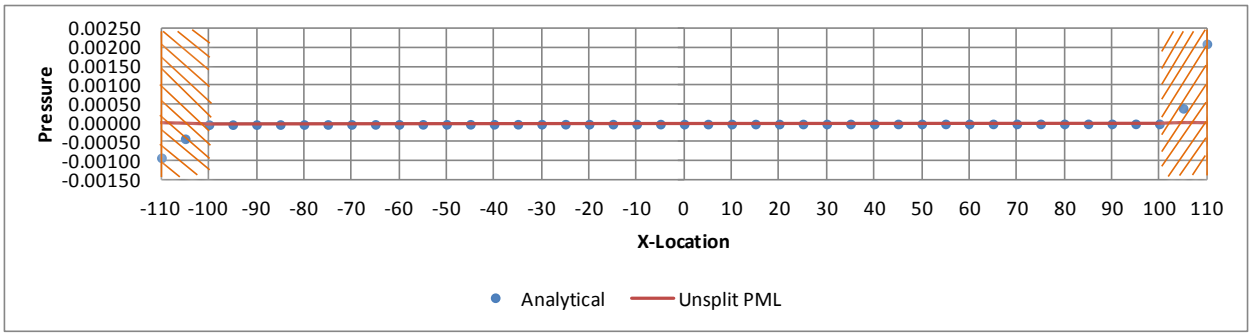

(b)

Figure 4.6. Pressure along line y = 0 for M = 0.5 at t = 600: (a) analytical vs. split PML, (b) analytical vs. unsplit PML, with $\sigma_m = \alpha = 2$ and NPML = 10.

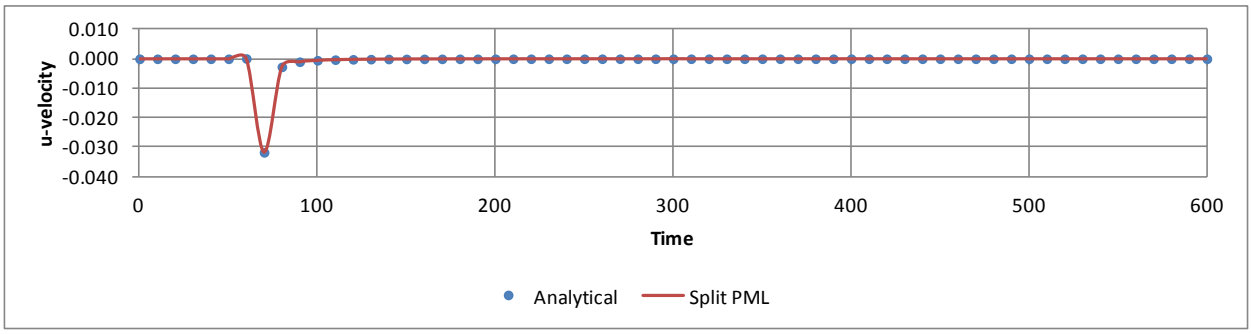

(a)

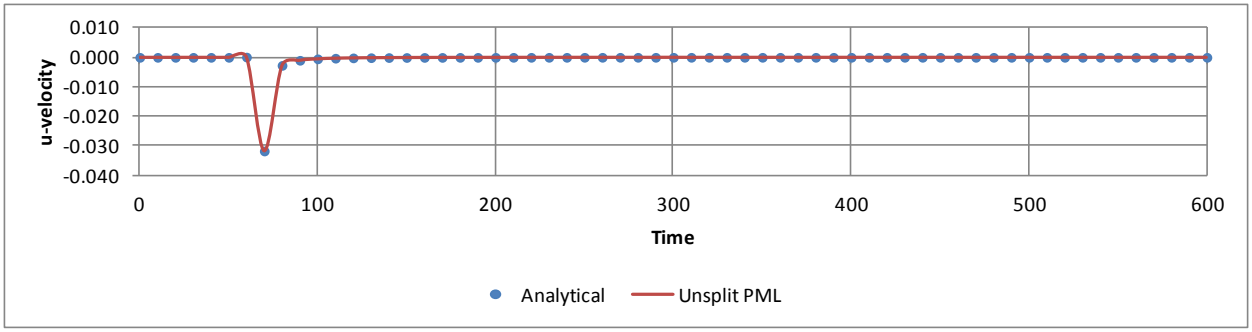

(b)

Figure 4.7. u-velocity as a function of time at Euler and PML domain interface at selected point (100, 0) for M = 0.5: (a) analytical vs. split PML, (b) analytical vs. unsplit PML, with $\sigma_m = \alpha = 2$ and NPML = 10.

4.4.1 Effect of Space-Time Transformation for High Subsonic Flow and Long-Time Integration

Now, both split- and unsplit-PML formulations are simulated with the same initial conditions given by equations (4.25)–(4.28) for a mean flow along the x-axis with M = 0.8. The values of σ_m = 1.5 and $\alpha = 2$ are selected with a time-step size of 0.1. Figure 4.8 shows the u velocity contours obtained using the split-form PML.

Reflections that appear predominantly from the right side boundary are visible at a time level of around $t = 550$. These reflections result in a spurious solution and subsequently lead to divergence. On the other hand, it is observed from Figure 4.9 that the unsplit formulation, which involves a space-time transformation with complex change of variables, provides a stable reflection-free solution. The waves not only leave the Euler domain smoothly but also are effectively damped in the PML domain before hitting the outermost boundaries.

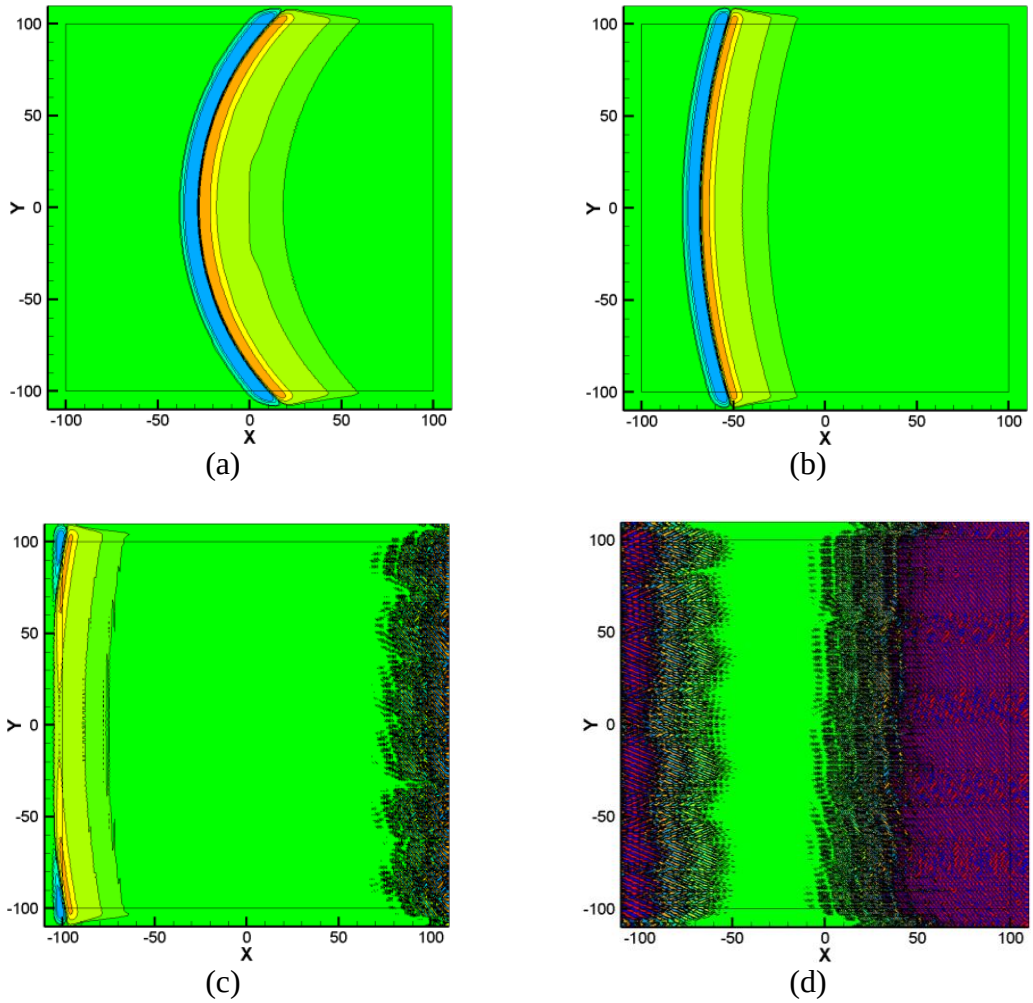

Figure 4.8. u-velocity contours obtained using split PML formulation at values of ±0.1, ±0.05, ±0.01, ±0.005, ±0.001, and ±0.0005 showing acoustic and vorticity pulses for M = 0.8: (a) t = 150, (b) t = 350, (c) t = 550, and (d) t = 700, with $\sigma_m = 1.5$, $\alpha = 2$, and NPML = 10.

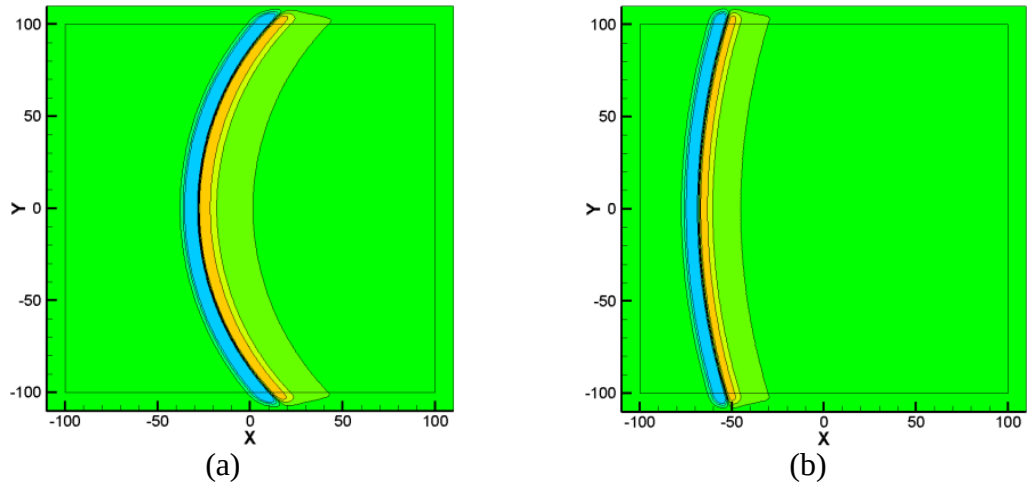

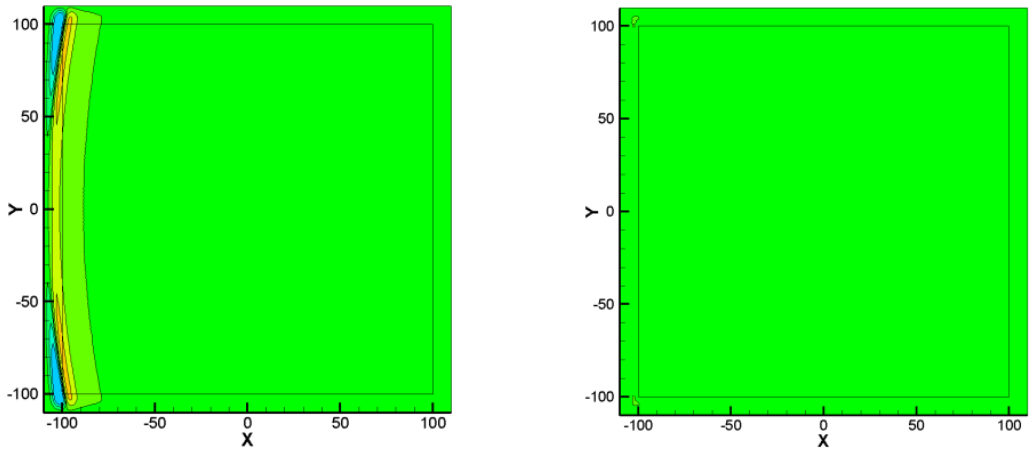

Figure 4.9. u-velocity contours obtained using unsplit PML formulation at values of ±0.1, ±0.05, ±0.01, ±0.005, ±0.001, and ±0.0005 showing acoustic and vorticity pulses for M= 0.8: (a) t = 150, (b) t = 350, (c) t = 550, and (d) t = 700, with $\sigma_m = 1.5$, $\alpha = 2$, and NPML = 10.

Figures 4.10(a) and (b) present a comparison of the split-form PML solution with the analytical solution along line $y = 0$ at $t = 700$ for u velocity and pressure, respectively. These plots clearly show the growing solution due to the reflections from the boundaries in the split formulation. Hu [16] attributes this instability of the split formulation to the amplification of the acoustic waves that have a positive group velocity but a negative phase velocity in the direction of the mean flow. It has been shown that this growth rate increases with M and σ_x for a uniform mean flow along the x-axis, and it would be difficult to suppress the instability occurring in flows with a high Mach number [16]. With the transformation, the convective acoustic waves are made nonconvective with the group velocities of all linear waves in the same direction as that of the phase velocities in order to obtain stable PML equations. A comparison of the unsplit-form PML solution with the analytical solution is presented in Figure 4.11. It is observed that the numerical solution matches well with the analytical solution, thus demonstrating the stability of the unsplit-PML formulation. The u velocity as a function of time

at a selected point (100, 0) on the Euler and PML domain interface is shown in Figure 4.12. The diverging solution from the split-form of the PML formulation is clearly seen in Figure 4.12(a). It is also observed in Figure 4.12(b) that the unsplit-PML formulation predicts a solution that compares very well with the analytical solution.

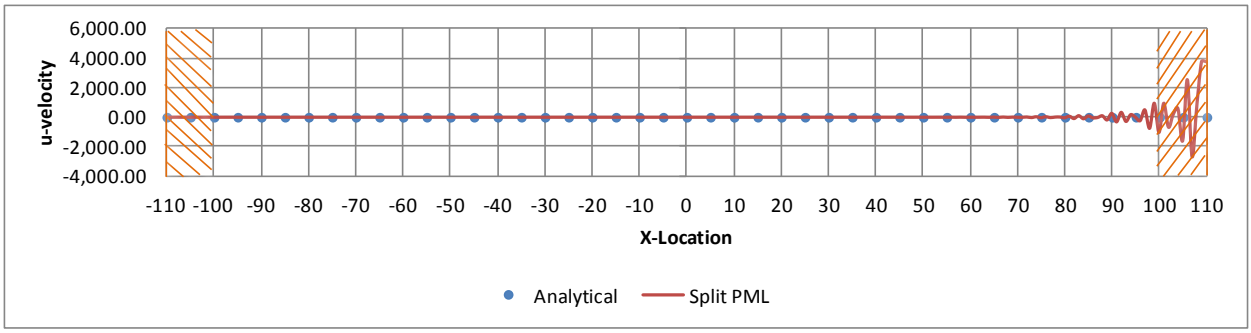

(a)

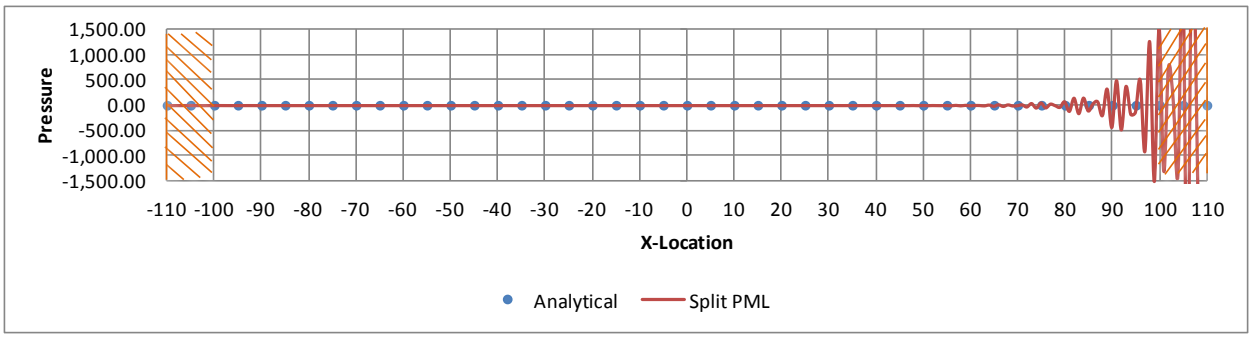

(b)

Figure 4.10. Comparison of split-form PML solution with analytical solution along line y = 0 for M = 0.8 at t = 700: (a) u-velocity and (b) pressure, with $\sigma_m = 1.5$, $\alpha = 2$, and NPML = 10.

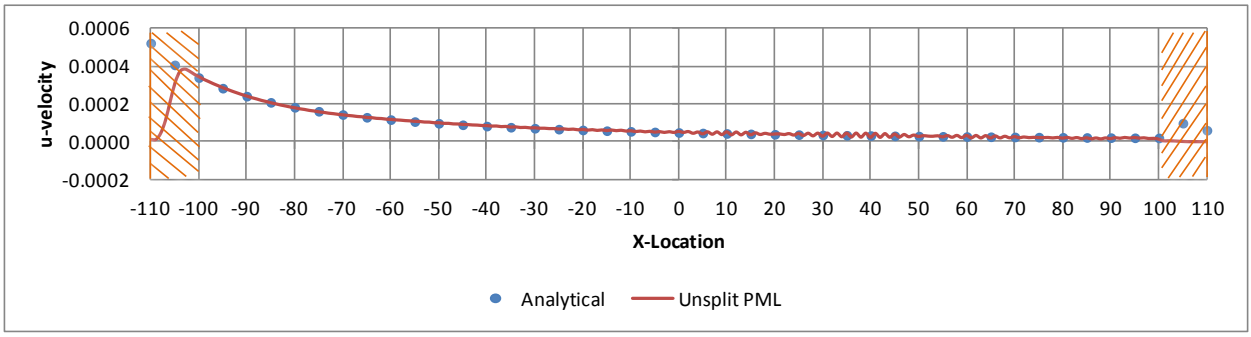

(a)

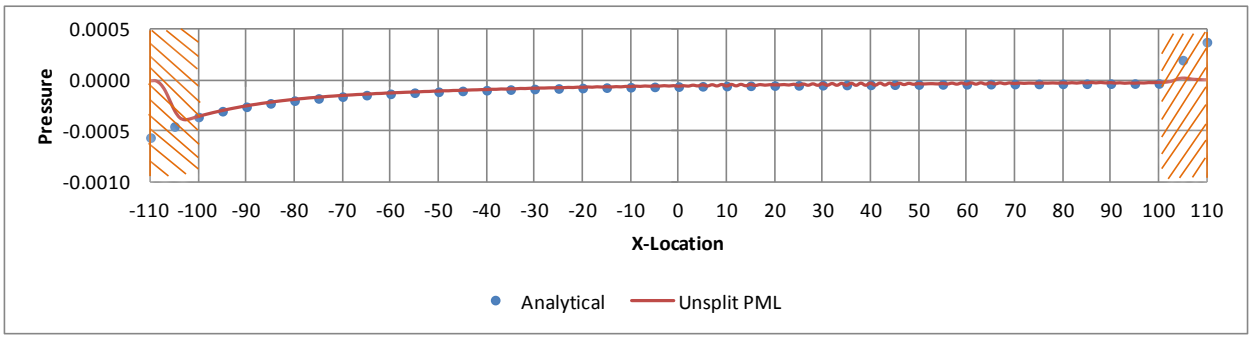

(b)

Figure 4.11. Comparison of unsplit-form PML solution with analytical solution along line y = 0 for M = 0.8 at t = 700: (a) u-velocity and (b) pressure, with $\sigma_m = 1.5$, $\alpha = 2$, and NPML = 10.

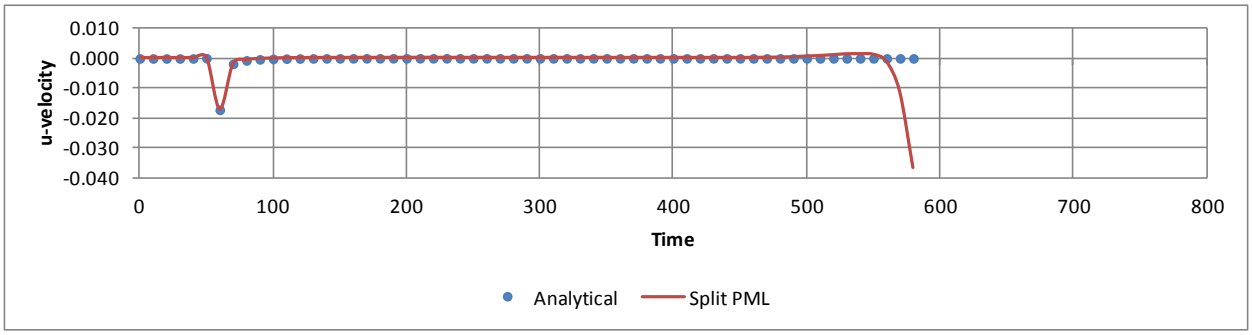

(a)

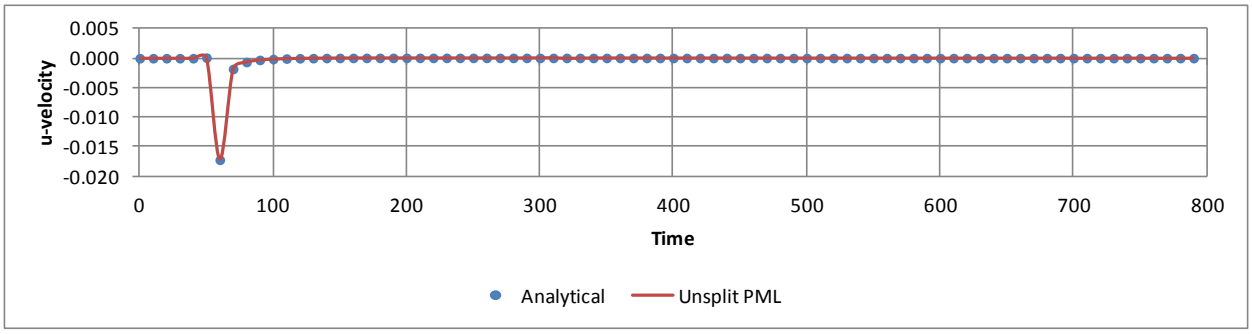

(b)

Figure 4.12 u-velocity as a function of time at Euler and PML domain interface at selected point (100, 0) for M = 0.8: (a) analytical vs. split PML, (b) analytical vs. unsplit PML, with $\sigma_m = 1.5$, $\alpha = 2$, and NPML = 10.

4.4.2 Stability Analysis Using Dispersion Relation

To investigate the instability issue, it is necessary to carry out a dispersion analysis according to Hu [16]. When a plane wave solution of the elementary form $\boldsymbol{Q}_0 e^{ik_x x + ik_y y - i\omega t}$ is assumed, the disturbance governed by the LEE can be considered a superposition of vorticity, entropy, and acoustic modal wave fields [11, 23, 24], where k_x and k_y are the wave numbers in the x- and y-directions, respectively; ω is the angular frequency; and $\boldsymbol{Q}_0$ is the amplitude of the wave. To satisfy the governing equations, k_x, k_y, and ω must be related by an equation called the dispersion relation. The dispersion relations for the LEE, equation (4.3), are

$$\left(\omega - Mk_x\right)^2 - k_x^2 - k_y^2 = 0 \tag{4.35}$$

for the acoustic waves and

$$\left(\omega - Mk_x\right) = 0 \tag{4.36}$$

for the vorticity and entropy waves [16, 25]. With the complex change of variables, equation (4.17), the dispersion relations for the split formulation and the unsplit formulation with a space-time transformation for the acoustic waves are given by equations (4.37) and (4.38) respectively, as

$$\left(\omega - M\frac{k_x}{1+\frac{i\sigma_x}{\omega}}\right)^2 - \left(\frac{k_x}{1+\frac{i\sigma_x}{\omega}}\right)^2 - \left(\frac{k_y}{1+\frac{i\sigma_y}{\omega}}\right)^2 = 0 \tag{4.37}$$

$$\frac{\left(\omega+i\sigma_x\right)^2\left(\omega+i\sigma_y\right)^2}{\left(1-M^2\right)^2} - \left(\omega+i\sigma_y\right)^2\left(k_x + \frac{M}{1-M^2}\omega\right)^2 - \frac{1}{1-M^2}\left(\omega+i\sigma_x\right)^2 k_y^2 = 0 \tag{4.38}$$

Equations (4.37) and (4.38) are solved numerically for the frequency for real values of the wavenumber. The exponential solutions will be stable provided the imaginary part ($\Im\omega$) of

the four roots of ω is negative. The angular frequencies are calculated for a chosen range of wavenumbers $|k_x| \leq 5$ and $|k_y| \leq 5$. Figures 4.13—4.16 show the maximum $\Im\omega$ obtained from the dispersion relations. Solid and dashed lines represent contours of positive and negative imaginary roots, respectively. Even though imaginary roots of lower values with a positive sign are shown in Figure 4.13(a), the dominant negative roots result in a stable accurate solution for the split formulation, as shown previously in Figures 4.2—4.7 for M = 0.5.

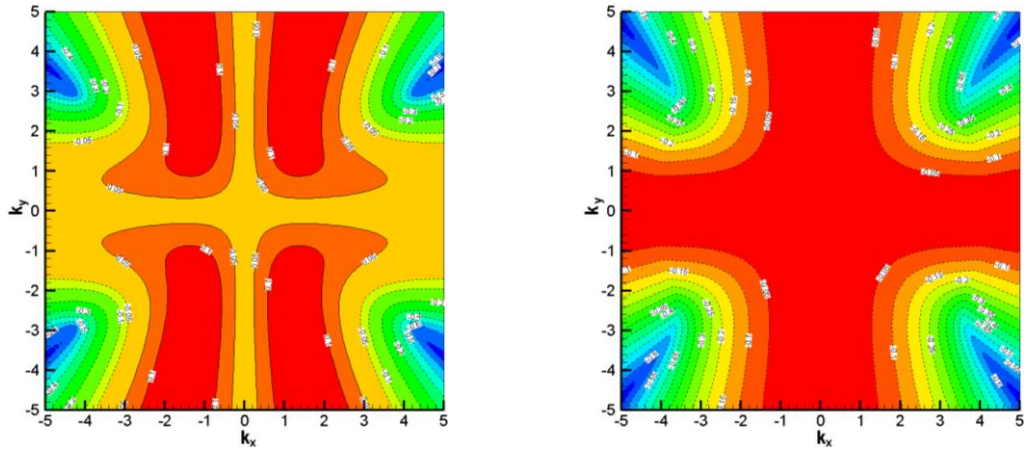

(a) (b)

Figure 4.13. Contours of maximum $\Im\omega$, imaginary part of ω, of four roots solved numerically from equation (4.37) with M = 0.5: (a) $\sigma_x = 2.0$ and $\sigma_y = 0$, (b) $\sigma_x = 0$ and $\sigma_y = 2.0$.

In Figure 4.14, negative imaginary roots are shown for equation (4.38) of the unsplit formulation, resulting in a stable solution. However, for a high subsonic number, M = 0.8, the split-form dispersion equation, equation (4.37), has a positive $\Im\omega$, as can be seen in Figure 4.15(a), thus leading to exponential growth of the solution in the PML domain. This follows the trend between the Mach number, M, and the damping parameter, σ_x, as discussed in section 4.4.1. On the other hand, the dispersion equation, equation (4.38), has all negative imaginary

roots, as shown in Figures 4.16(a) and (b), which eventually lead to a decaying solution in the PML domain.

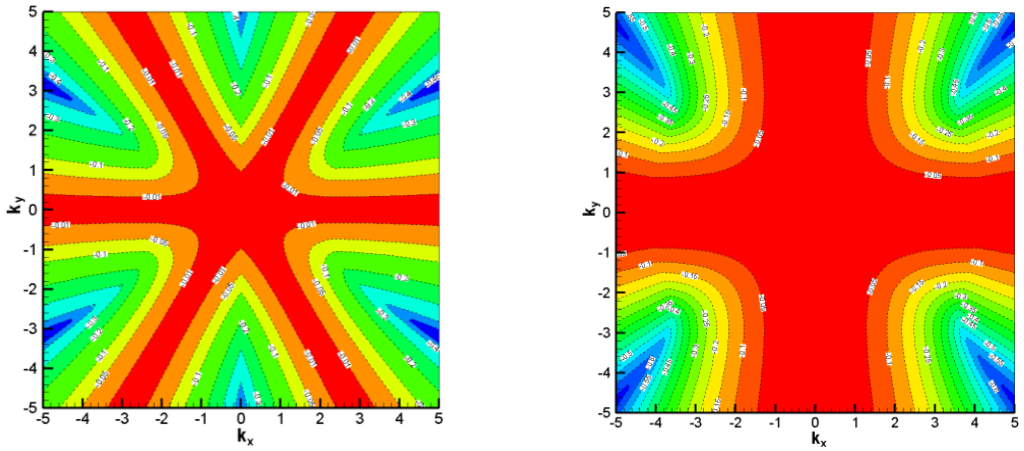

Figure 4.14. Contours of maximum $\Im\omega$, imaginary part of ω, of four roots solved numerically from equation (4.38) with M = 0.5: (a) $\sigma_x = 2.0$ and $\sigma_y = 0$, (b) $\sigma_x = 0$ and $\sigma_y = 2.0$.

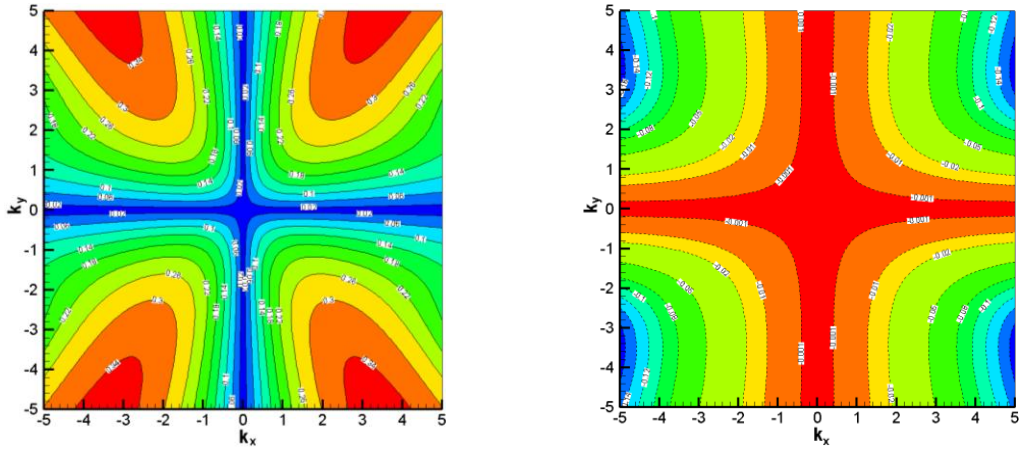

Figure 4.15. Contours of maximum $\Im\omega$, imaginary part of ω, of four roots solved numerically from equation (4.37) with M = 0.8: (a) $\sigma_x = 2.0$ and $\sigma_y = 0$, (b) $\sigma_x = 0$ and $\sigma_y = 2.0$.

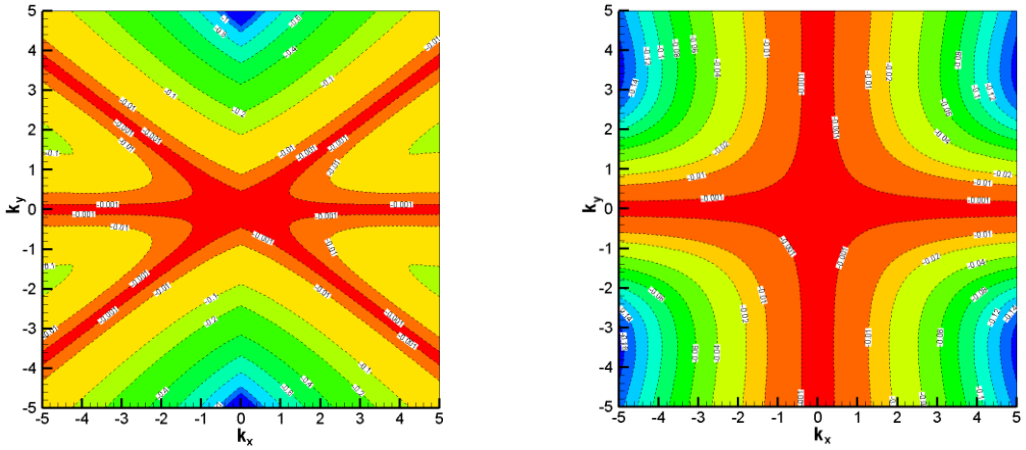

(a) (b)

Figure 4.16. Contours of maximum $\Im\omega$, imaginary part of ω, of four roots solved numerically from equation (4.38) with M = 0.8: (a) $\sigma_x = 2.0$ and $\sigma_y = 0$, (b) $\sigma_x = 0$ and $\sigma_y = 2.0$.

4.4.3 Effect of Time-Step Size on Stability of PML Formulations

Most unsteady fluid-flow analyses are carried out with a smaller time-step size in order to provide a stable accurate solution. Since PML formulations are a function of multiple variables, viz., the number of layers used in the PML domain, the maximum value of damping and its distribution rate in the PML domain, and the error associated with the numerical approximations of the schemes used in the computations, it is a challenging task to identify an appropriate combination of the PML parameters for a given flow problem. Moreover, with regard to stability, the time-step size plays a key role in the long-time behavior of the computational scheme. Simulations with a large time-step size resulted in a diverging solution for both split and unsplit formulations for the initial value problem considered in section 4.4. Thus, it was necessary to investigate and verify if the time-step size used in the simulations could be a possible cause of the instability associated with the PML equations. Furthermore, this investigation provides the range of time-step size and PML parameters for which numerical schemes produce accurate results with an effective PML.

An unsteady acoustic source case is found to be a well-suited candidate for this investigation. The LEE, equation (4.3), is solved with the source term, equation (4.39), added to the energy equation [26]:

$$p(x,y,t)=\frac{1}{2}\exp\left[-(\ln 2)\frac{x^2+y^2}{2}\right]\sin(\omega t) \tag{4.39}$$

where the frequency of the source is $\omega = 2\pi/30$, and the mean-flow Mach number is $M = 0.8$. Due to the presence of mean flow, acoustic waves have a larger wavelength at the downstream boundary than at the upstream boundary. The following example is used to illustrate the effectiveness of PML equations for both long and short waves: The Euler domain is [-100, 100] x [-100, 100]. A PML domain with ten layers on all four sides of the interior domain is used. The source is located at the origin. Several numerical simulations are carried out using the unsplit formulation for a wide range of PML parameters with various time-step sizes. Time-step sizes of 0.5, 0.2, 0.1, 0.05, 0.01, and 0.001 are used. The PML parameters, σ and α, are varied from 0.5 to 4.0 in steps of 0.5, thus providing various combinations of time-step size and PML parameters.

Figure 4.17(a) shows the pressure along line $y = 0$ at $t = 600$. The PML region is shown by the hatched section. The damping of the solution from the Euler-PML interface to the outermost boundary of the PML domain is clearly observed on both sides of the physical space i.e., the solution is reduced to nearly zero as it approaches the outermost boundary of the PML. It is also observed that the solution obtained from the unsplit-PML formulation compares very well with the reference solution obtained from a large computational domain. The pressure as a function of time at a selected point on the Euler and PML domain interface shows a clear sinusoidal wave in Figure 4.17(b).

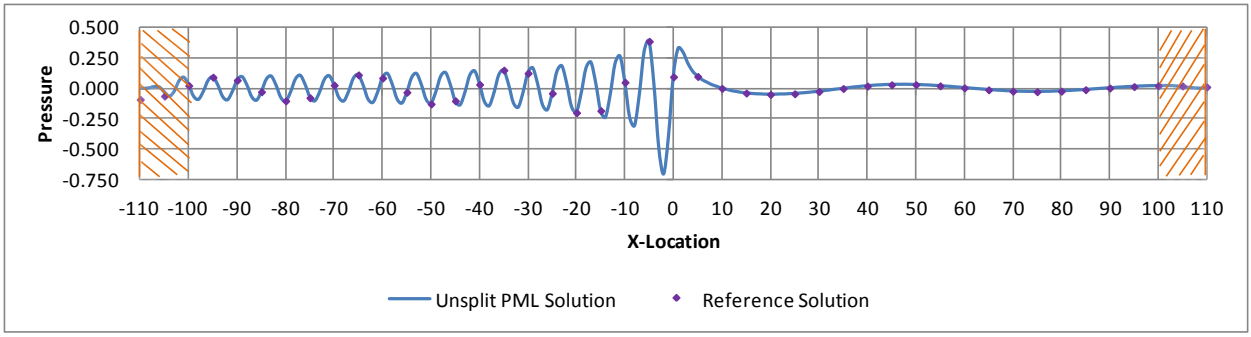

(a)

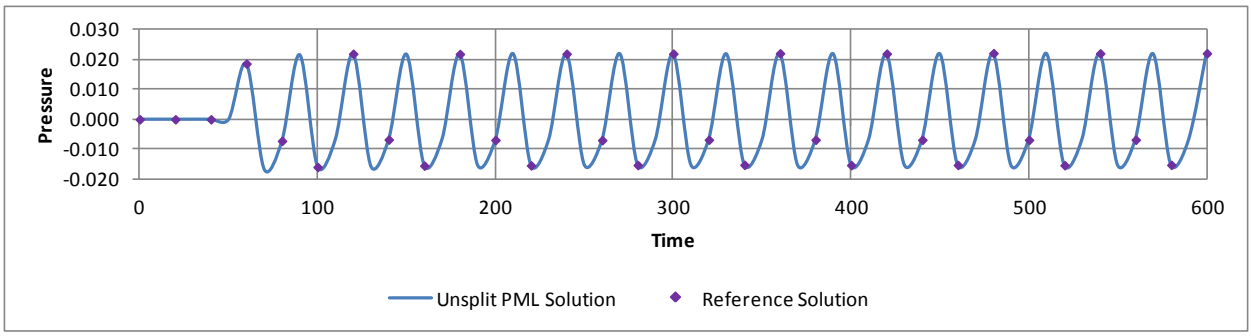

(b)

Figure 4.17. Pressure obtained with unsplit PML: (a) along line y = 0 at t = 600 and (b) at a selected point (100, 0) as a function of time, for M = 0.8, with $\Delta t = 0.05$, $\sigma_m = 1.5$, $\alpha = 2$, and NPML = 10.

Figure 4.18(a) shows the pressure contours at t = 600, along with reflections, obtained with the split formulation. From various numerical simulations, it was found that reflections arise around the time level of t = 450 in the split-formulation solution, and the scheme fails even for a very small time-step size. These reflections grow with time and eventually spoil the entire solution. On the other hand, a clean solution is seen in Figure 4.18(b), an unsplit formulation with a proper space-time transformation. It is further found that the unsplit PML formulation produces excellent results for small time-step sizes. However, in order to perform effectively, it must be ensured that the PML domain is provided with sufficient damping, which is a necessary condition for any PML formulation. From the investigations, it was found that the unsplit PML formulation performs well for PML parameters of σ and α ranging between 1.5 and 4.0, with a

time-step size ranging between 0.001 and 0.1. Although the unsplit-PML formulation converges for a solution for PML parameters of values lower than 1.5, results indicate inaccuracies in the solution.

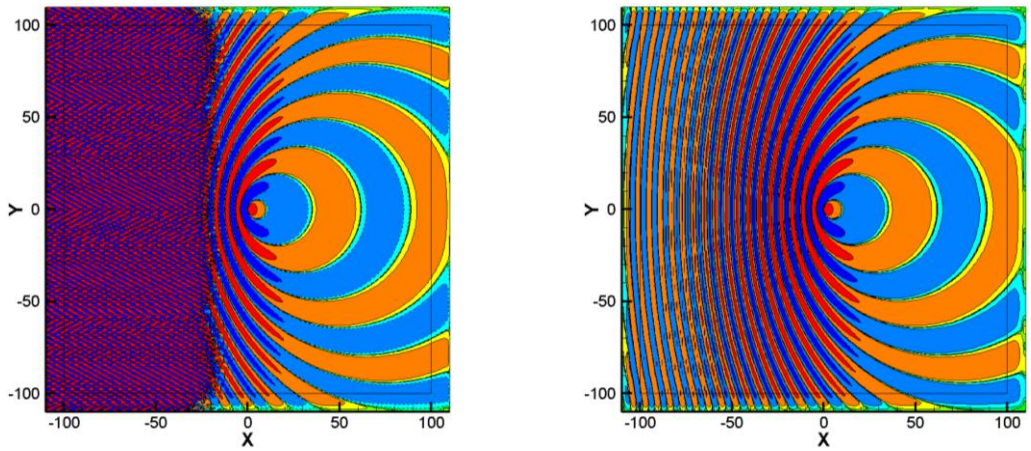

Figure 4.18. Pressure contours at values of ±0.1, ±0.01, and ±0.001, for M = 0.8 at t = 600: (a) split-form PML solution and (b) unsplit-PML solution, with $\Delta t = 0.05$, $\sigma_m = 1.5$, $\alpha = 2$, and NPML = 10.

CHAPTER 5

PML FOR NONLINEAR EULER EQUATIONS

5.1 2-D Nonlinear Euler Equations

Recalling the two-dimensional Euler equations discussed in section 2.3, in a conservative form, the two-dimensional Euler equations are written in Cartesian coordinates as

$$\frac{\partial Q}{\partial t}+\frac{\partial E}{\partial x}+\frac{\partial F}{\partial y}=0 \tag{5.1}$$

where

$$Q=\begin{bmatrix}\rho\\ \rho u\\ \rho v\\ \rho e_t\end{bmatrix};\quad E=\begin{bmatrix}\rho u\\ \rho u^2+p\\ \rho uv\\ \rho hu\end{bmatrix};\quad F=\begin{bmatrix}\rho v\\ \rho vu\\ \rho v^2+p\\ \rho hv\end{bmatrix} \tag{5.2}$$

and

$$h=e_t+\frac{p}{\rho};\quad e_t=e_i+\frac{u^2+v^2}{2};\quad p=\rho e_i(\gamma-1);\quad p=(\gamma-1)\rho\left(e_t-\frac{u^2+v^2}{2}\right) \tag{5.3}$$

in which u and v are the velocity components in the x- and y-directions, respectively; p is the pressure; ρ is the density; h is the enthalpy; e_t is the total energy per unit mass; e_i is the internal energy per unit mass; and γ is the ratio of specific heats and equals 1.4.

The two-dimensional Euler equations, equation (5.1), in generalized coordinates are given by

$$\frac{\partial \bar{Q}}{\partial \tau}+\frac{\partial \bar{E}}{\partial \xi}+\frac{\partial \bar{F}}{\partial \eta}=0 \tag{5.4}$$

where

$$\bar{Q} = \frac{Q}{J}\ ;\ \bar{E} = \frac{1}{J}\left[\xi_t Q + \xi_x E + \xi_y F\right]; \bar{F} = \frac{1}{J}\left[\eta_t Q + \eta_x E + \eta_y F\right] \tag{5.5}$$

and J is the Jacobian of transformation.

5.2 Pseudo Mean-flow

In a nonlinear simulation, the total variable Q could be quite large and may not be most efficient absorbing it completely in the PML domain. Therefore, a pseudo mean-flow, as shown in Figure 5.1, is introduced in the PML domain as equation (5.6), and only the fluctuation needs to be absorbed in the PML domain [17].

$$Q = \bar{Q}_p + Q' \tag{5.6}$$

where $\bar{Q}_p$ is the time-independent pseudo mean-flow, and Q' is the time-dependent fluctuation.

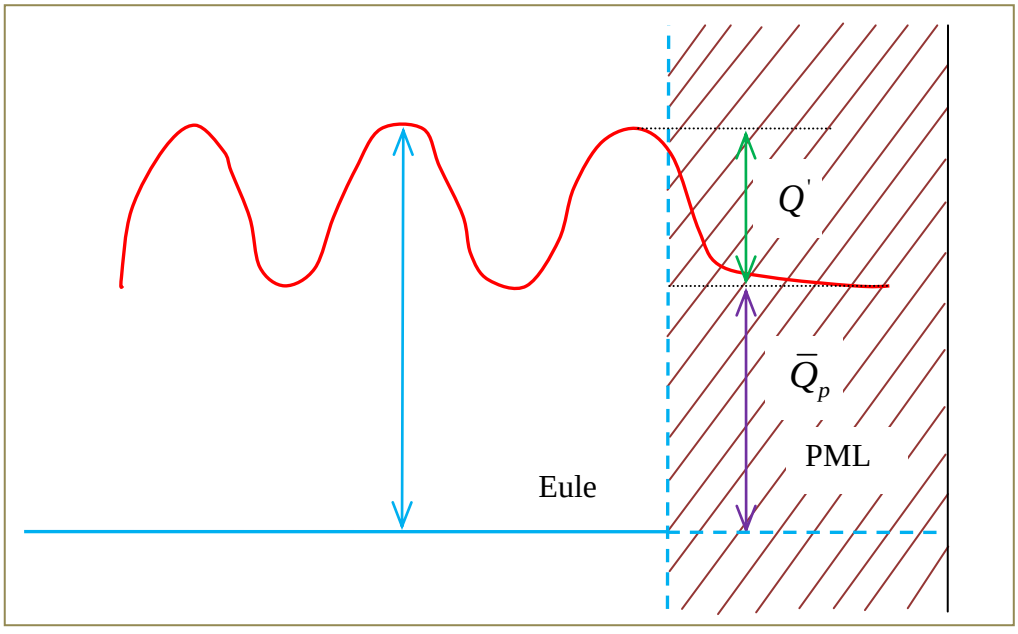

Figure 5.1. Schematic showing total pseudo mean-flow variables and absorption of fluctuations in PML domain.

The only requirement of this pseudo mean-flow is that it satisfies steady-state Euler equations, as given by equation (5.7), in order to carry out the linearization of the nonlinear Euler equations inside the PML domain and construct the PML formulation in such a way that only the time-dependent fluctuations need to be reduced to nearly zero inside the PML domain.

$$\frac{\partial \bar{E}_p}{\partial x} + \frac{\partial \bar{F}_p}{\partial y} = 0 \tag{5.7}$$

It may not be possible to find an exact pseudo mean-flow for a given flow problem. For example, in the case of a wall-bounded compressible flow governed by Navier-Stokes equations, the solution near the boundaries may not be known at the beginning of the numerical simulation, in which case, a similarity solution can be used as the pseudo mean-flow [27]. But, these approximate solutions may not define an accurate pseudo mean-flow. Therefore, the pseudo mean-flow should be judiciously chosen according to the problem at hand. Hence, the choice of $\bar{Q}_p$ is not unique. But any known solution or a parallel flow that satisfies the steady Euler equation, equation (5.7), appropriate to the actual flow problem can be used as a pseudo mean-flow in the construction of PML equation. Once a suitable pseudo mean-flow is identified, PML equations are constructed in such a way that the nonlinear fluctuations, Q', are absorbed in the PML domain. These fluctuations inside the PML domain depend on the choice of the most appropriately selected pseudo mean-flow, $\bar{Q}_p$. It must be reemphasized here that the solution inside the PML domain has no physical significance, and the foremost objective is that the fluctuations are reduced to nearly zero inside the PML domain, thus guaranteeing a nonreflecting outer boundary.

The Euler equations in terms of fluctuations can be written using equations (5.1) and (5.7) as

$$\frac{\partial Q'}{\partial t}+\frac{\partial\left(E-\bar{E}_p\right)}{\partial x}+\frac{\partial\left(F-\bar{F}_p\right)}{\partial y}=0 \tag{5.8}$$

5.3 PML for Nonlinear Euler Equations in Split Form

A three-step PML procedure, as presented in Chapter 4.3, is used for the construction of the PML equation for nonlinear Euler equations as well, in terms of fluctuating terms as given by equation (5.8). In order to preserve the dispersion relation of the waves supported by equation (5.8), a proper space-time transformation needs to be identified before applying the complex change of variables [17, 21]. Therefore, a dispersion analysis needs to be performed to identify the proper space-time transformation. In other words, the proper space-time transformation is identified in order to correct the dispersion relation with consistent phase and group velocities in the transformed coordinates. But the analysis is more challenging than the procedure involved in the dispersion analysis of the LEE. The PML equations in unsplit form for Navier-Stokes equations obtained using the space-time transformation, equation (4.15), required the introduction of an advection term to improve the stability of the PML formulation [27]. In this research effort, a proper space-time transformation of the form

$$\bar{t}=t+\beta x \tag{5.9}$$

is used [17, 21]. Here, β is a function of phase speed. For uniform mean flows, there exists an exact dispersion relation for the acoustic wave, and the value of β can be evaluated. The phase speed is obtained from the dispersion diagram by identifying the zero group velocity points for the chosen number of acoustic modes. The slope of the line formed by these zero group velocity points is the phase speed and β is the negative inverse of this phase speed. But for nonuniform shear flows (for jets, shear layers, wakes, and boundary layers, for example) in the absence of an explicit and direct relationship between the phase speed and the arbitrary mean flow profile, the

spectral collocation method provides a general way of determining the dispersion relations for an arbitrary mean flow [21], and the values of the phase speed and β are extracted from the spectral collocation method for flows with nonuniform arbitrary mean flow. The idea here is to find an appropriate value of β in such a way that the phase and group velocities of the waves supported by non-linear Euler equations are consistent [21] for the problem at hand. Thus, the value of β is very critical for the stability of the PML.

It has been shown that Euler equations support entropy, vorticity, and acoustic waves. The entropy wave consists of density fluctuations alone, whereas the vorticity wave consists of velocity fluctuations alone. Both entropy and vorticity waves are convected downstream by the uniform mean flow without distortion [28]. Acoustic waves involve fluctuations in all physical variables, and due to their dispersive nature, they are given major emphasis. For cases where a linearization is carried out over a uniform mean-flow, it has been shown [21] that for cases where the mean density is constant, i.e., the non-dimensionalized mean density $\overline{\rho}(y)=1$, the expression given by equation (5.10) can be used as an empirical formula to calculate the value of β.

$$\beta = \frac{\overline{U}_m}{1-\overline{U}_m^2} \quad \text{where} \quad \overline{U}_m = \frac{1}{b-1}\int_a^b \overline{U}(y)\,dy \quad , \quad y \in [a,b] \tag{5.10}$$

The transformation given by equation (5.9) changes the partial derivatives of equation (5.8) to

$$\frac{\partial}{\partial t} \to \frac{\partial}{\partial \overline{t}}; \quad \frac{\partial}{\partial x} \to \frac{\partial}{\partial x} + \beta \frac{\partial}{\partial \overline{t}}; \text{ and } \quad \frac{\partial}{\partial y} \to \frac{\partial}{\partial y} \tag{5.11}$$

Thus, applying the transformation, equation (5.9), to equation (5.8) results in

$$\frac{\partial Q'}{\partial \overline{t}} + \beta \frac{\partial \left(E - \overline{E}_p\right)}{\partial \overline{t}} + \frac{\partial \left(E - \overline{E}_p\right)}{\partial x} + \frac{\partial \left(F - \overline{F}_p\right)}{\partial y} = 0 \tag{5.12}$$

Consider equation (5.12) in the frequency domain by replacing $\frac{\partial}{\partial \overline{t}}$ with $-i\omega$. Then equation (5.12) in the frequency domain can be written as

$$-i\omega\tilde{Q}' - i\omega\beta\left(\tilde{E} - \tilde{\bar{E}}_p\right) + \frac{\partial\left(\tilde{E} - \tilde{\bar{E}}_p\right)}{\partial x} + \frac{\partial\left(\tilde{F} - \tilde{\bar{F}}_p\right)}{\partial y} = 0 \tag{5.13}$$

where a tilde denotes the time Fourier-transformed quantity. Now, by applying the PML complex change of variables obtained as per equation (1.1)

$$x = \left(1 + \frac{i\sigma_x}{\omega}\right)x, \quad y = \left(1 + \frac{i\sigma_y}{\omega}\right)y \tag{5.14}$$

in the frequency domain, equation (5.13) takes the form

$$(-i\omega)\left(\tilde{Q}' + \beta\left(\tilde{E} - \tilde{\bar{E}}_p\right)\right) + \frac{1}{\left(1 + \frac{i\sigma_x}{\overline{\omega}}\right)}\frac{\partial\left(\tilde{E} - \tilde{\bar{E}}_p\right)}{\partial x} + \frac{1}{\left(1 + \frac{i\sigma_y}{\overline{\omega}}\right)}\frac{\partial\left(\tilde{F} - \tilde{\bar{F}}_p\right)}{\partial y} = 0 \tag{5.15}$$

where $\overline{\omega}$ is the frequency in the transformed equation, which is equal to ω. The $\tilde{Q}'$ can be split into sub-components $\tilde{Q}_1'$ and $\tilde{Q}_2'$, and equation (5.15) can be written in the frequency domain in split form as

$$(-i\omega)\left(\tilde{Q}_1' + \beta\left(\tilde{E} - \tilde{\bar{E}}_p\right)\right) + \frac{1}{\left(1 + \frac{i\sigma_x}{\overline{\omega}}\right)}\frac{\partial\left(\tilde{E} - \tilde{\bar{E}}_p\right)}{\partial x} = 0 \tag{5.16}$$

$$(-i\omega)\tilde{Q}_2' + \frac{1}{\left(1 + \frac{i\sigma_y}{\overline{\omega}}\right)}\frac{\partial\left(\tilde{F} - \tilde{\bar{F}}_p\right)}{\partial y} = 0 \tag{5.17}$$

Now, multiplying equation (5.16) by $\left(1 + \frac{i\sigma_x}{\overline{\omega}}\right)$ and equation (5.17) by $\left(1 + \frac{i\sigma_y}{\overline{\omega}}\right)$ yields

$$(-i\omega)\left(\tilde{Q}_1^{'}+\beta\left(\tilde{E}-\tilde{\bar{E}}_p\right)\right)+\sigma_x\left(\tilde{Q}_1^{'}+\beta\left(\tilde{E}-\tilde{\bar{E}}_p\right)\right)+\frac{\partial\left(\tilde{E}-\tilde{\bar{E}}_p\right)}{\partial x}=0 \tag{5.18}$$

$$-i\omega\tilde{Q}_2^{'}+\sigma_y\tilde{Q}_2^{'}+\frac{\partial\left(\tilde{F}-\tilde{\bar{F}}_p\right)}{\partial y}=0 \tag{5.19}$$

Equations (5.18) and (5.19) can be written in the time domain as

$$\frac{\partial Q_1^{'}}{\partial\bar{t}}+\beta\frac{\partial\left(E-\bar{E}_p\right)}{\partial\bar{t}}+\sigma_x\left(Q_1^{'}+\beta\left(E-\bar{E}_p\right)\right)+\frac{\partial\left(E-\bar{E}_p\right)}{\partial x}=0 \tag{5.20}$$

$$\frac{\partial Q_2^{'}}{\partial\bar{t}}+\sigma_y Q_2^{'}+\frac{\partial\left(F-\bar{F}_p\right)}{\partial y}=0 \tag{5.21}$$

Equations (5.20) and (5.21) form the PML equations for absorbing $Q^{'}$ in the PML domain. Adding equations (5.20) and (5.21) and replacing $Q_1^{'}$ with $Q^{'}-Q_2^{'}$ yields

$$\begin{aligned}\frac{\partial\left(Q^{'}-Q_2^{'}\right)}{\partial\bar{t}}+\beta\frac{\partial\left(E-\bar{E}_p\right)}{\partial\bar{t}}+\sigma_x\left(Q^{'}-Q_2^{'}+\beta\left(E-\bar{E}_p\right)\right)+\frac{\partial\left(E-\bar{E}_p\right)}{\partial x}\\ +\frac{\partial Q_2^{'}}{\partial\bar{t}}+\sigma_y Q_2^{'}+\frac{\partial\left(F-\bar{F}_p\right)}{\partial y}=0\end{aligned} \tag{5.22}$$

Using the fact that $\bar{Q}_p$ satisfies the steady Euler equations as given by equation (5.7), equation (5.22) is rewritten in the original x and t variables as

$$\frac{\partial Q^{'}}{\partial t}+\sigma_x\left(Q^{'}-Q_2^{'}\right)+\sigma_y Q_2^{'}+\sigma_x\beta\left(E-\bar{E}_p\right)+\frac{\partial E}{\partial x}+\frac{\partial F}{\partial y}=0 \tag{5.23}$$

By introducing an auxiliary variable q in such a way that $q = Q_2^{'}$ and by equation (5.6), equation (5.23) can be written as

$$\frac{\partial Q}{\partial t}-\frac{\partial\bar{Q}_p}{\partial t}+\frac{\partial E}{\partial x}+\frac{\partial F}{\partial y}+\sigma_x\left(Q-\bar{Q}_p-q\right)+\sigma_y q+\sigma_x\beta\left(E-\bar{E}_p\right)=0 \tag{5.24}$$

Thus, the pseudo mean-flow is defined as time independent and satisfies the steady-state Euler equation as given by equation (5.7). Applying this fact, equation (5.24) is written as

$$\frac{\partial Q}{\partial t}+\frac{\partial E}{\partial x}+\frac{\partial F}{\partial y}+H=0 \tag{5.25}$$

where

$$H=\sigma_x\left(Q-\bar{Q}_p-q\right)+\sigma_y q+\sigma_x\beta\left(E-\bar{E}_p\right) \tag{5.26}$$

And from equation (5.21),

$$\frac{\partial q}{\partial t}+\sigma_y q+\frac{\partial\left(F-\bar{F}_p\right)}{\partial y}=0 \tag{5.27}$$

Equations (5.25) and (5.27) are the governing split-form PML equations of the nonlinear Euler equations in a Cartesian coordinate system. Based on equation (5.4), the PML formulation in the Cartesian coordinate system can be transformed into the generalized coordinate system as

$$\frac{\partial \bar{Q}}{\partial \tau}+\frac{\partial \bar{E}}{\partial \xi}+\frac{\partial \bar{F}}{\partial \eta}+\bar{H}=0 \tag{5.28}$$

where

$$\bar{H}=\sigma_\xi\left(\bar{Q}-\bar{\bar{Q}}_p-\bar{q}\right)+\sigma_\eta\bar{q}+\sigma_\xi\beta\left(\bar{E}-\bar{\bar{E}}_p\right) \tag{5.29}$$

and

$$\frac{\partial \bar{q}}{\partial \tau}+\sigma_\eta\bar{q}+\frac{\partial\left(\bar{F}-\bar{\bar{F}}_p\right)}{\partial \eta}=0 \tag{5.30}$$

Equations (5.28) and (5.30) are solved in the computational space. By a reverse-transformation, the physical variables are calculated in the Cartesian coordinates. In this split formulation, only one auxiliary variable needs to be calculated within the PML domain, where

σ_x or σ_y is a non-zero value. Thus, it is not necessary to calculate this auxiliary variable within the interior domain, where the absorption coefficients are zero.

5.4 Numerical Results

In order to demonstrate the effectiveness of PML in a generalized coordinate system, three physical domains of different shapes are considered: the physical domains, viz., square domain with uniform grid spacing, tapered domain, and arbitrary-shaped domain with nonuniform grid spacing in Cartesian coordinates, as shown in Figures 5.2, 5.3, and 5.4, respectively.

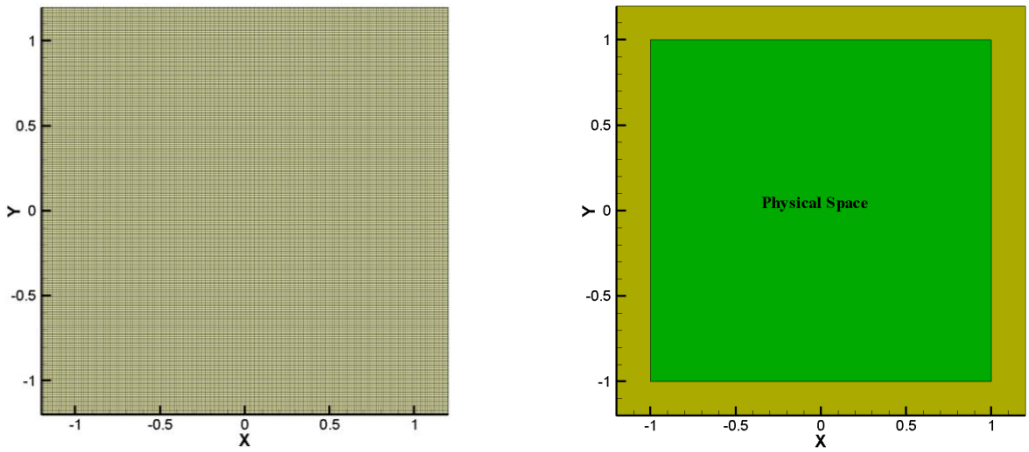

(a) (b)

Figure 5.2. Square physical domain with uniform grid: (a) grid structure, (b) PML domain (shaded region in olive green) and physical space. Number of layers in PML domain = 20.

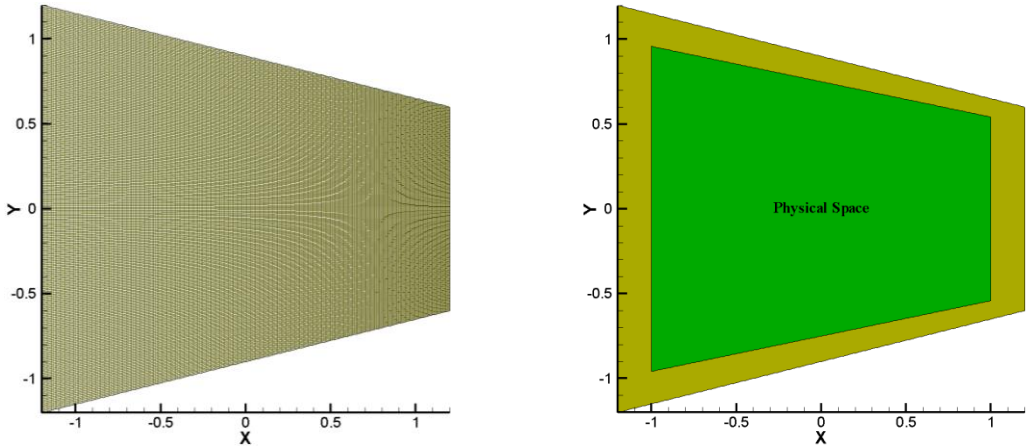

Figure 5.3. Tapered physical domain with nonuniform grid: (a) grid structure, (b) PML domain (shaded region in olive green) and physical space. Number of layers in PML domain = 20.

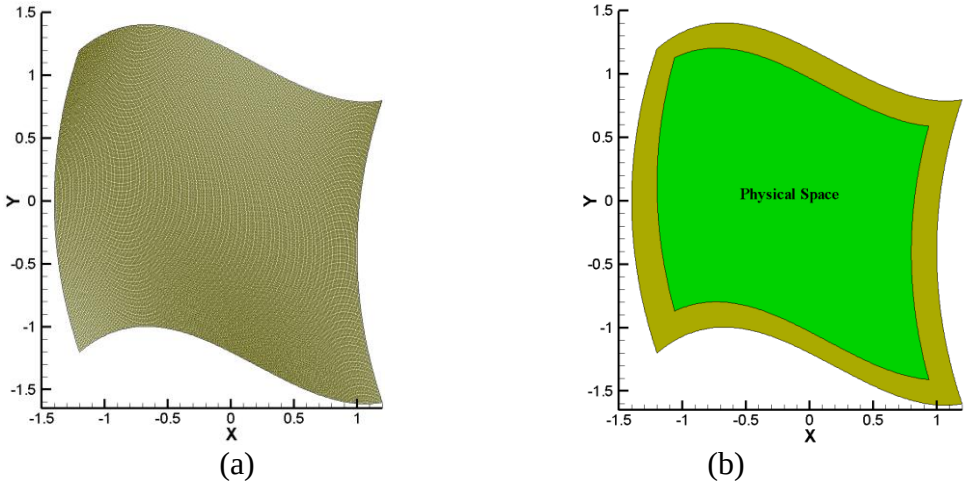

Figure 5.4. Arbitrary physical domain with nonuniform grid: (a) grid structure, (b) PML domain (shaded region in olive green) and physical space. Number of layers in PML domain = 20.

The square domain with a uniform grid is of the size [-1.2, 1.2] x [-1.2, 1.2]. The non-rectangular physical domain tapered on the top and bottom boundaries is obtained by changing the lower and upper-right vertices of the square domain as (-1.2, -0.6) and (1.2, 0.6). The physical domain of arbitrary shape is obtained by using a third-order polynomial for the top and bottom boundaries and a second-order polynomial for the left and right boundaries. The physical

domains include a PML domain, the region shaded in olive green in Figures 5.2(b), 5.3(b), and 5.4(b), with 20 grid points appended on the four sides. Thus, the square domain uses a uniform grid spacing of $\Delta x = \Delta y = 0.01$, the non-rectangular tapered domain uses a grid spacing of $\Delta x = 0.01$ and a varying grid spacing of Δy in the physical space, and the physical domain of arbitrary shape has a varying grid spacing of both Δx and Δy. For all three physical domains, the grid spacing is uniform in the computational space, i.e., generalized coordinates, and is $\Delta\xi = \Delta\eta = 1.0$.

A reference length of 0.01 m, speed of sound of 340.26855 m/s, and mean-flow density of 1.225813 kg/m^3 are used in arriving at the length, velocity, density, and pressure scales for nondimensionalization. Unless otherwise specified explicitly, a global nondimensional time-step size of 0.001 is used in the calculations. For a mean-flow velocity of $\bar{u}_p = 0.5$, using the empirical formula given by equation (5.10), the parameter β is calculated to be 0.66667.

5.4.1 Extrapolation Boundary Condition

Benefits of the PML formulation will not be realized until the solution is compared with that of other techniques. For this, a computational domain with four open boundaries is considered. An initial value problem with a two-dimensional strong acoustic pulse [17] analogous to category three of benchmark problems of computational aeroacoustics [22] is used, and the Euler domain is initialized with the initial conditions as given by equations (5.31)–(5.34). These equations include a strong acoustic pulse, initially located at the origin, $(x_a, y_a) = (0, 0)$. The values of σ_m = 500.0 and α = 2.5 are used in the computational domain.

$$\rho = 1.0 \tag{5.31}$$

$$p = \frac{1}{\gamma} + \exp\left[-(\ln 2)\left(\frac{(x - x_a)^2 + (y - y_a)^2}{0.2^2} \right) \right] \tag{5.32}$$

$$u = U_0 = 0.5 \tag{5.33}$$

$$v = V_0 = 0.0 \tag{5.34}$$

The pseudo mean-flow inside the PML domain is initialized by equations (5.35)–(5.38).

$$\bar{\rho}_p = 1.0 \tag{5.35}$$

$$\bar{p}_p = \frac{1}{\gamma} \tag{5.36}$$

$$\bar{u}_p = 0.5 \tag{5.37}$$

$$\bar{v}_p = 0.0 \tag{5.38}$$

Figure 5.5 shows the pressure contours obtained from a small computational domain without a PML layer, [-1.0, 1.0] x [-1.0, 1.0], with zero-order extrapolation on the outermost boundaries. It can be seen from Figure 5.5(b) that the outgoing waves are not smooth closer to the right boundary. At $t =$ 1.0, shown in Figure 5.5(c), these ripples have spread into the domain and have affected the solution almost everywhere, subsequently resulting in a contaminated solution at $t =$ 2.0, as can be seen in Figure 5.5(d).

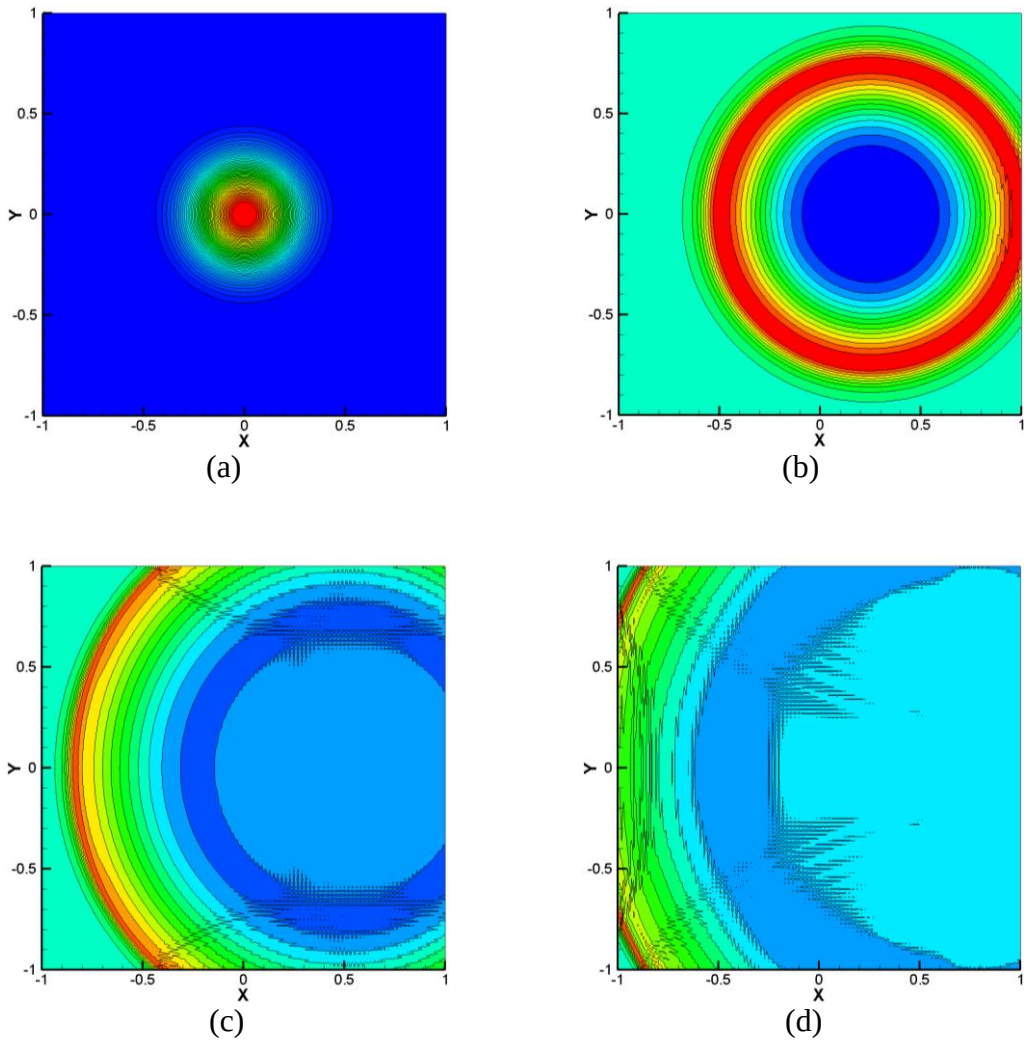

Figure 5.5. Pressure contours: (a) t = 0.0 with levels from 0.65 to 1.75 in steps of 0.02, (b) t = 0.5, (c) t = 1.0, and (d) t = 1.5 with levels from 0.65 to 0.9 and in steps of 0.02 obtained with zero-order extrapolation.

In order to reduce the dispersion, the same case was simulated again with a TVD scheme, and the solution is shown in Figure 5.6. Even though the solution appears to be oscillation-free, it is quite evident from Figures 5.6(c) and (d) that the waves are not smooth due to reflections from the outflow boundaries. In order to verify the effect of a simple extrapolation scheme on a small computational domain, a reference solution is obtained by computing the flow with the same spatial and temporal resolution but in a much larger domain in such a way that for the time levels

considered, the waves do not reach the boundaries so that the numerical solution is not affected by the boundary condition. The pressure contours obtained from the reference simulation is shown in Figure 5.7. For clarity, only the region of interest is shown in Figure 5.7. A clear solution is observed at all time levels.

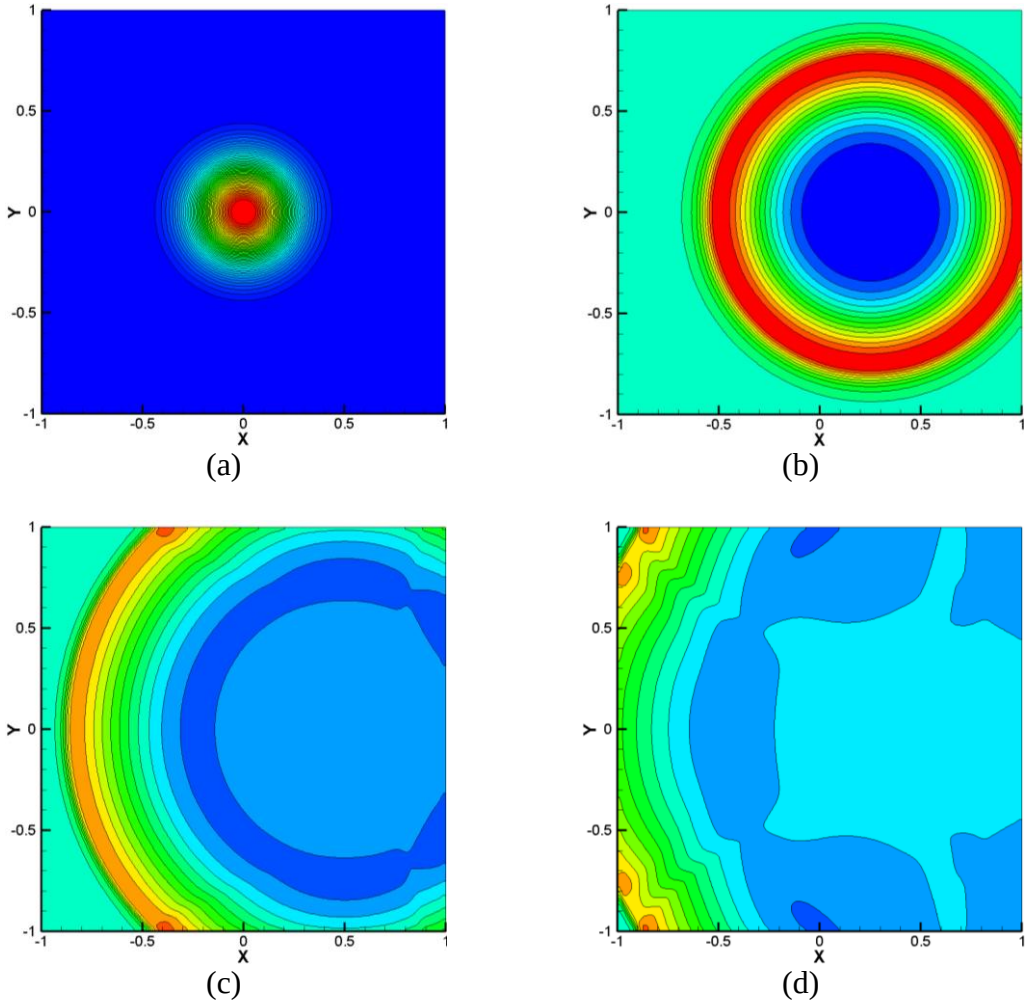

Figure 5.6. Pressure contours: (a) t = 0.0 with levels from 0.65 to 1.75 in steps of 0.02, (b) t = 0.5, (c) t = 1.0, and (d) t = 1.5 with levels from 0.65 to 0.9 and in steps of 0.02 obtained with TVD scheme and zero-order extrapolation.

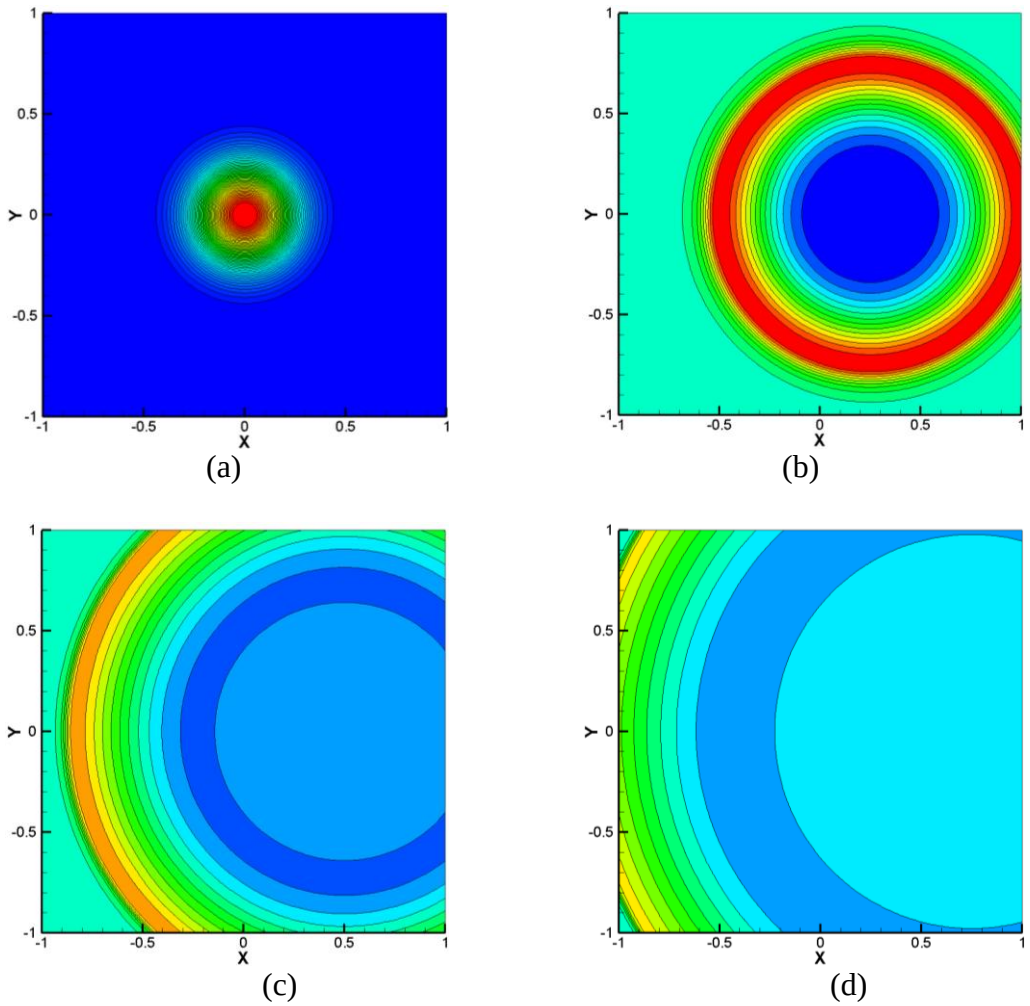

Figure 5.7. Pressure contours: (a) t = 0.0 with levels from 0.65 to 1.75 in steps of 0.02, (b) t = 0.5, (c) t = 1.0, and (d) t = 1.5 with levels from 0.65 to 0.9 and in steps of 0.02 obtained from large computational domain.

The comparison of pressure at $t =$ 1.5 and $t =$ 2.0 along line $y = 0$ obtained from both the small computational domain with the zero-order extrapolation scheme and the reference solution is shown in Figures 5.8 and 5.9, respectively. In Figure 5.8, although the solution appears to differ only by a small amount at $t =$ 1.5, it is clearly visible that the solution obtained from the small computational domain without TVD is oscillating due to reflections as well as dispersion.

The application of TVD has reduced the dispersion error and is observed in both Figures 5.8 and 5.9. Although the difference in the solution obtained with TVD and the reference solution appears to be small, it is inevitable that the error due to reflections from the boundaries will grow with time and eventually result in a spurious solution. This demonstrates that a simple extrapolation boundary treatment requires a large computational domain for accurate results, but at the cost of increased computational time and effort.

This can be avoided by appending a PML domain on the four sides of the smaller computational domain in such a way that the PML domain absorbs the incoming waves and thus prevents any reflection back into the domain from the boundaries.

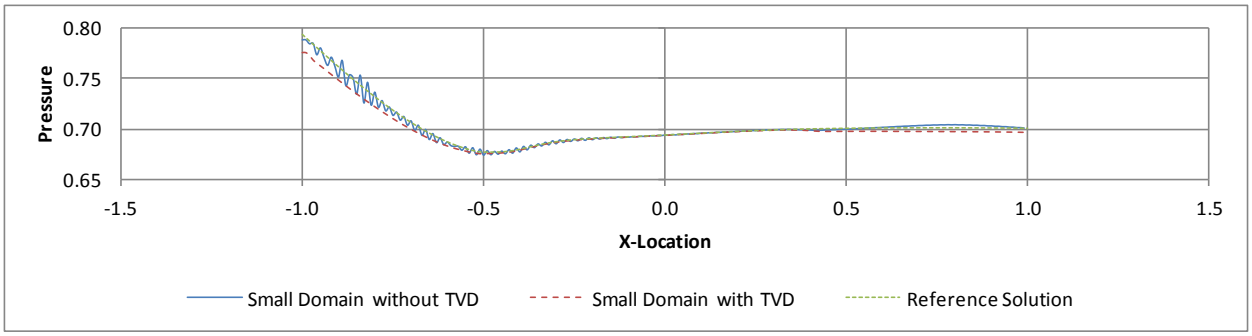

Figure 5.8. Comparison of pressure along line y = 0 at t = 1.5 obtained from reference case and small computational domain with simple extrapolation on boundaries.

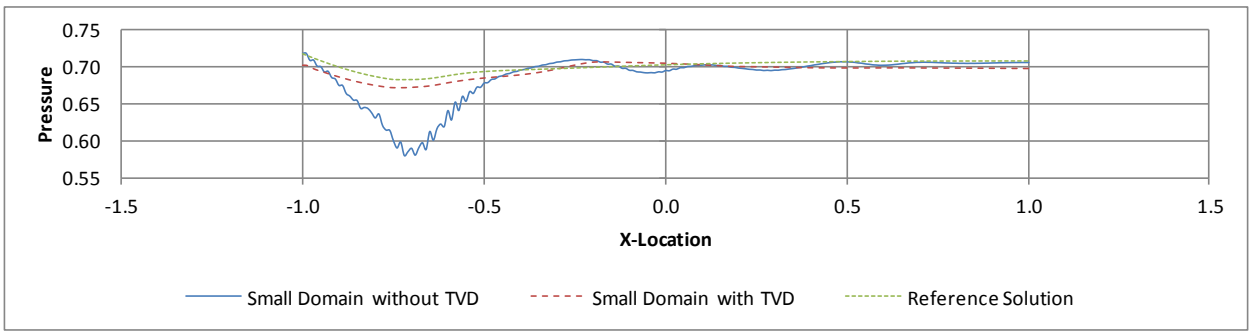

Figure 5.9. Comparison of pressure along line y = 0 at t = 2.0 obtained from reference case and small computational domain with simple extrapolation on boundaries.

5.4.2 Advection of Isentropic Vortex

Advection of the isentropic vortex is considered in this case, where the initial conditions, equations (5.39)–(5.42), are given by the work of Hu [17] as

$$\rho(x,t)=\left(1-\frac{1}{2}(\gamma-1)U_{\max}^{2}e^{1-\frac{r^2}{b^2}}\right)^{1/(\gamma-1)} \tag{5.39}$$

$$p(x,t)=\frac{1}{\gamma}\left(1-\frac{1}{2}(\gamma-1)U_{\max}^{2}e^{1-\frac{r^2}{b^2}}\right)^{\gamma/(\gamma-1)} \tag{5.40}$$

$$u(x,t)=U_0-\frac{U_{\max}^{'}}{b}re^{\frac{1}{2}\left(1-\frac{r^2}{b^2}\right)}\sin\theta \tag{5.41}$$

$$v(x,t)=V_0+\frac{U_{\max}^{'}}{b}re^{\frac{1}{2}\left(1-\frac{r^2}{b^2}\right)}\cos\theta \tag{5.42}$$

where

$$r=\sqrt{(x-U_0t)^2+(y-V_0t)^2},\ U_{\max}^{'}=0.25,\ b=0.2 \tag{5.43}$$

and

$$\left[U_{0,}V_0\right]=[0.5,0] \tag{5.44}$$

The values of σ_m = 50.0 and α = 2.0 are selected. The v-velocity contours at progressive time frames are shown in Figures 5.10, 5.11, and 5.12, obtained from domains with uniform and nonuniform grid structures. The contour plots clearly demonstrate that the PML formulation effectively dampens the waves entering the PML domain, with no reflections seen.

In order to validate the results obtained from the PML formulation, the numerical solutions are compared with that of the analytical solution, whereas the analytical solution is obtained in a straight forward manner for the advection of the given wave form as a function of time. The comparison of the v-velocity profile along line y = 0 plotted at various time levels is

shown in Figure 5.13. The solution obtained from both tapered and arbitrary-shaped domains with nonuniform grid spacing compared very well with the reference solution, and the solution from the tapered domain is used in the comparison. These plots clearly demonstrate how well the numerical solutions match the analytical solution in the Euler domain. The hatched regions shown in Figure 5.13 represent the PML domain. The damping of the wave entering the PML domain can be clearly seen in Figures 5.13(d)–(g). It is also observed that the numerical solution approaches the proposed $\bar{v}_p$ as the wave approaches the outermost boundary of the PML domain on the right. In this case, the entire v-velocity of the wave entering the PML domain is comprised of the time-independent fluctuation and is effectively absorbed by the PML domain. It must be noted that the solution inside the PML domain is non-physical and is of no significance as long as it is not reflected at the boundaries and does not contaminate the interior solution.

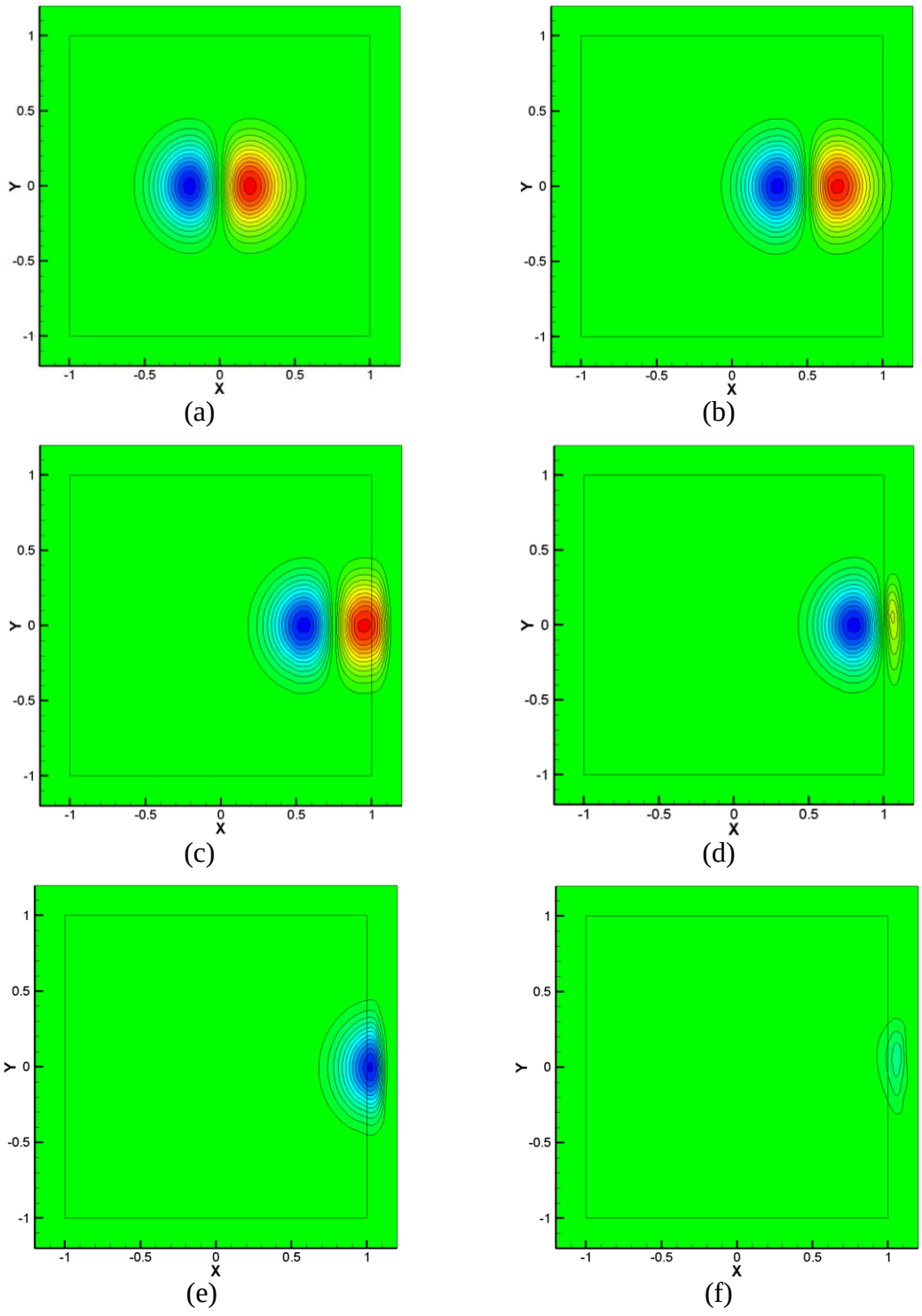

Figure 5.10. v-velocity contour levels from ± 0.02 to ± 0.24 with step of 0.02: (a) t = 0.0, (b) t = 1.0, (c) t = 1.5, (d) t = 2.0, (e) t = 2.5, and (f) t = 3.0.

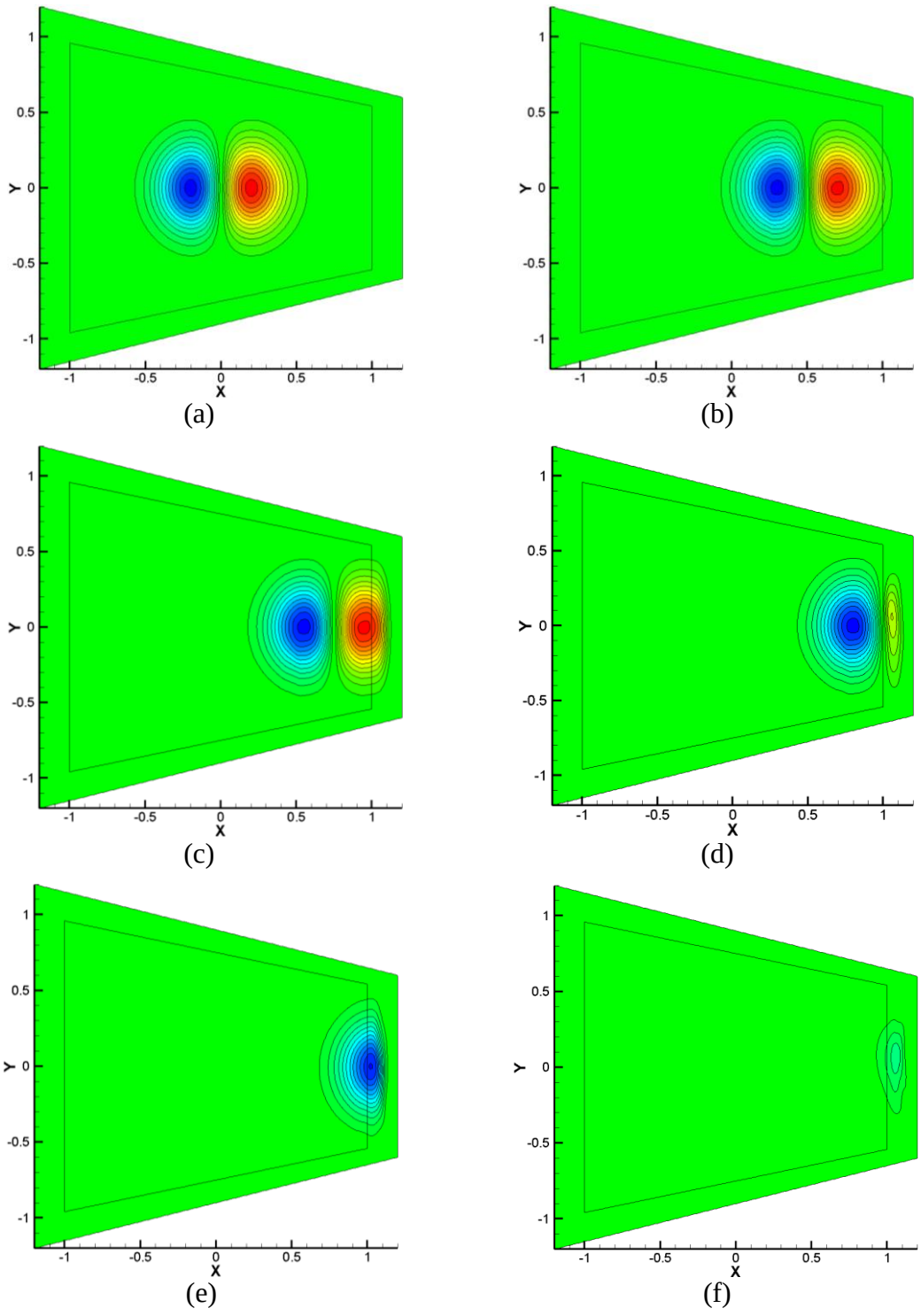

Figure 5.11 v-velocity contour levels from ± 0.02 to ± 0.24 with step of 0.02: (a) t = 0.0, (b) t = 1.0, (c) t = 1.5, (d) t = 2.0, (e) t = 2.5, and (f) t = 3.0.

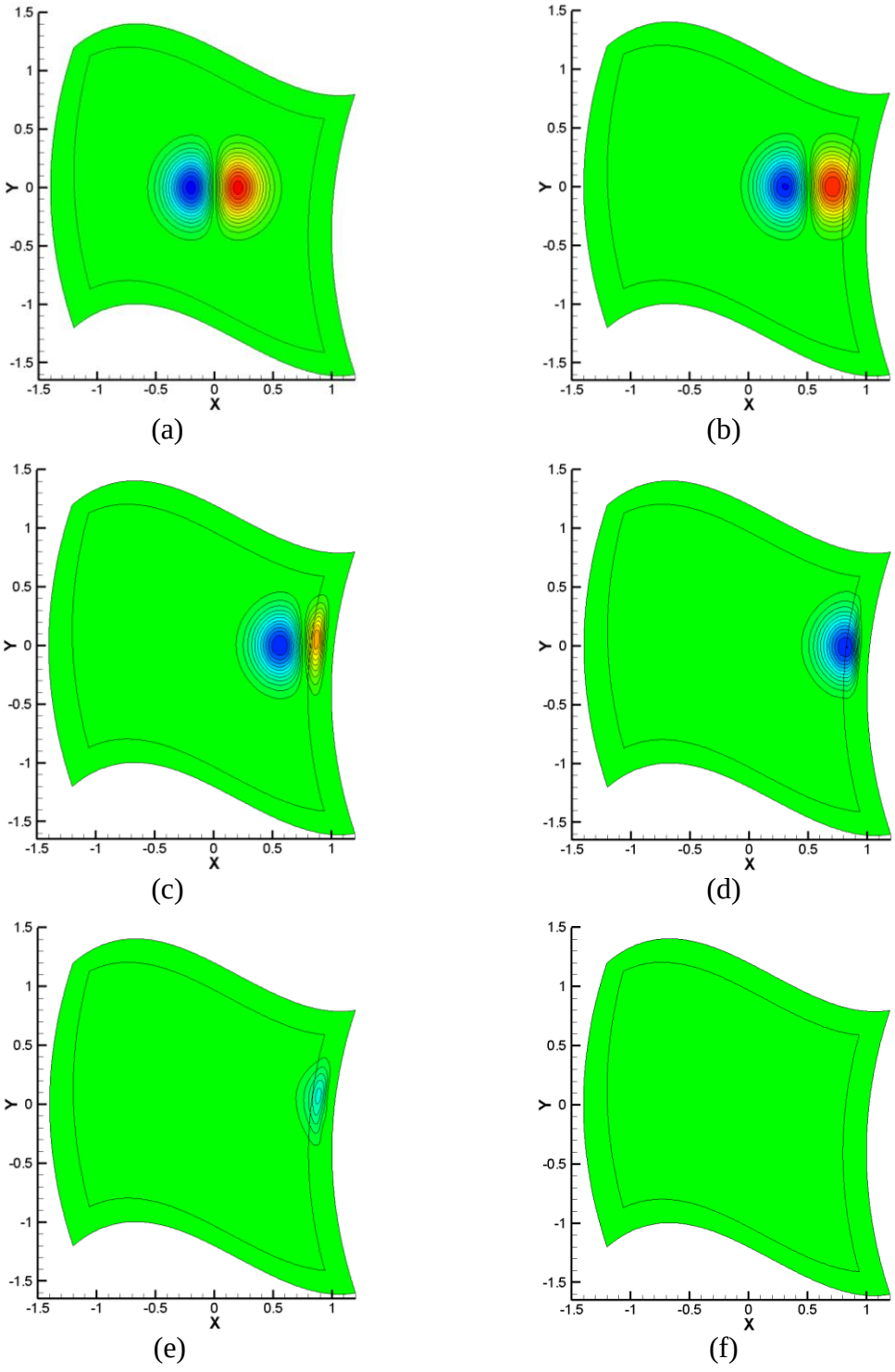

Figure 5.12 v-velocity contour levels from ± 0.02 to ± 0.24 with step of 0.02: (a) t = 0.0, (b) t = 1.0, (c) t = 1.5, (d) t = 2.0, (e) t = 2.5, and (f) t = 3.0.

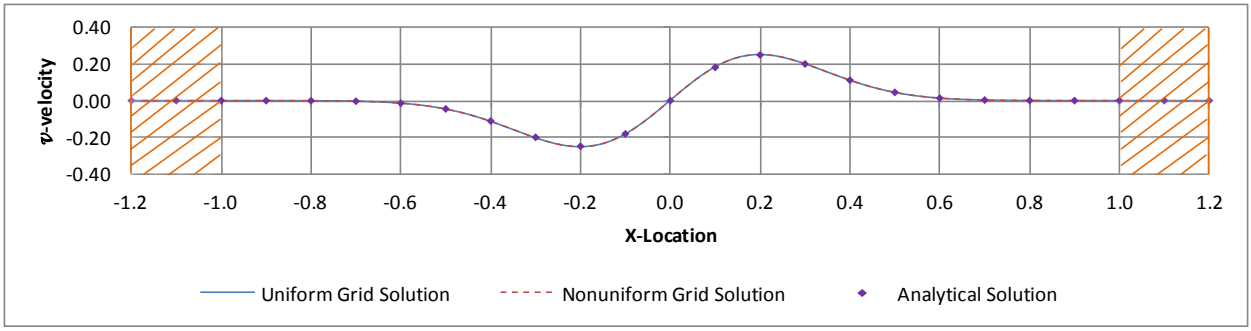
v-velocity
0.40
0.20
0.00
-0.20
-0.40
-1.2
-1.0
-0.8
-0.6
-0.4
-0.2
0.0
0.2
0.4
0.6
0.8
1.0
1.2
X-Location
Uniform Grid Solution
Nonuniform Grid Solution
Analytical Solution

(a)

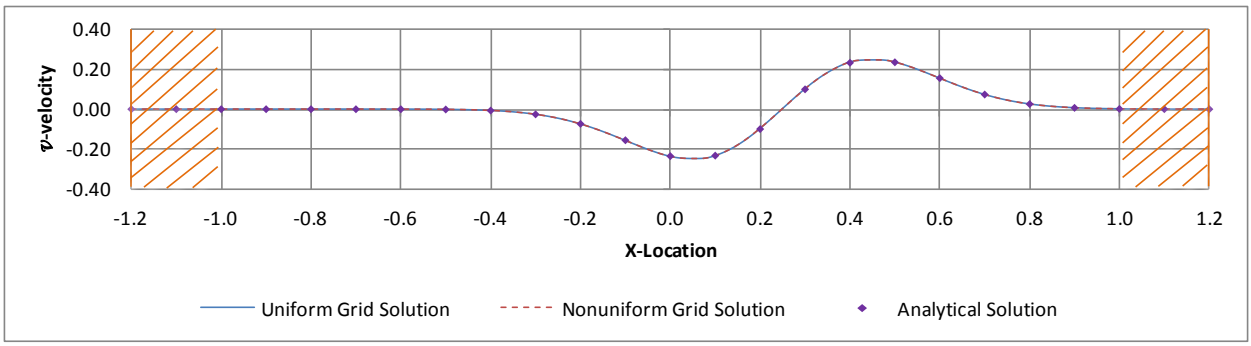
v-velocity
0.40
0.20
0.00
-0.20
-0.40
-1.2
-1.0
-0.8
-0.6
-0.4
-0.2
0.0
0.2
0.4
0.6
0.8
1.0
1.2
X-Location
Uniform Grid Solution
Nonuniform Grid Solution
Analytical Solution

(b)

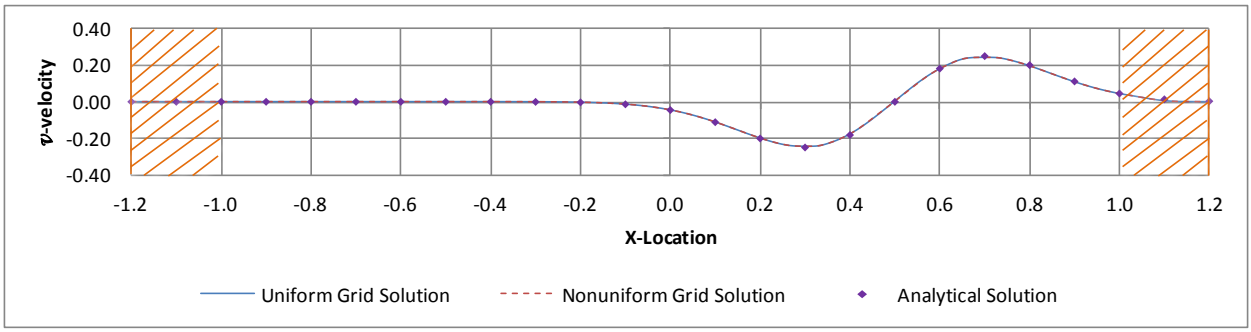
v-velocity
0.40
0.20
0.00
-0.20
-0.40
-1.2
-1.0
-0.8
-0.6
-0.4
-0.2
0.0
0.2
0.4
0.6
0.8
1.0
1.2
X-Location
Uniform Grid Solution
Nonuniform Grid Solution
Analytical Solution

(c)

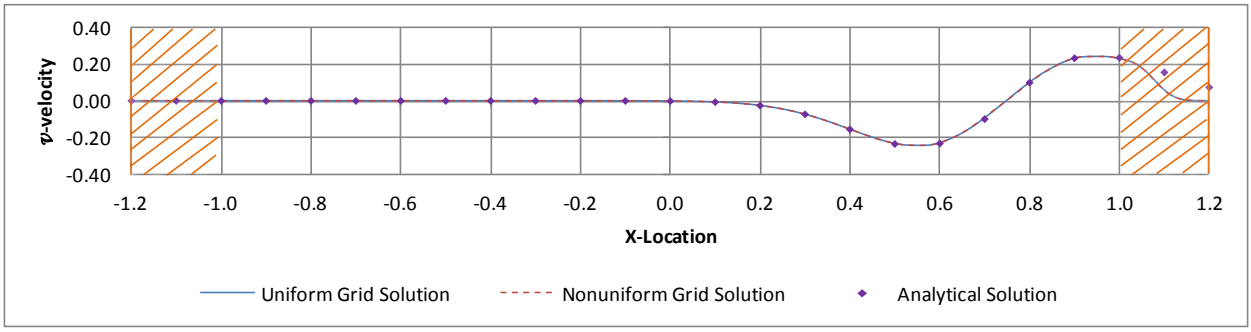
v-velocity
0.40
0.20
0.00
-0.20
-0.40
-1.2
-1.0
-0.8
-0.6
-0.4
-0.2
0.0
0.2
0.4
0.6
0.8
1.0
1.2
X-Location
Uniform Grid Solution
Nonuniform Grid Solution
Analytical Solution

(d)

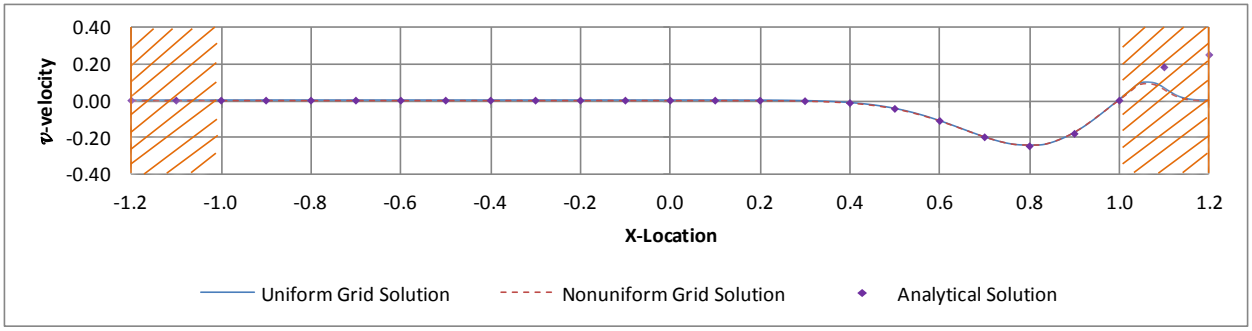

(e)

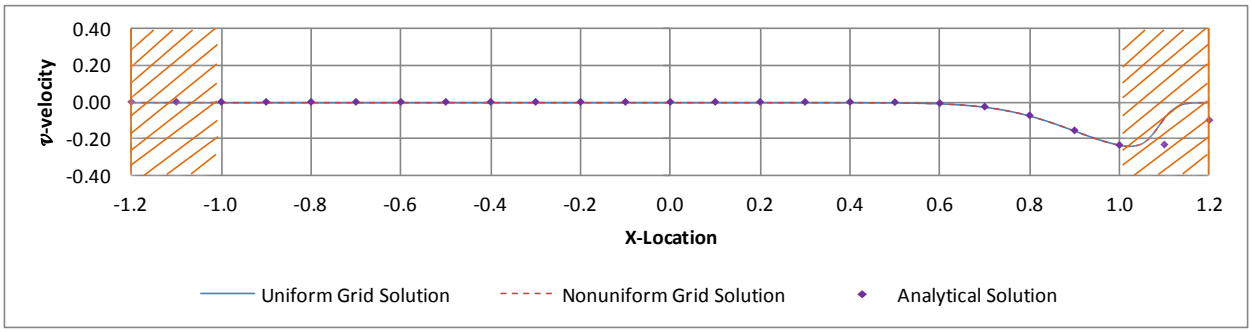

(f)

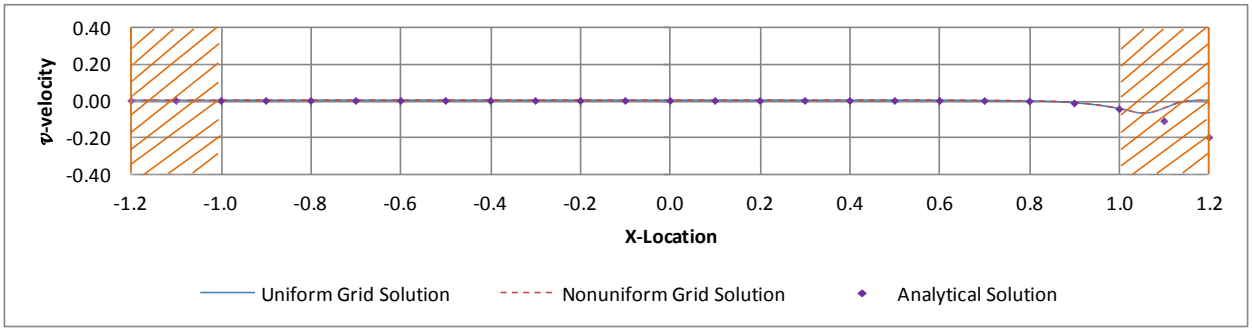

(g)

Figure 5.13 Comparison of analytical solution with PML solution for v-velocity along y = 0: (a) t = 0, (b) t = 0.5, (c) t = 1.0, (d) t = 1.5, (e) t = 2.0, (f) t = 2.5, and (g) t = 3.0.

Figure 5.14 shows a comparison of the PML solution with the reference solution for v-velocity at a point (1, 0) on the Euler-PML interface. It can be seen that the PML solution matches well with the reference solution, clearly demonstrating the PML as a nonreflecting boundary condition.

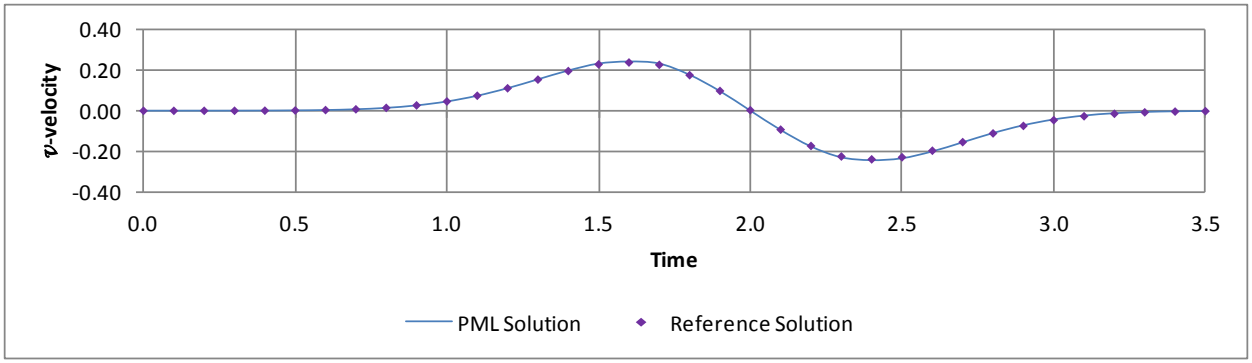

Figure 5.14 Comparison of PML solution with reference solution for v-velocity at Euler-PML interface at point (1, 0) as function of time.

5.4.3 Pressure Pulse

The initial conditions for this strong pressure pulse case are the same as those provided in section 5.4.1, but the major difference is that the nonlinear Euler equations are numerically solved with PML boundaries. The values of σ_m = 500.0 and α = 2.5 are selected. Figures 5.15, 5.16, and 5.17 show the pressure contours at various time levels obtained from domains with uniform and nonuniform grids. At all time levels, the pressure wave is seen to travel smoothly through the nonlinear regime and absorbed effectively in the PML domain with very minimal reflection.

The pressure profile along line $y = 0$ at various time levels is presented in Figure 5.18. The solutions obtained from the tapered domain and the domain with an arbitrary shape matched the reference solution very well, and only the solution from the tapered domain is presented as a nonuniform grid solution in Figure 5.18. The hatched region represents the solution in the PML domain. It can be seen that the acoustic pulse entering the PML domain is dampened, and the solution approaches $1/\gamma$, the proposed $\overline{p}_p$, in the PML domain, thus indicating the damping of the fluctuation term appearing in equation (5.32). It is observed that the solutions obtained with PML boundary conditions match well with that of the reference solution.

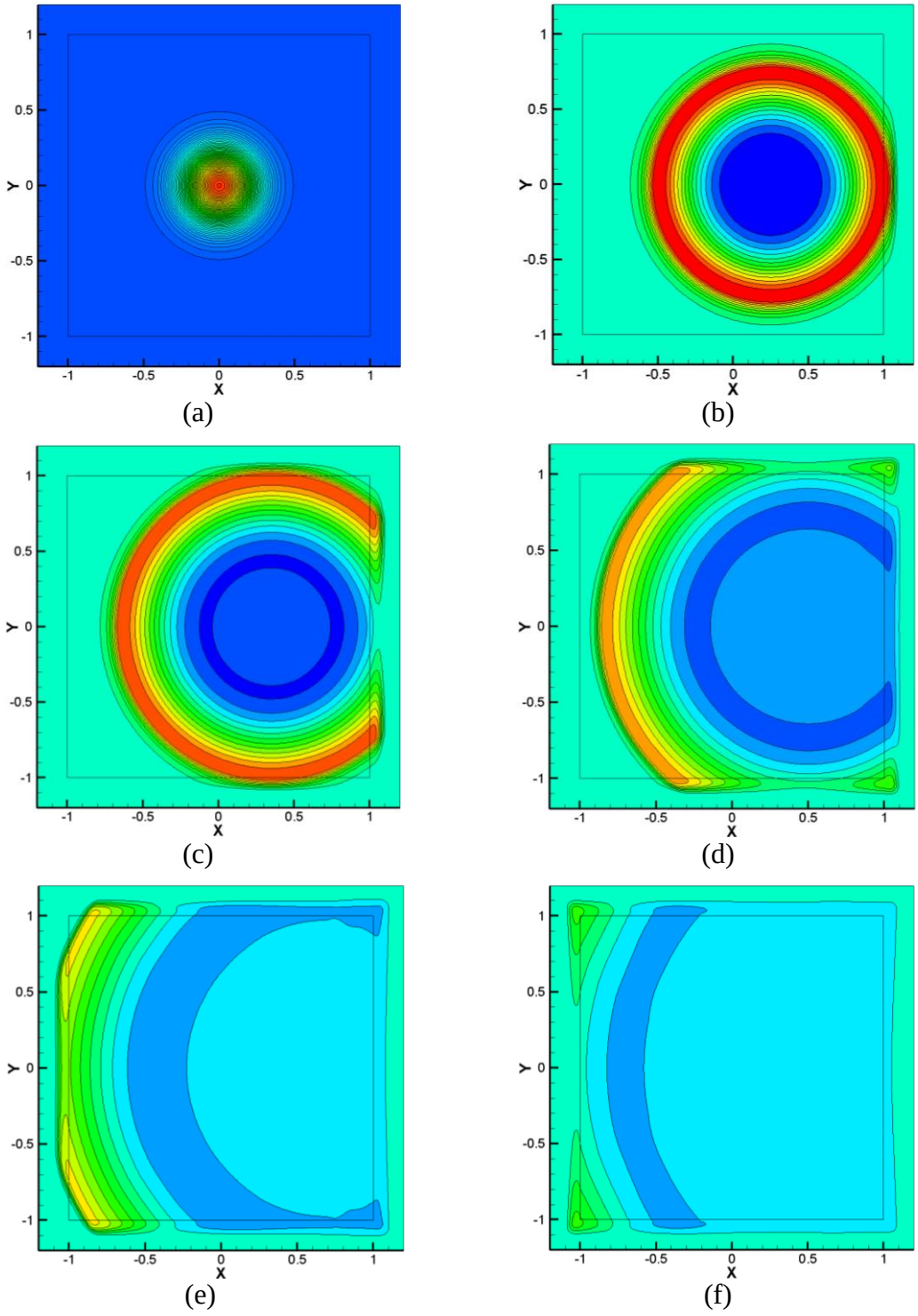

Figure 5.15. Pressure contours: (a) t = 0.0 with levels from 0.65 to 1.75 in steps of 0.02, (b) t = 0.5, (c) t = 0.7, (d) t = 1.0, (e) t = 1.5, and (f) t = 2.0 with levels from 0.65 to 0.9 and step of 0.02.

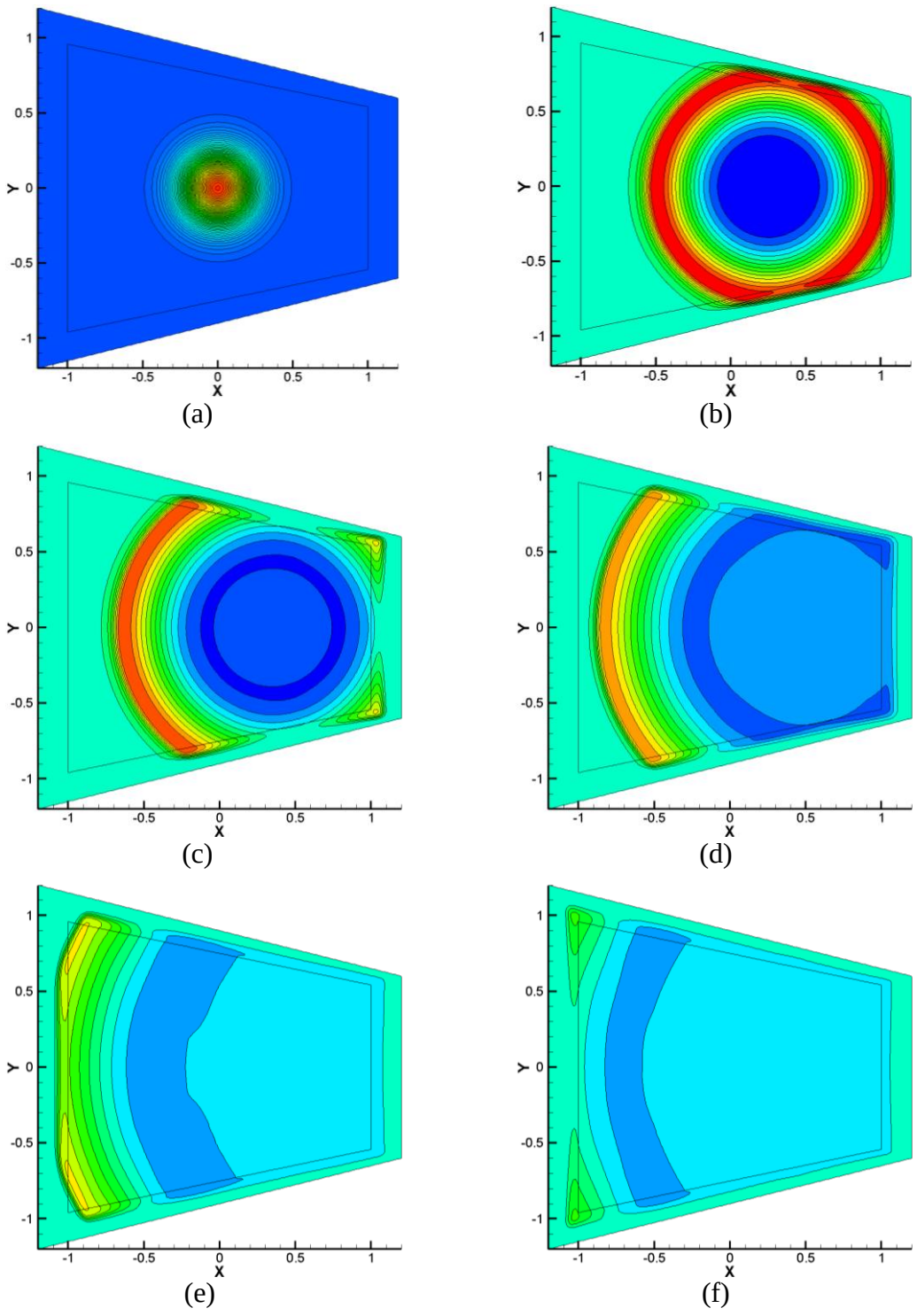

Figure 5.16. Pressure contours: (a) t = 0.0 with levels from 0.65 to 1.75 in steps of 0.02, (b) t = 0.5, (c) t = 0.7, (d) t = 1.0, (e) t = 1.5, and (f) t = 2.0 with levels from 0.65 to 0.9 and step of 0.02.

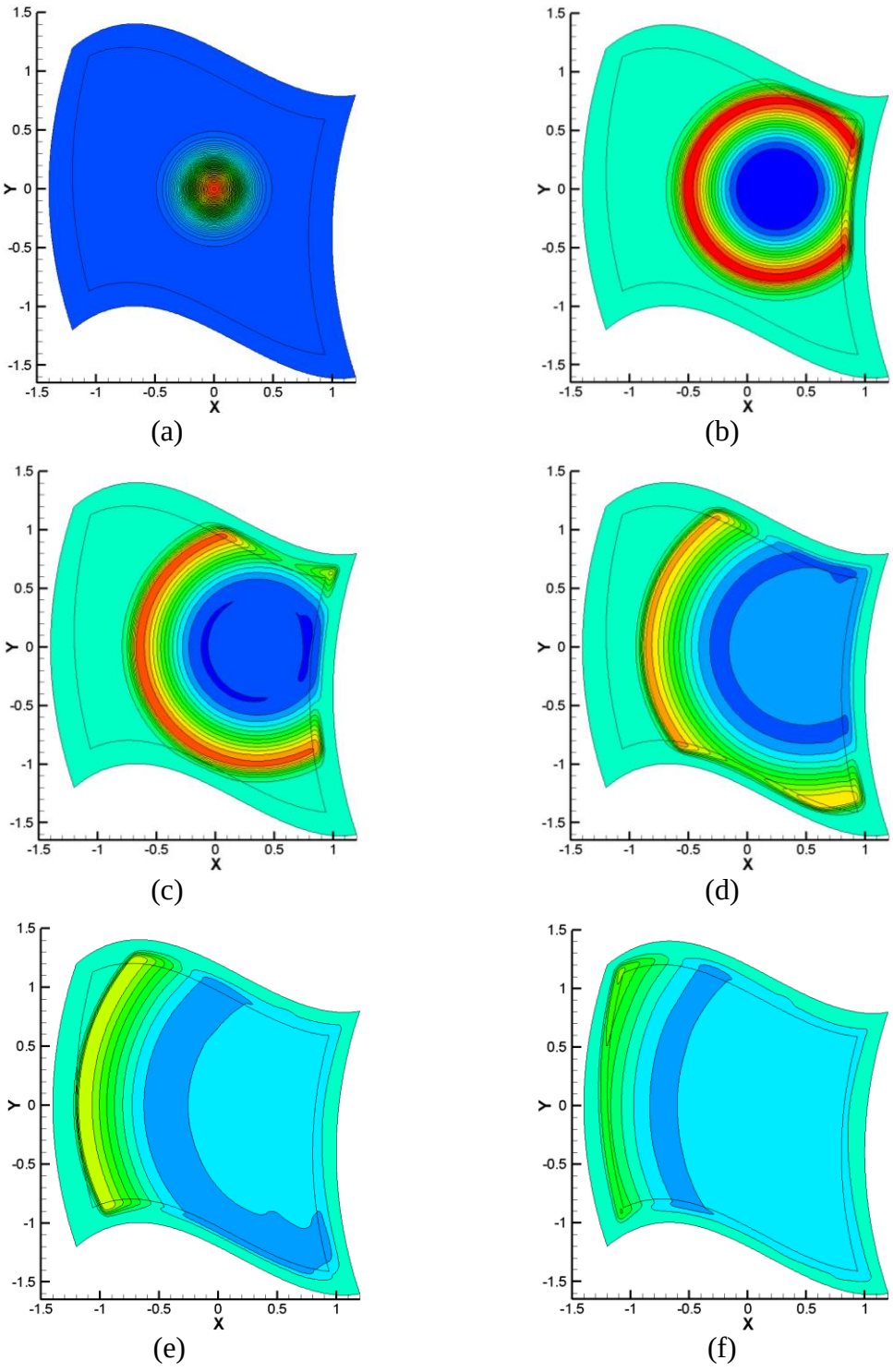

Figure 5.17 Pressure contours: (a) t = 0.0 with levels from 0.65 to 1.75 in steps of 0.02, (b) t = 0.5, (c) t = 0.7, (d) t = 1.0, (e) t = 1.5, and (f) t = 2.0 with levels from 0.65 to 0.9 and step of 0.02.

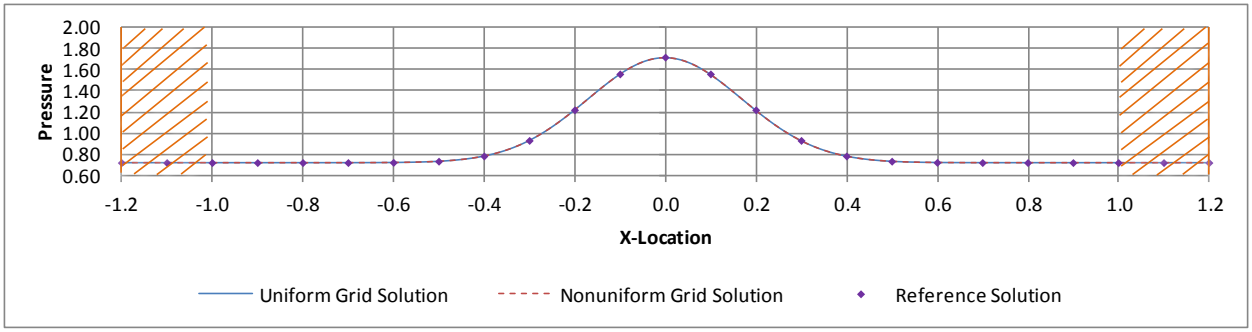
Pressure
2.00
1.80
1.60
1.40
1.20
1.00
0.80
0.60
-1.2 -1.0 -0.8 -0.6 -0.4 -0.2 0.0 0.2 0.4 0.6 0.8 1.0 1.2
X-Location
Uniform Grid Solution
Nonuniform Grid Solution
Reference Solution

(a)

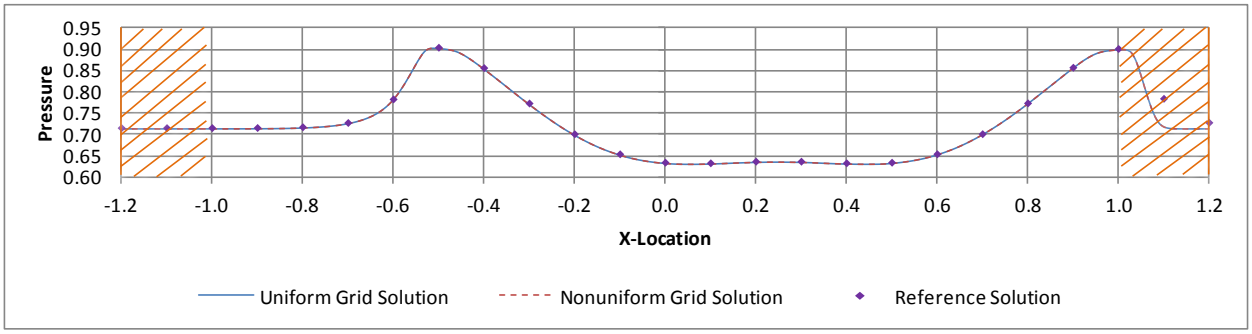
Pressure
0.95
0.90
0.85
0.80
0.75
0.70
0.65
0.60
-1.2 -1.0 -0.8 -0.6 -0.4 -0.2 0.0 0.2 0.4 0.6 0.8 1.0 1.2
X-Location
Uniform Grid Solution
Nonuniform Grid Solution
Reference Solution

(b)

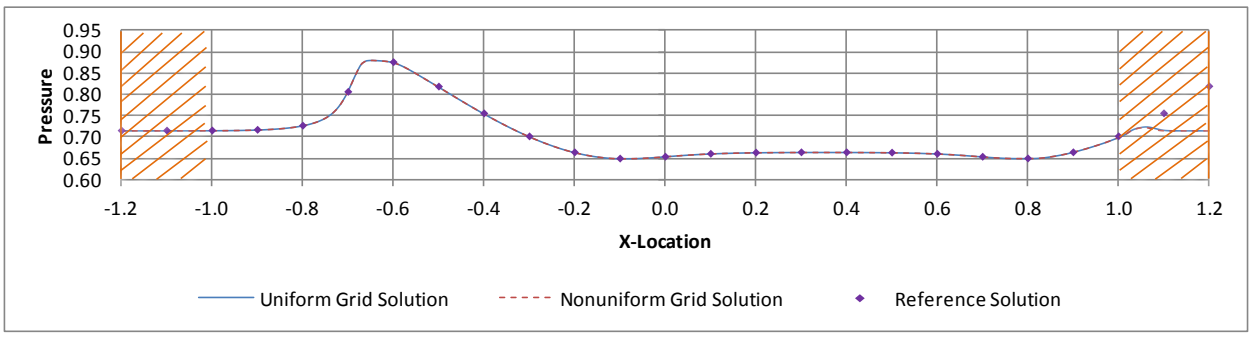
Pressure
0.95
0.90
0.85
0.80
0.75
0.70
0.65
0.60
-1.2 -1.0 -0.8 -0.6 -0.4 -0.2 0.0 0.2 0.4 0.6 0.8 1.0 1.2
X-Location
Uniform Grid Solution
Nonuniform Grid Solution
Reference Solution

(c)

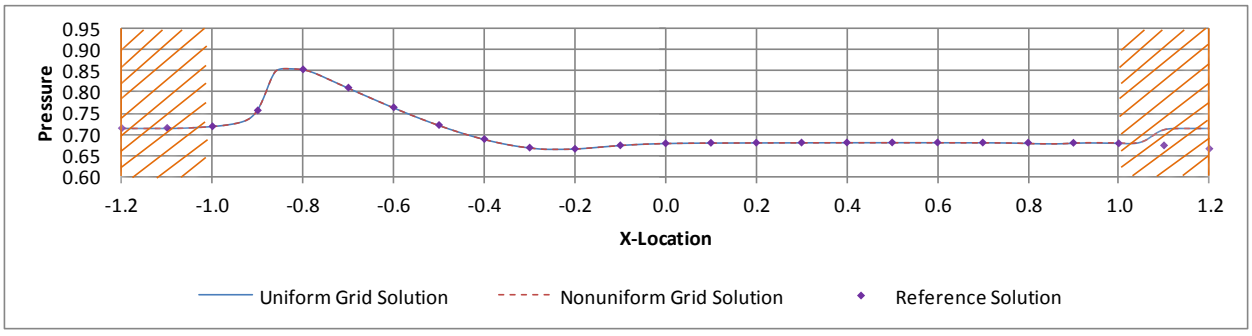
Pressure
0.95
0.90
0.85
0.80
0.75
0.70
0.65
0.60
-1.2 -1.0 -0.8 -0.6 -0.4 -0.2 0.0 0.2 0.4 0.6 0.8 1.0 1.2
X-Location
Uniform Grid Solution
Nonuniform Grid Solution
Reference Solution

(d)

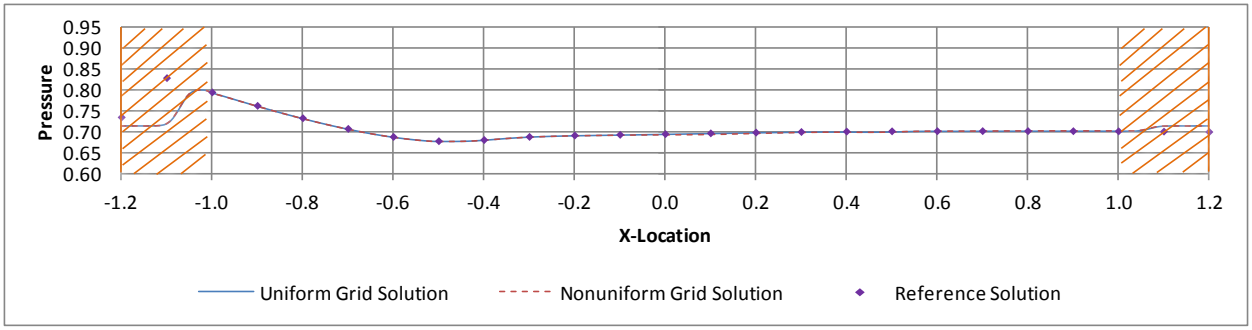

(e)

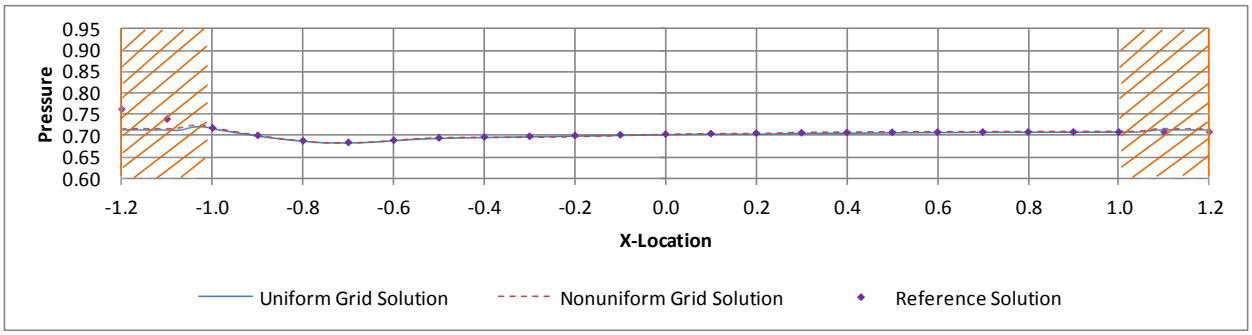

(f)

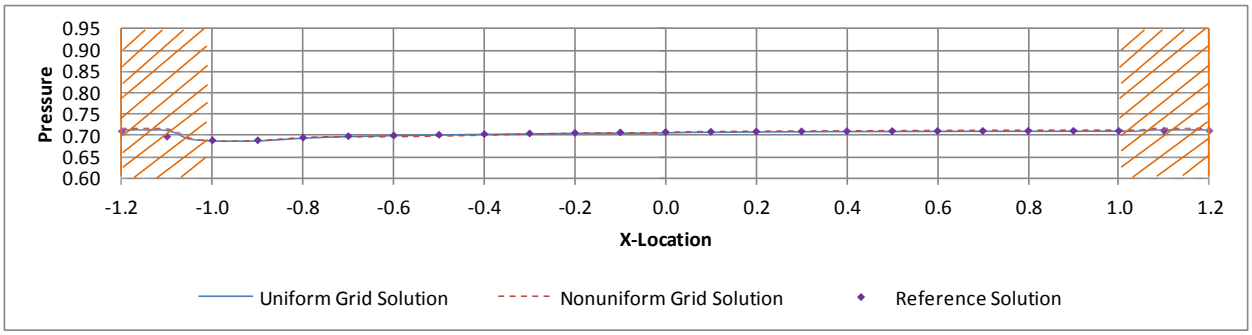

(g)

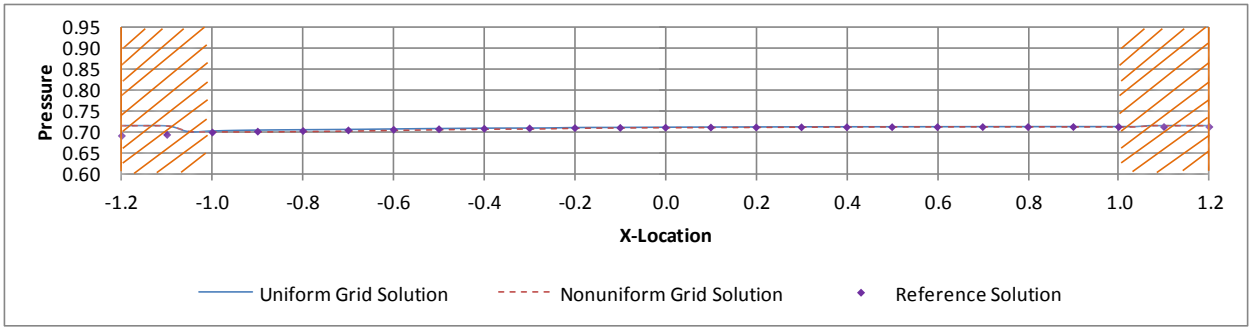

(h)

Figure 5.18 Pressure along y = 0: (a) t = 0, (b) t = 0.5, (c) t = 0.7, (d) t = 1.0, (e) t = 1.5, (f) t = 2.0, (g) t = 2.5, and (h) t = 3.0.

A point (1, 0) is chosen on the Euler-PML domain interface to appraise the effectiveness of the PML boundary condition. The solution for pressure obtained using the PML boundary condition is checked with that of the reference solution at this interface and is shown in Figure 5.19. A good match between the solutions is observed.

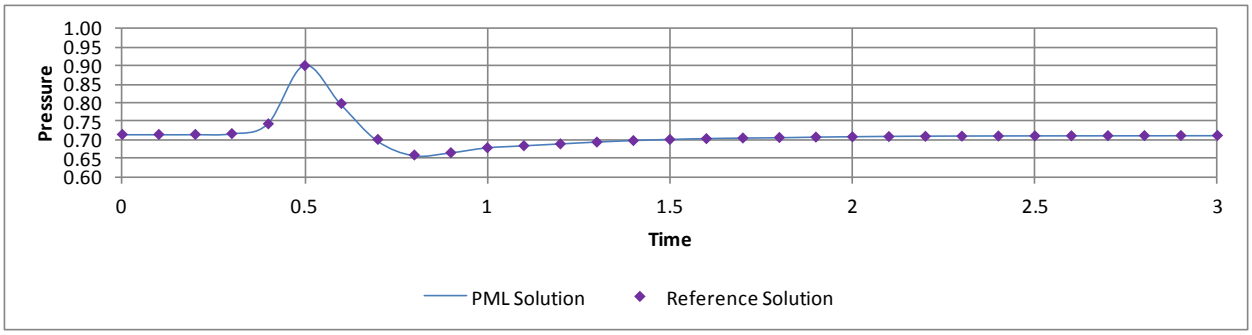

Fig. 5.19 Comparison of PML solution with reference solution for pressure at Euler-PML interface at point (1, 0) as function of time.

5.4.4 Acoustic Radiation from Oscillating Piston

5.4.4.1 Rectangular Domain with Uniform Grid Spacing

In this case, acoustic radiation from an oscillating piston in a wall is simulated to demonstrate the effectiveness of the PML boundary condition. The boundary condition defining the piston and the wall used in this case is analogous to problem 2 of the category 4 benchmark problem found in a NASA Conference Publication [22]. The rectangular physical domain, Figure 5.20, used in this simulation is of the size [-105, 105] x [0, 105] with a uniform spacing of $\Delta x = \Delta y = 0.5$. The physical domain includes a PML domain with ten layers, the region shaded in olive green in Figure 5.21, appended to the three sides of the physical space. The piston, blue line in Figures 5.20 and 5.21, is located at $-10 \leq x \leq 10,\ y = 0$. Hatching defines the wall for $-105 \leq x < -10$ and $10 < x \leq 105,\ y = 0$. In the computational space, i.e., generalized coordinates, the grid spacing is $\Delta\xi = \Delta\eta = 1.0$. A nondimensional global time-step size of 0.01 is used.

The entire domain is initialized with the conditions as given by equations (5.45)–(5.48).

$$\rho = 1.0 \tag{5.45}$$

$$p = \frac{1}{\gamma} \tag{5.46}$$

$$u = U_0 \tag{5.47}$$

$$v = 0.0 \tag{5.48}$$

Two numerical simulations are carried out for $u = U_0 = 0.0$ and $u = U_0 = 0.5$. Simple extrapolation is used on the outermost boundaries of the PML domain. The velocity of the piston is defined by equation (5.49). The wall boundary condition is enforced by specifying the zero

normal component of velocity along $y = 0$. Zero-order extrapolation is used to calculate the other physical variables on the wall and the piston.

$$v = A\sin\left(\pi t/20\right) \tag{5.49}$$

where A is the amplitude and equal to 0.2.

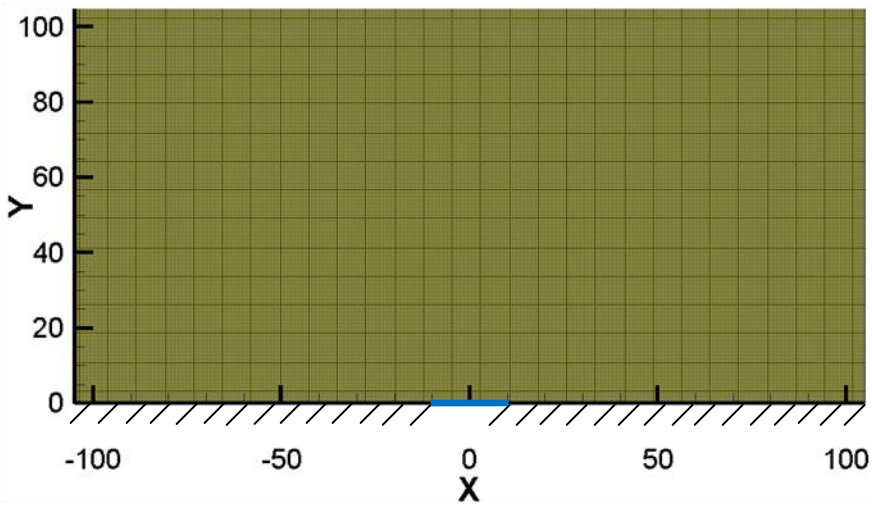

Figure 5.20. Rectangular domain with uniform grid structure showing piston (blue line) and wall (hatched section). Number of layers in PML domain = 10.

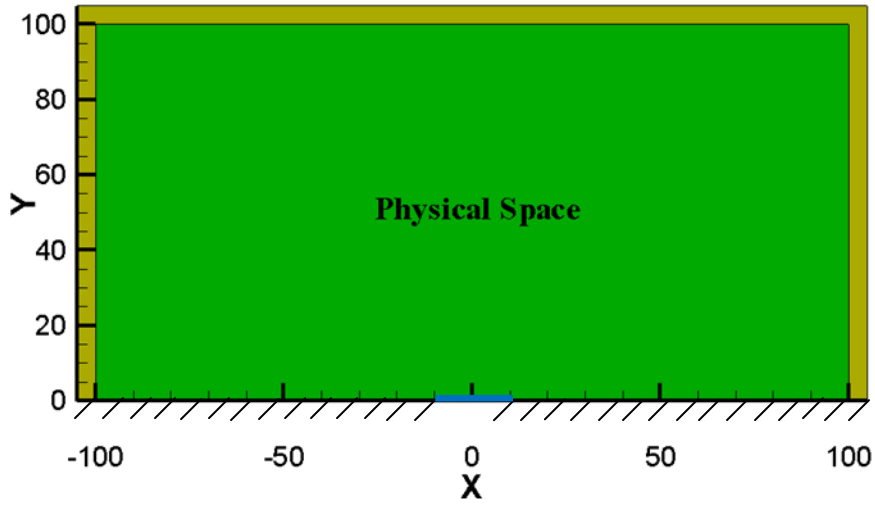

Figure 5.21. Rectangular domain showing physical space and PML domain (shaded region in olive green). Number of layers in PML domain = 10.

The pseudo mean-flow inside the PML domain is initialized by equations (5.50)–(5.53).

$$\bar{\rho}_p = 1.0 \tag{5.50}$$

$$\bar{p}_p = \frac{1}{\gamma} \tag{5.51}$$

$$\bar{u}_p = u \tag{5.52}$$

$$\bar{v}_p = 0.0 \tag{5.53}$$

The parameter β is appropriately calculated based on the chosen $\bar{u}_p$ using the empirical formula given by equation (5.10). The values of σ_m = 50.0 and α = 2.0 are used for the PML parameters in the computational domain.

Figures 5.22 and 5.26 show the pressure contours over a period of oscillation, from $t = 200$ to $t = 240$ in steps of ten, for $u = 0.0$ and $u = 0.5$ respectively. The damping of the perturbation of the pressure induced by the oscillating piston is clearly shown in the contour plots. A comparison of pressure along $x = 0$ (Figures 5.23 and 5.27) and along $y = 0$ (Figures 5.23 and 5.28), obtained with the PML boundary condition and from a reference case for $u = 0.0$ and $u = 0.5$, respectively, shows a clear match between the two solutions. The rectangular domain used for the reference case is of the size [-315, 315] x [0, 315]. Over a period of oscillation of the piston, it is observed that the solution obtained with PML compares very well with the solution from the reference case. Because the perturbation is dampened inside the PML domain, it can be seen that the solution for pressure approaches $1/\gamma$, the proposed $\bar{p}_p$, as per equation (5.50). Figures 5.25 and 5.29 show a comparison of the PML solution with that of the reference case for pressure as a function of time at the Euler-PML interface for $u = 0.0$ and

$u = 0.5$, respectively. Clear agreement between the solutions demonstrates that the PML boundary condition is an effective nonreflecting boundary condition.

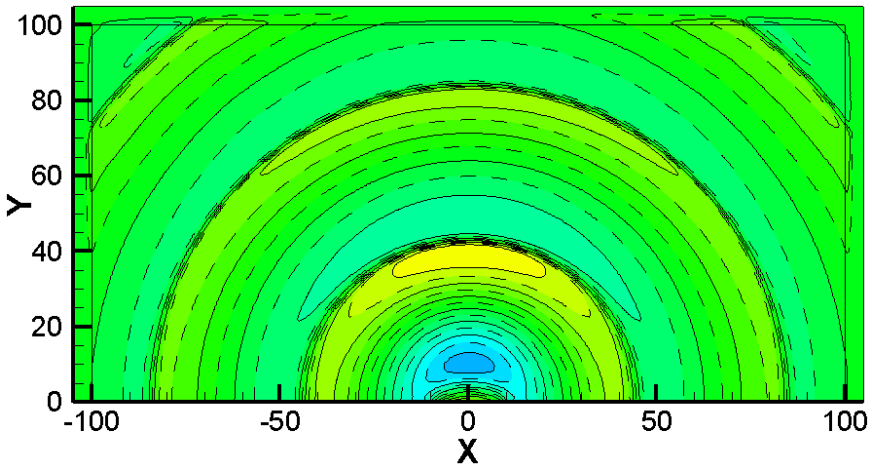

(a)

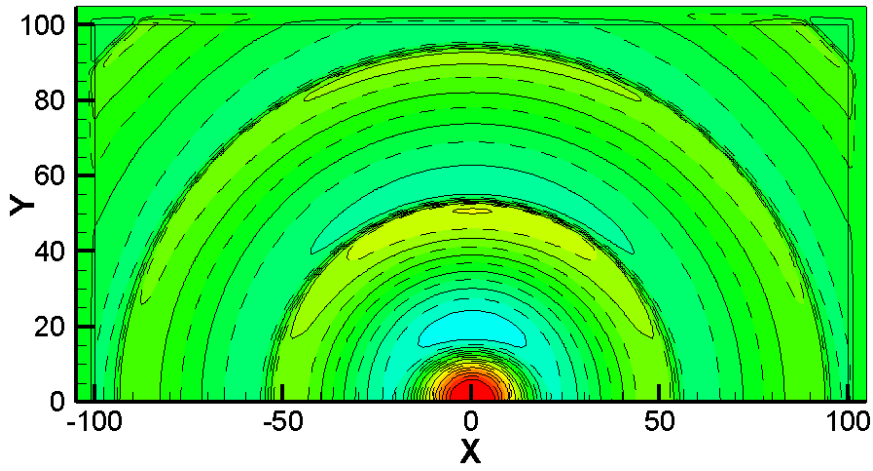

(b)

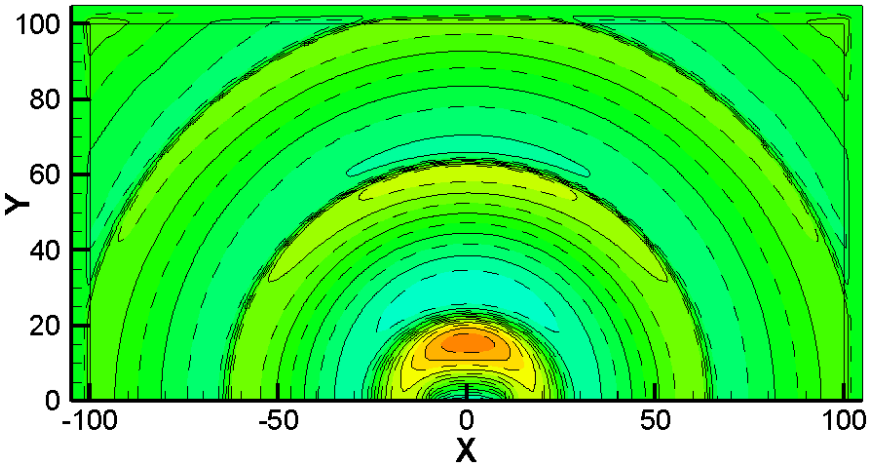

(c)

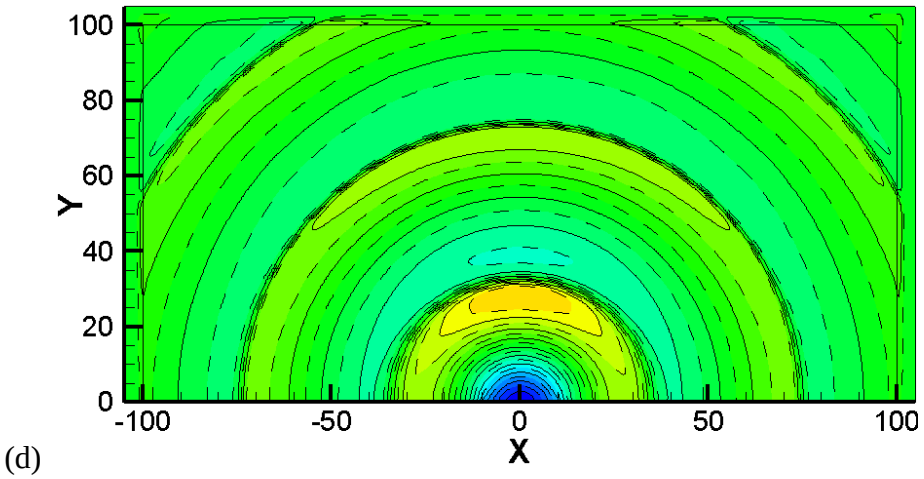

(d)

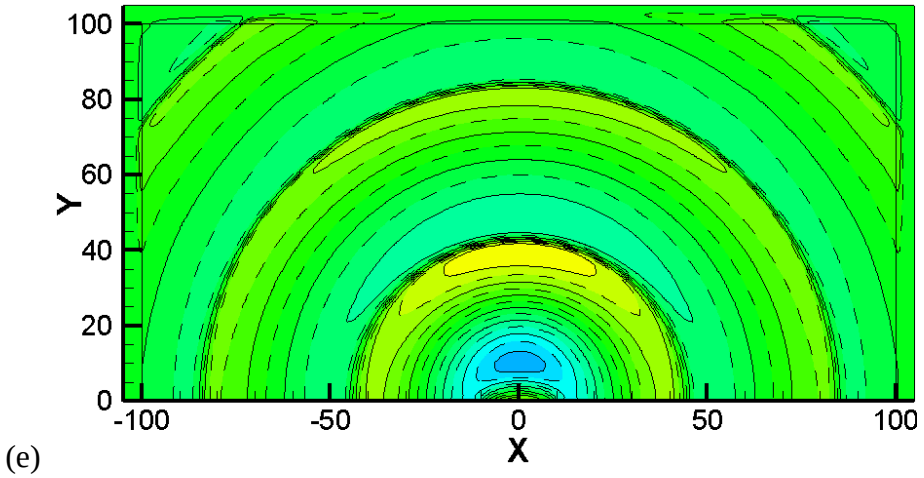

(e)

Figure 5.22. Pressure contours over period of piston oscillation: (a) t = 200, (b) t = 210, (c) t = 220, (d) t = 230, and (e) t = 240 with levels from 0.5 to 0.95 in steps of 0.02 for u = 0.0.

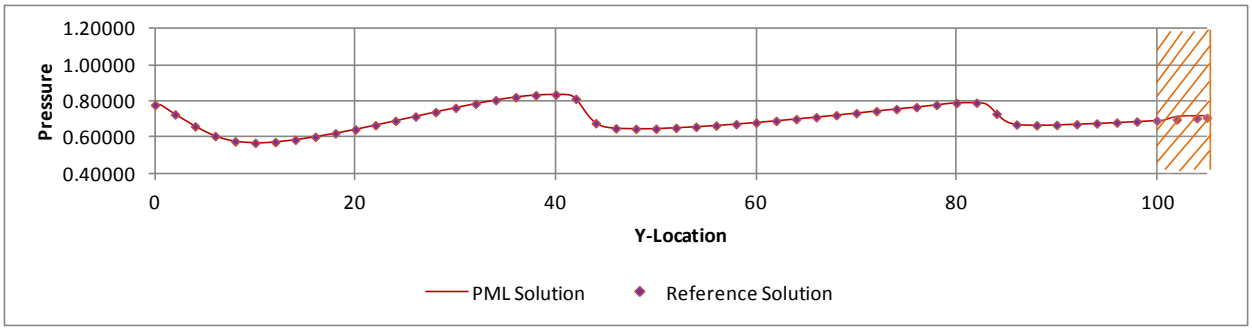

(a)

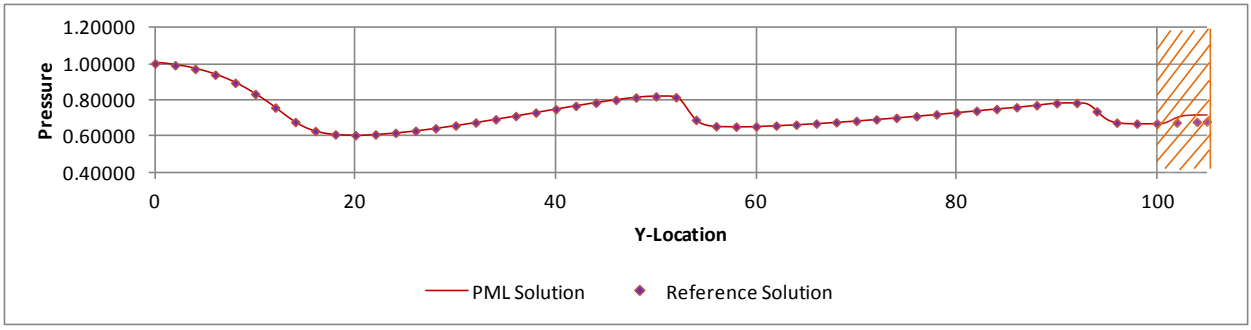

(b)

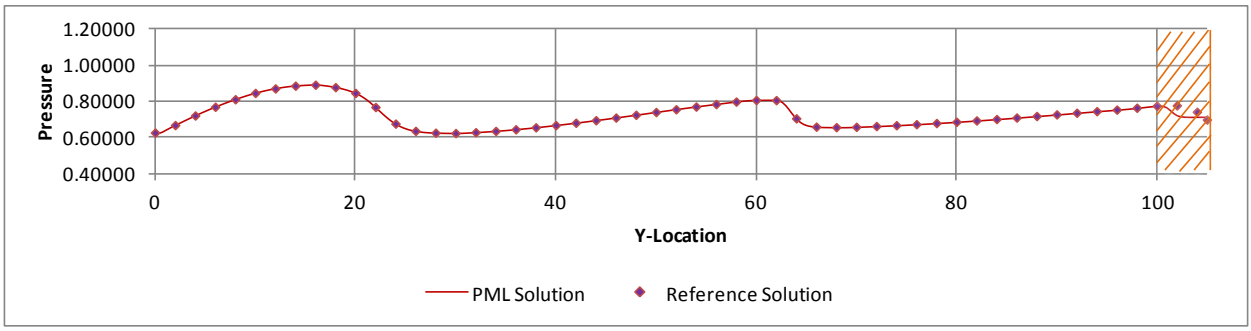

(c)

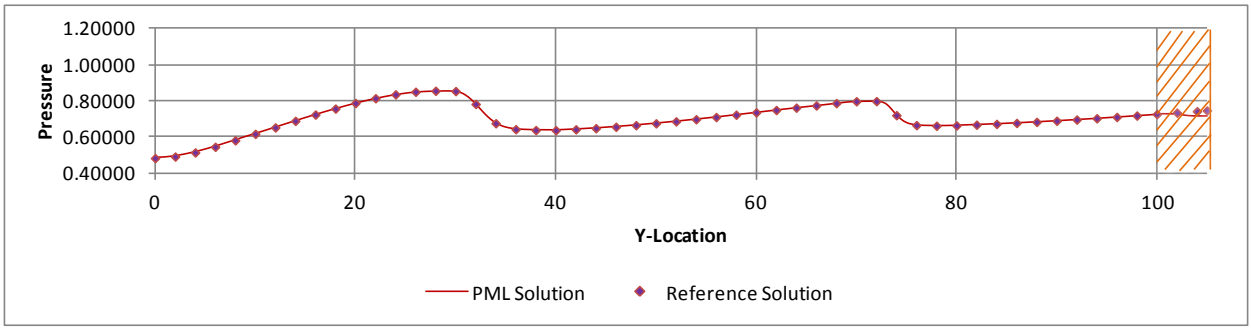

(d)

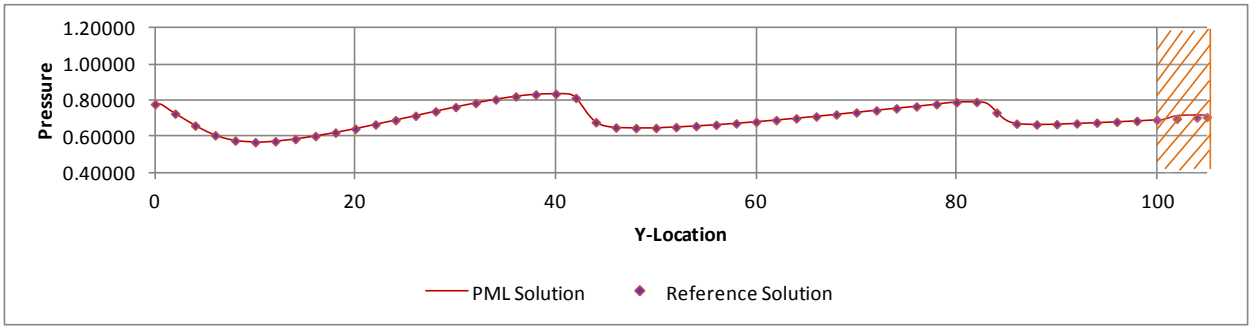

(e)

Figure 5.23. Pressure along x = 0 over period of piston oscillation: (a) t = 200, (b) t = 210, (c) t = 220, (d) t = 230, and (e) t = 240 for u = 0.0.

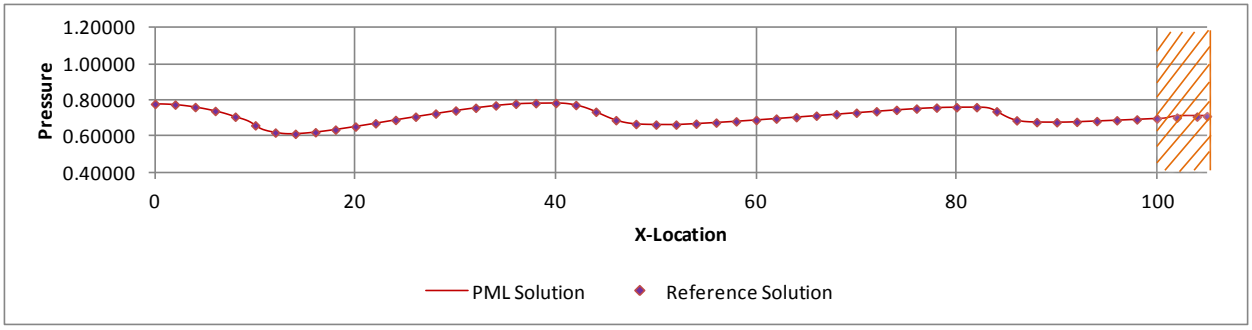
1.20000
1.00000
0.80000
0.60000
0.40000
Pressure
0
20
40
60
80
100
X-Location
PML Solution
Reference Solution

(a)

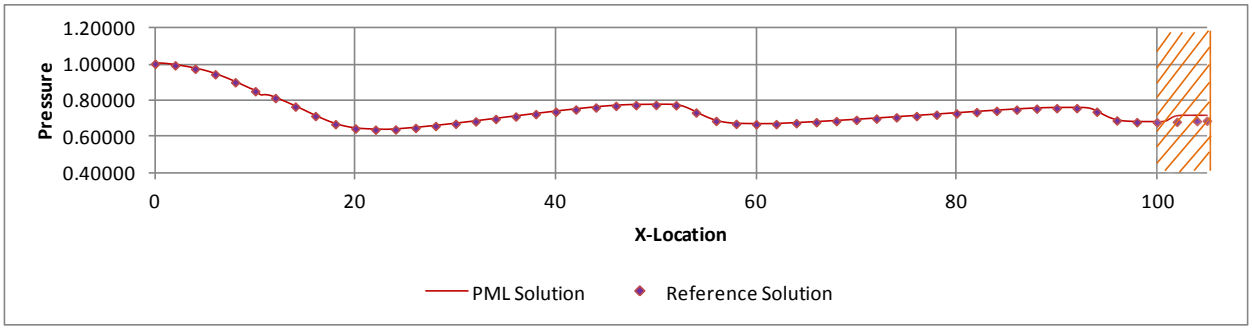
1.20000
1.00000
0.80000
0.60000
0.40000
Pressure
0
20
40
60
80
100
X-Location
PML Solution
Reference Solution

(b)

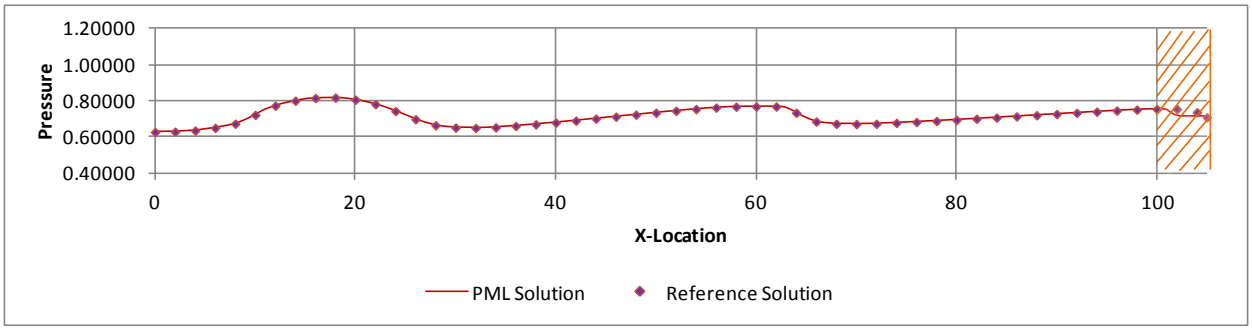
1.20000
1.00000
0.80000
0.60000
0.40000
Pressure
0
20
40
60
80
100
X-Location
PML Solution
Reference Solution

(c)

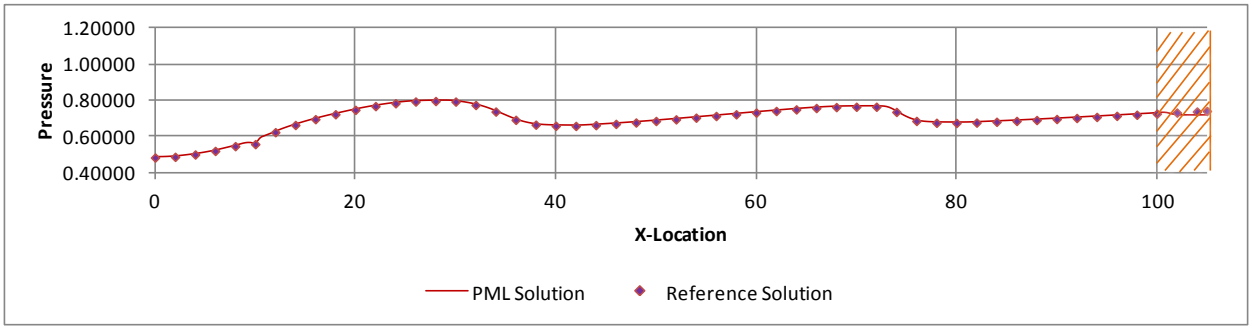
1.20000
1.00000
0.80000
0.60000
0.40000
Pressure
0
20
40
60
80
100
X-Location
PML Solution
Reference Solution

(d)

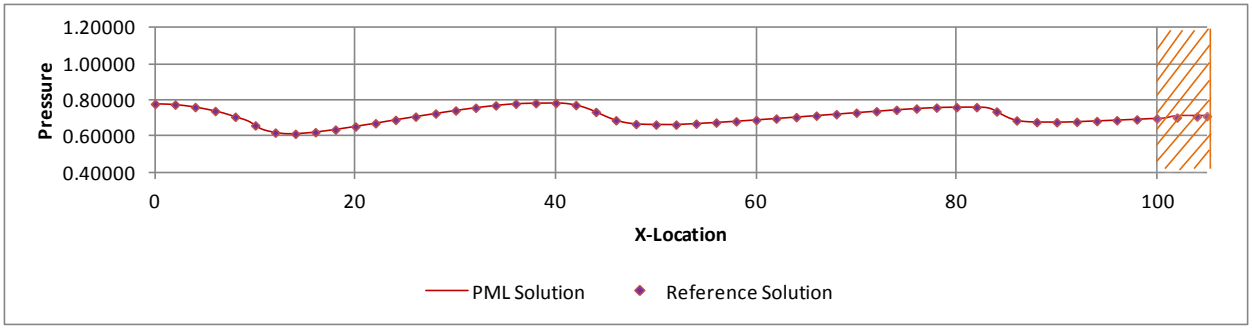

(e)

Figure 5.24. Pressure along y = 0 over period of piston oscillation: (a) t = 200, (b) t = 210, (c) t = 220, (d) t = 230, and (e) t = 240 for u = 0.0.

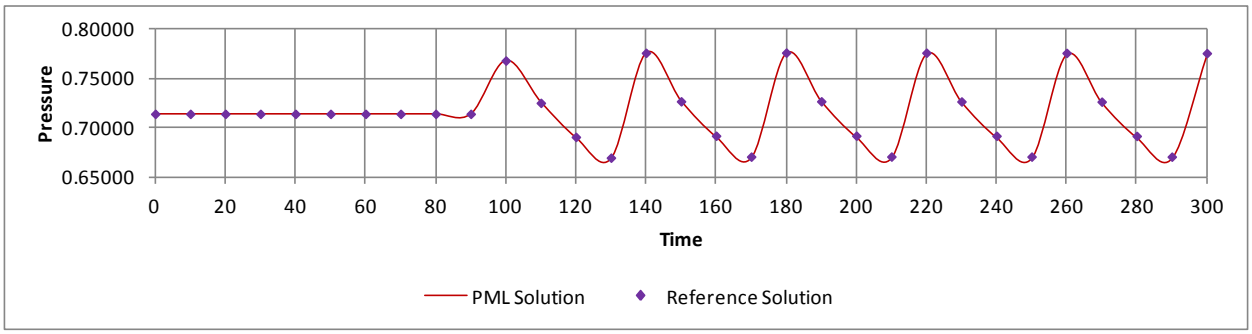

(a)

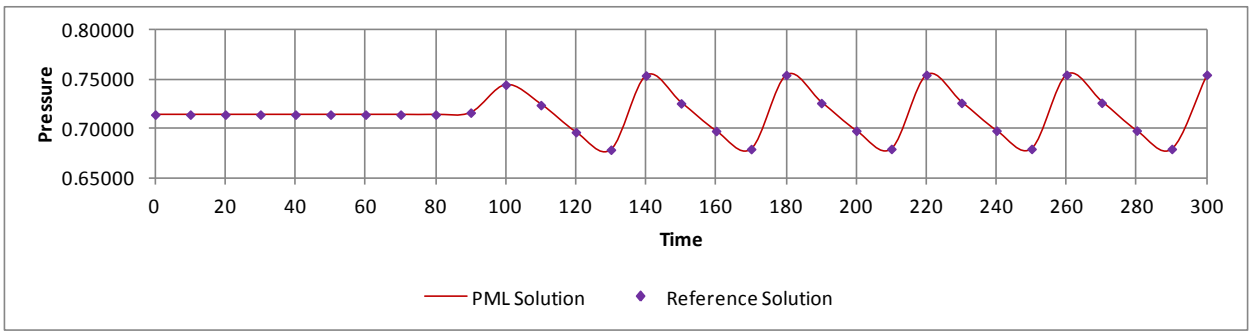

(b)

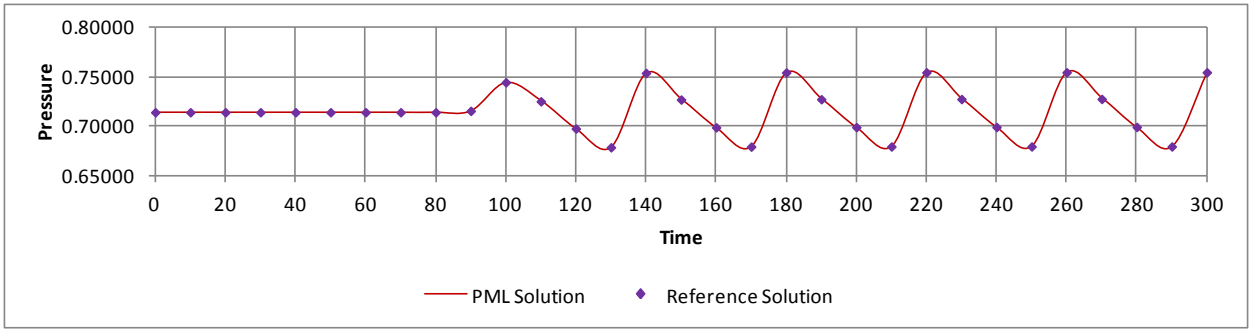

(c)

Figure 5.25. Pressure as function of time at Euler-PML interface at locations: (a) (0, 100), (b) (100, 0), and (c) (-100, 0) for u = 0.0.

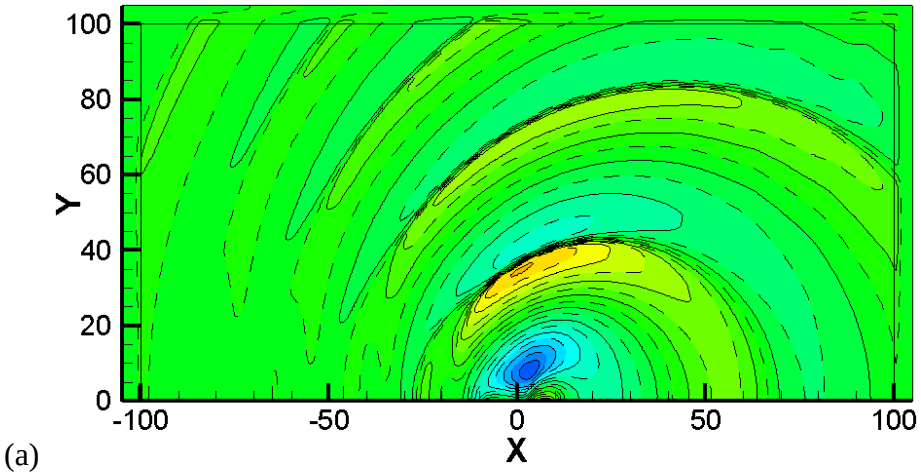

(a)

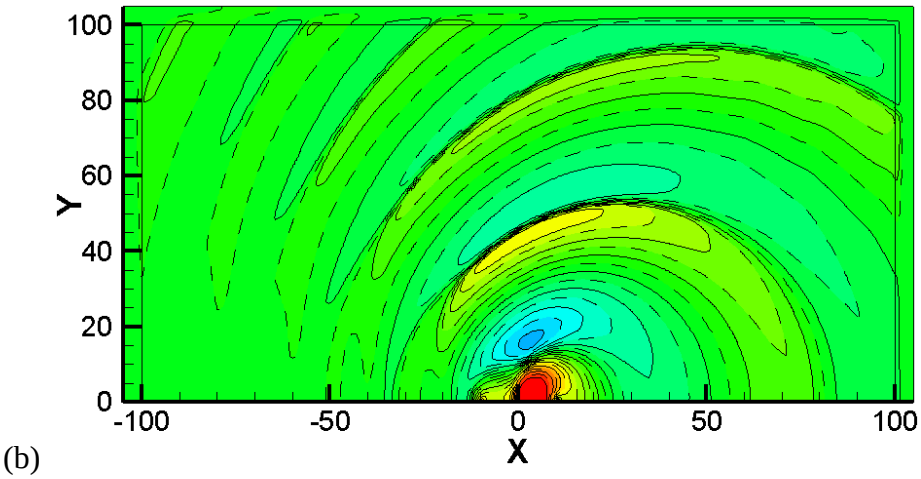

(b)

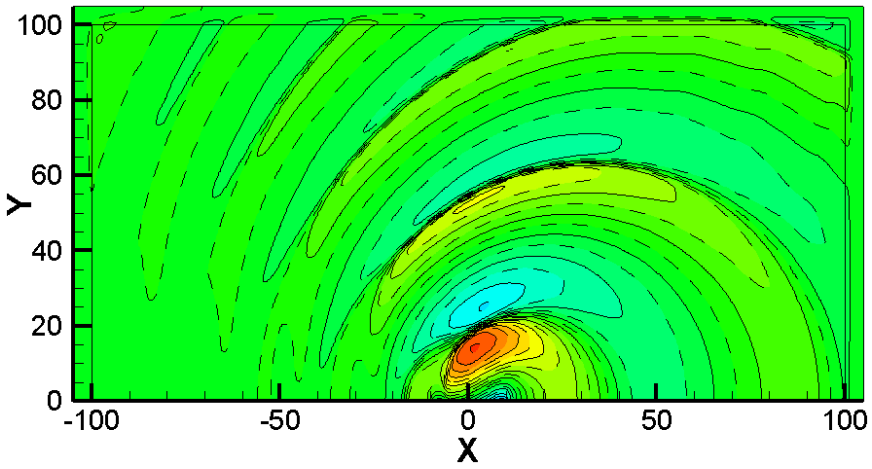

(c)

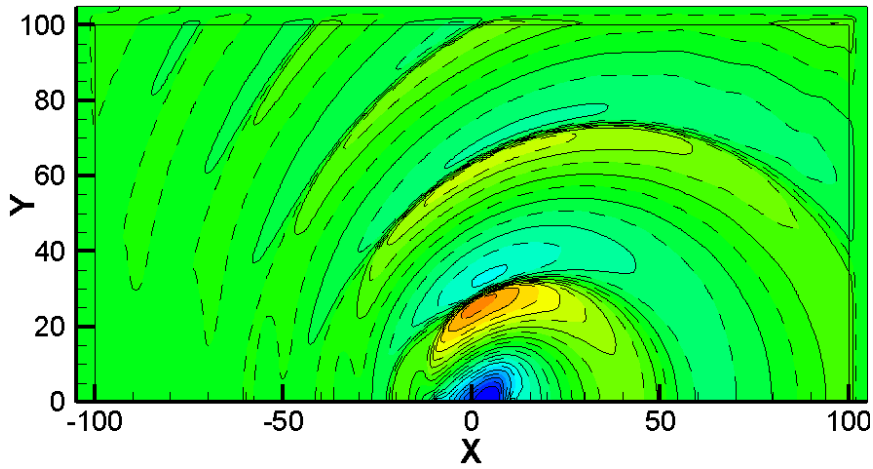

(d)

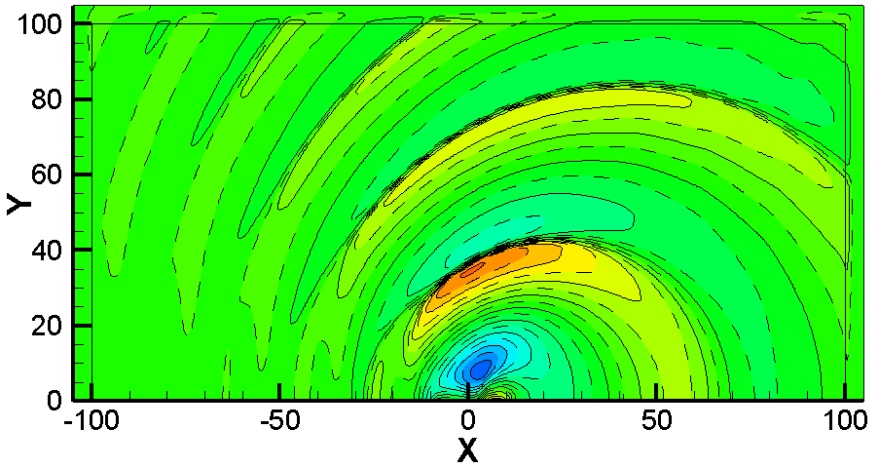

(e)

Figure 5.26. Pressure contours over period of piston oscillation: (a) t = 200, (b) t = 210, (c) t = 220, (d) t = 230, and (e) t = 240 with levels from 0.5 to 0.95 in steps of 0.02 for u = 0.5.

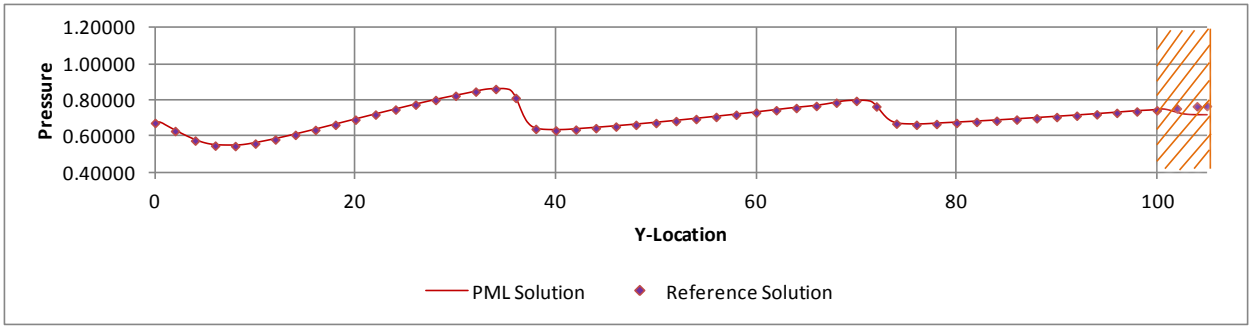
1.20000
1.00000
0.80000
0.60000
0.40000
Pressure
0
20
40
60
80
100
Y-Location
PML Solution
Reference Solution

(a)

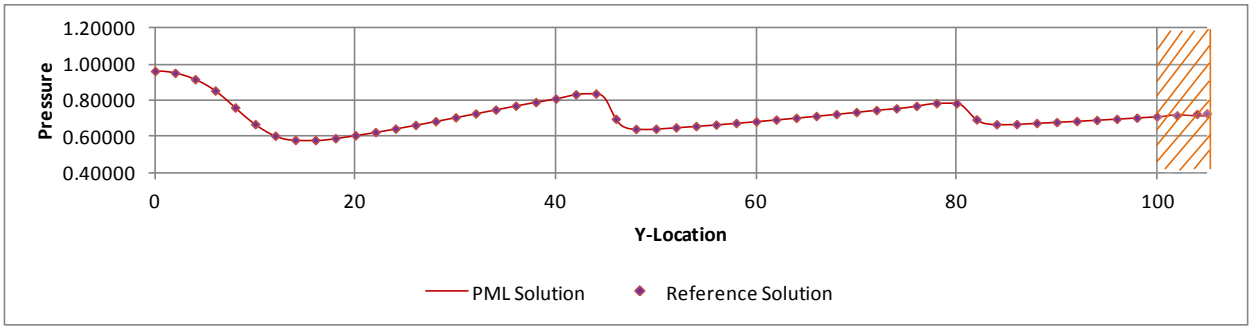
1.20000
1.00000
0.80000
0.60000
0.40000
Pressure
0
20
40
60
80
100
Y-Location
PML Solution
Reference Solution

(b)

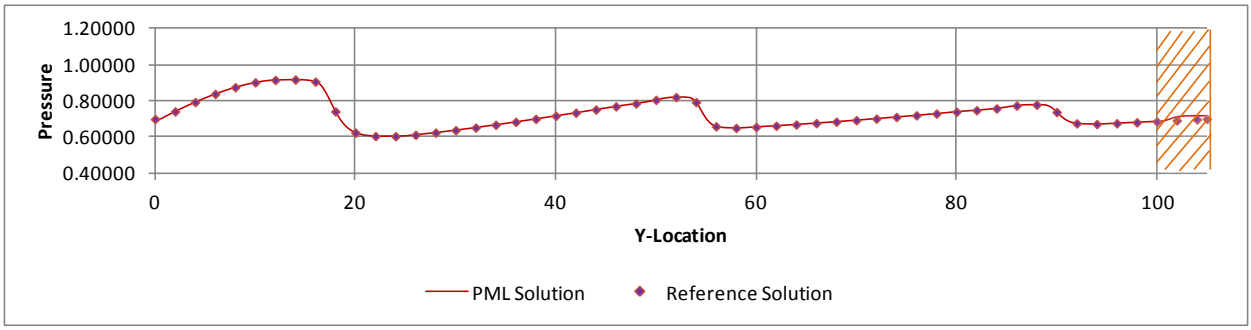
1.20000
1.00000
0.80000
0.60000
0.40000
Pressure
0
20
40
60
80
100
Y-Location
PML Solution
Reference Solution

(c)

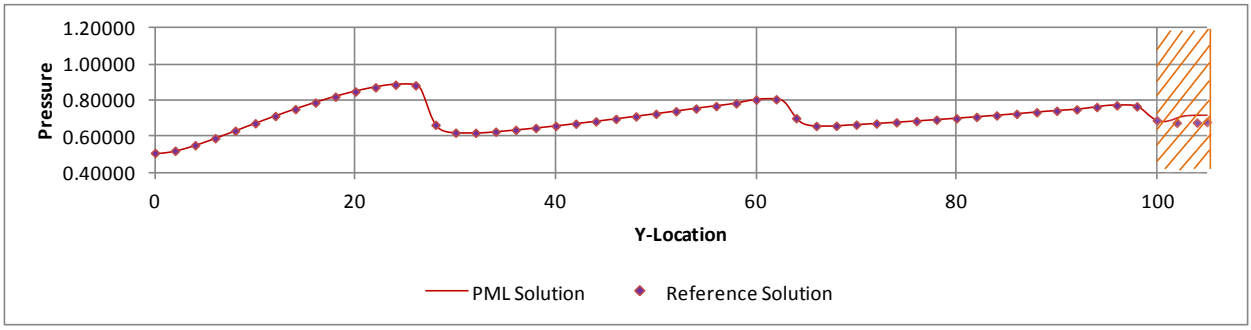
1.20000
1.00000
0.80000
0.60000
0.40000
Pressure
0
20
40
60
80
100
Y-Location
PML Solution
Reference Solution

(d)

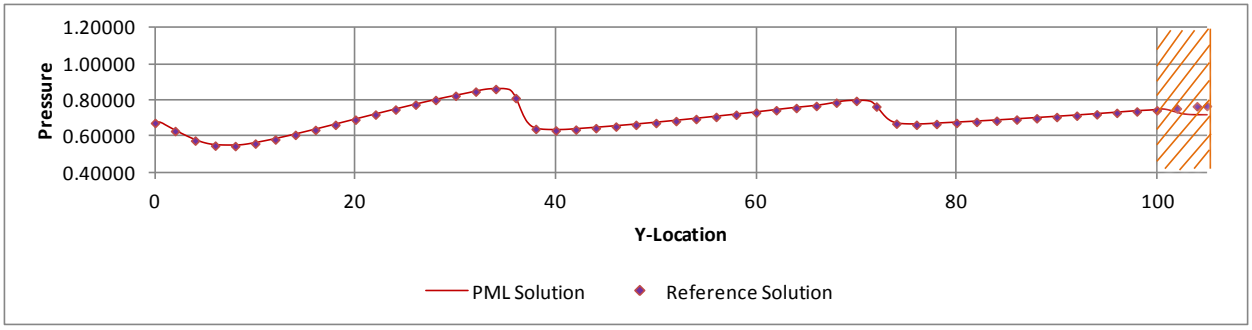

(e)

Figure 5.27. Pressure along x = 0 over period of piston oscillation: (a) t = 200, (b) t = 210, (c) t = 220, (d) t = 230, and (e) t = 240 for u = 0.5.

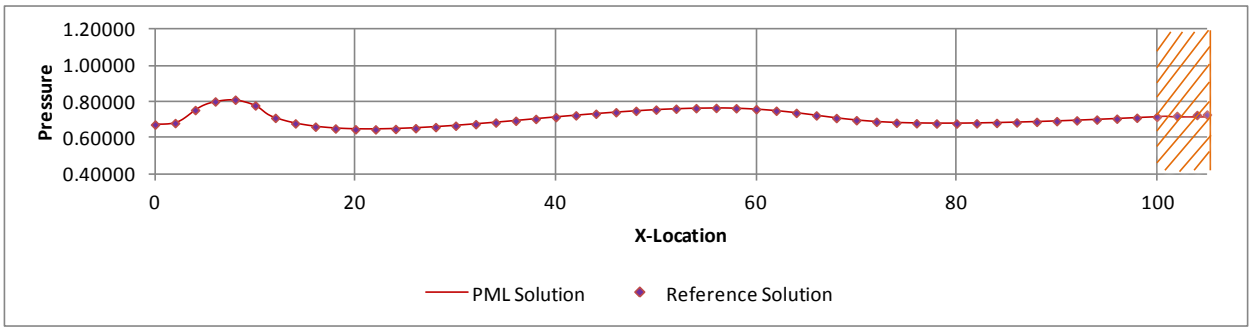

(a)

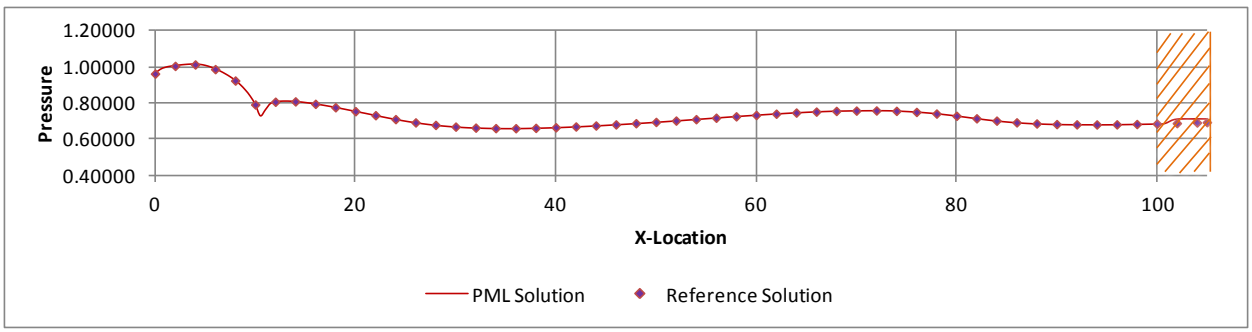

(b)

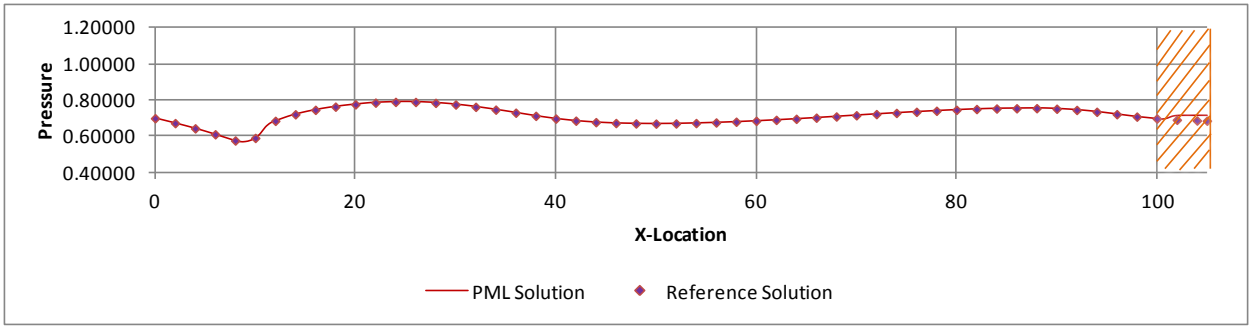

(c)

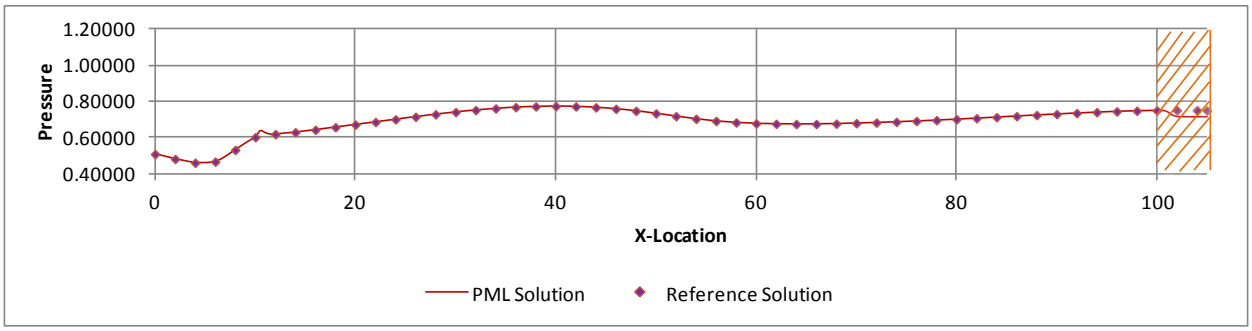

(d)

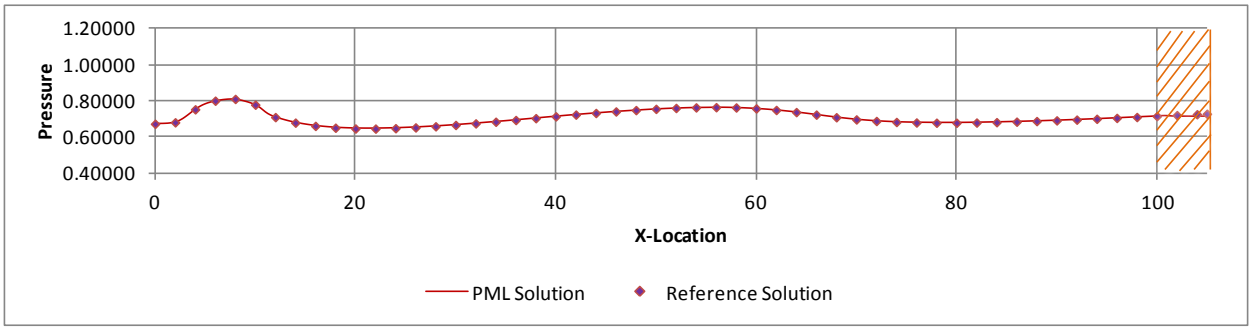

(e)

Figure 5.28. Pressure along y = 0 over period of piston oscillation: (a) t = 200, (b) t = 210, (c) t = 220, (d) t = 230, and (e) t = 240 for u = 0.5.

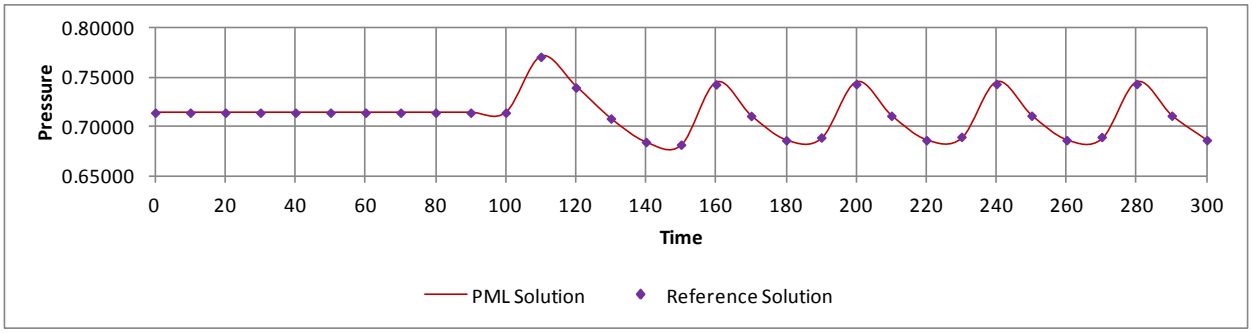

(a)

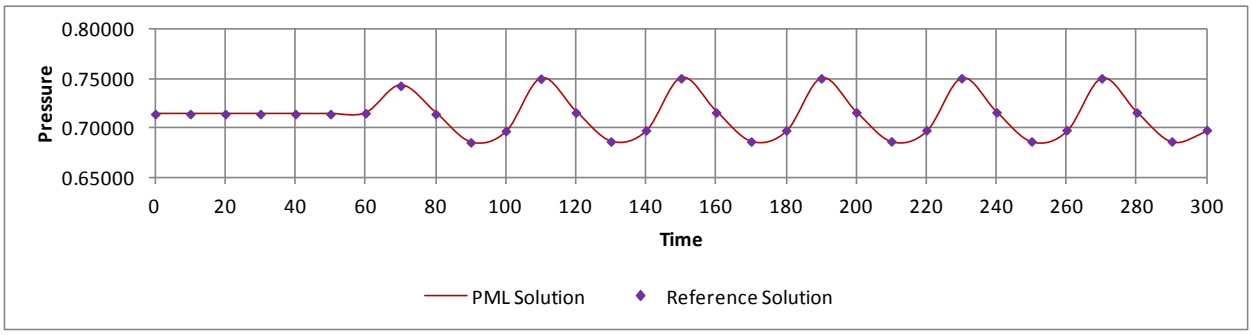

(b)

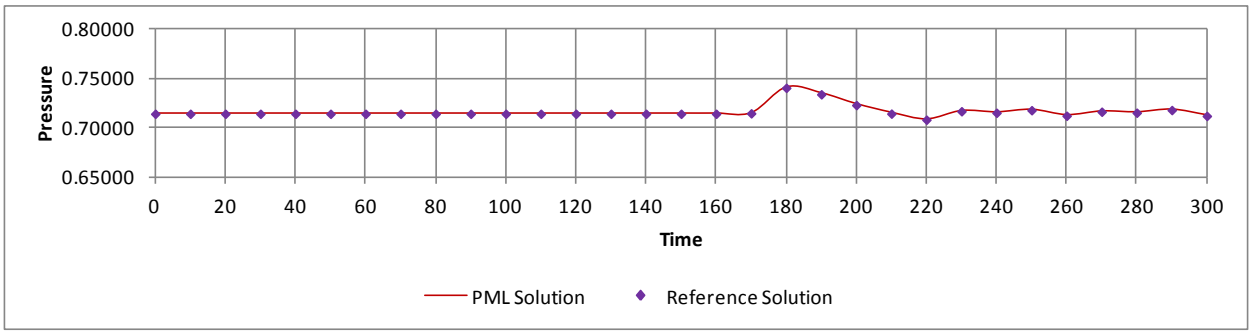

(c)

Figure 5.29 Pressure as function of time at Euler-PML interface at locations: (a) (0, 100), (b) (100, 0), and (c) (-100, 0) for u = 0.5.

5.4.4.2 Tapered Domain with Nonuniform Grid Spacing

In order to demonstrate the PML in a generalized coordinate system, a tapered domain with nonuniform grid spacing, Figures 5.30 and 5.31, is chosen. Except the taper introduced in the shape of the physical domain on the left and right side boundaries, all other parameters remain the same as that in section 5.4.4.1. The physical domain includes a PML domain with ten layers, the region shaded in olive green in Figure 5.31, appended to three sides of the physical space. In the computational space, i.e., generalized coordinates, grid spacing is $\Delta\xi = \Delta\eta = 1.0$. A nondimensional global time-step size of 0.01 is used in the numerical simulations. Two cases, viz., $u = U_0 = 0.0$ and $u = U_0 = 0.5$, are carried out in this tapered domain with nonuniform grid spacing for the oscillating piston.

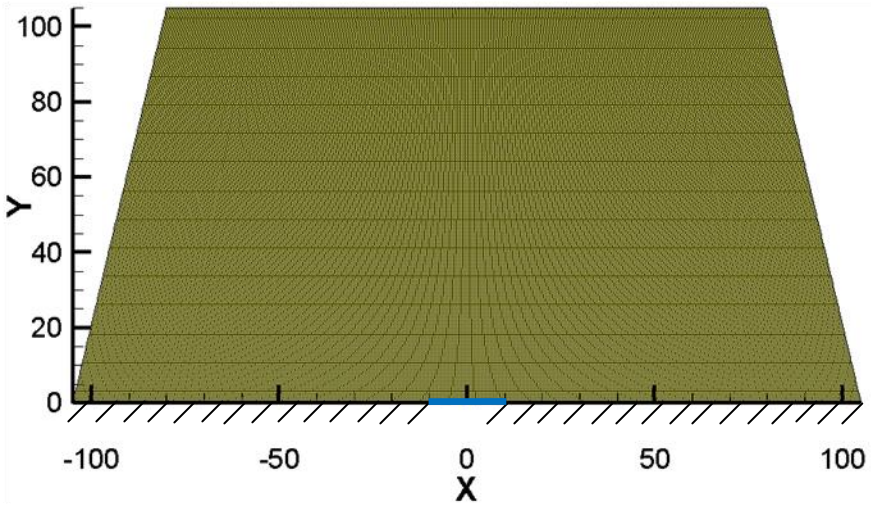

Figure 5.30. Tapered domain with nonuniform grid structure showing piston (blue line) and wall (hatched section). Number of layers in PML domain = 10.

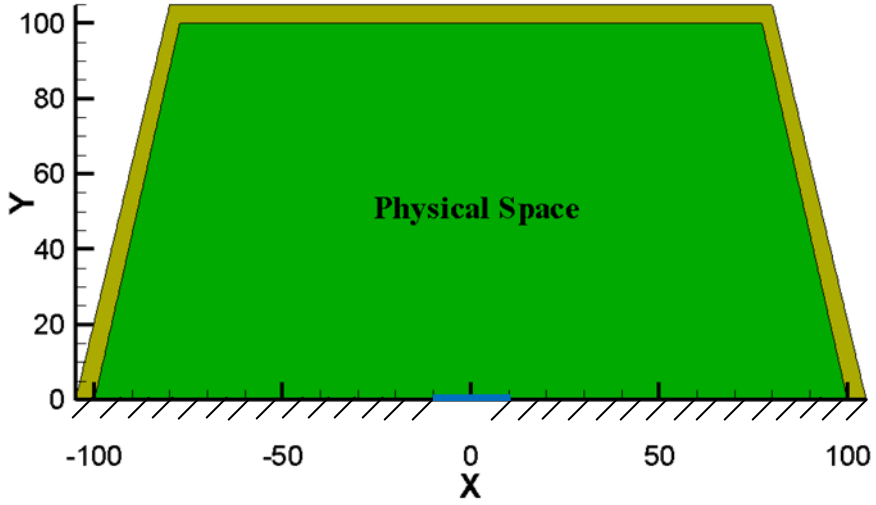

Figure 5.31. Tapered domain showing physical space and PML domain (shaded region in olive green). Number of layers in PML domain = 10.

Figures 5.32 and 5.36 show the pressure contours over a period of oscillation, from $t = 200$ to $t = 240$ in steps of ten, for $u = 0.0$ and $u = 0.5$, respectively. The comparison of pressure along $x = 0$ (Figures 5.33 and 5.37) and along $y = 0$ (Figures 5.34 and 5.38), obtained with PML boundary condition and from a reference case for $u = 0.0$ and $u = 0.5$, respectively,

shows a clear match between the two solutions. Over a period of oscillation of the piston, it is observed that the solution obtained with the PML compares very well with the solution from the reference case. Figures 5.35 and 5.39 show a comparison of the PML solution with that of the reference case for pressure as a function of time at the Euler-PML interface for $u = 0.0$ and $u = 0.5$, respectively.

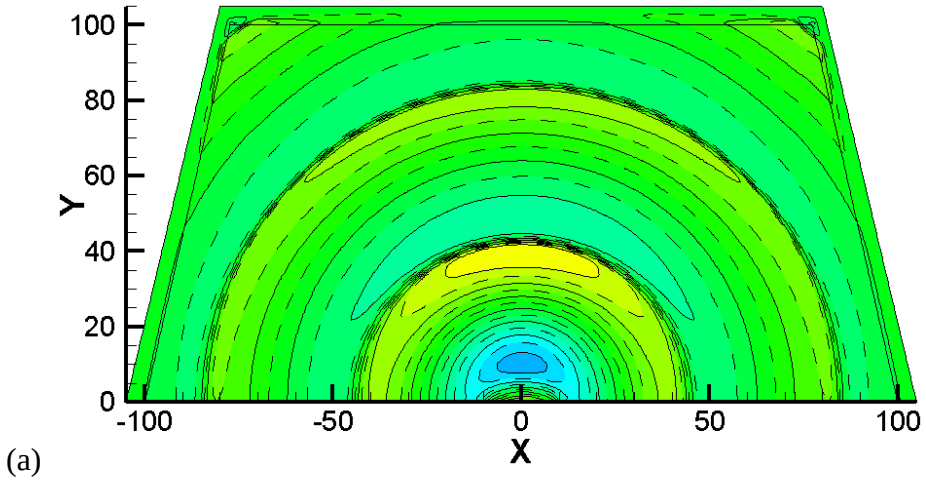

(a)

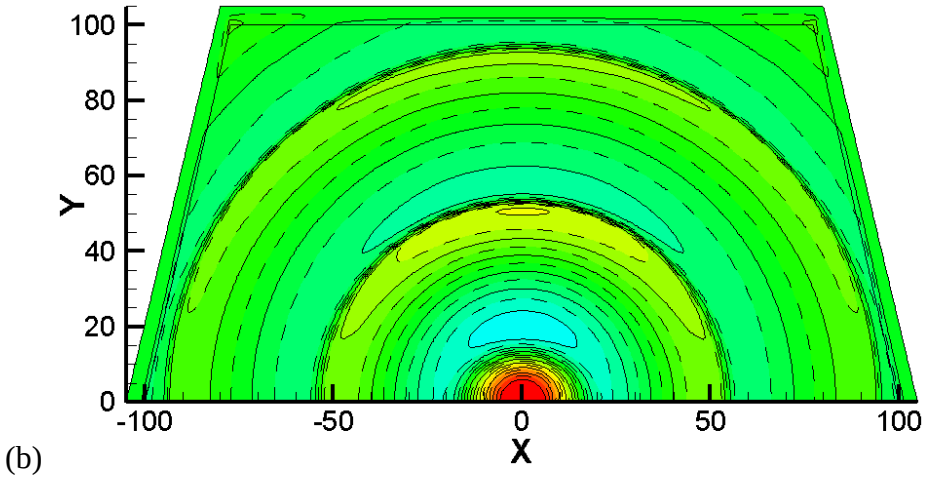

(b)

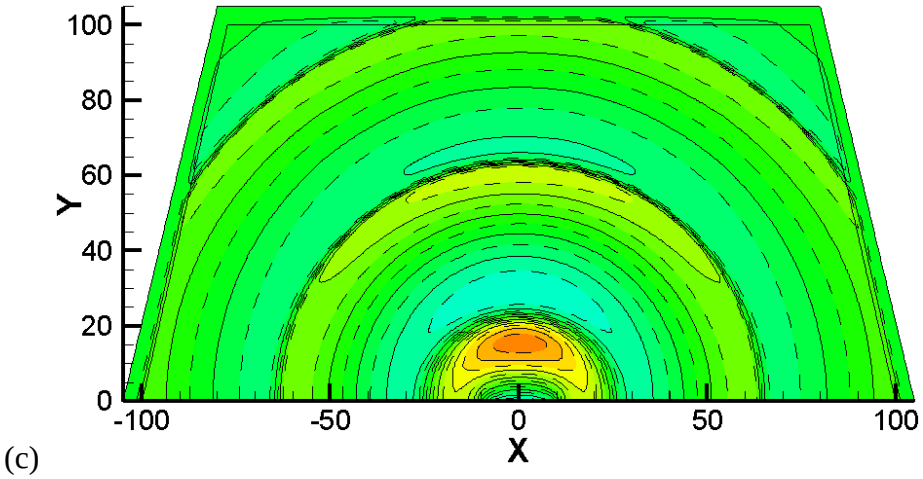

(c)

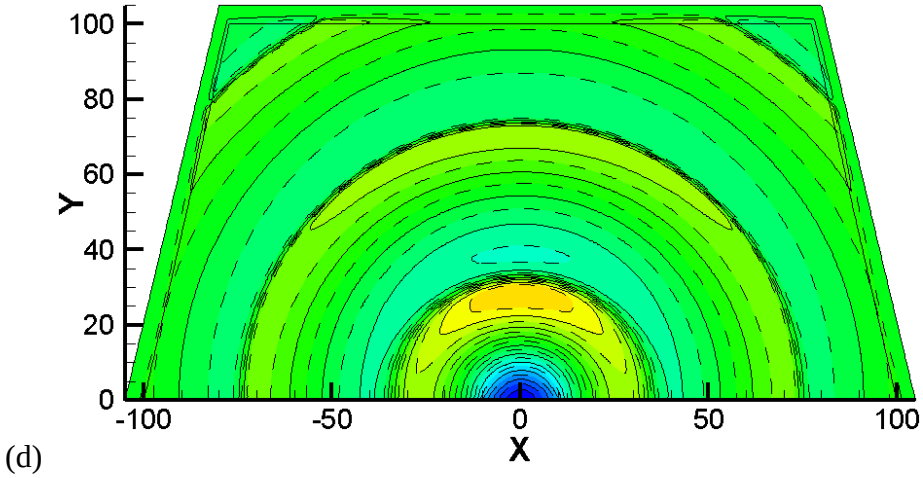

(d)

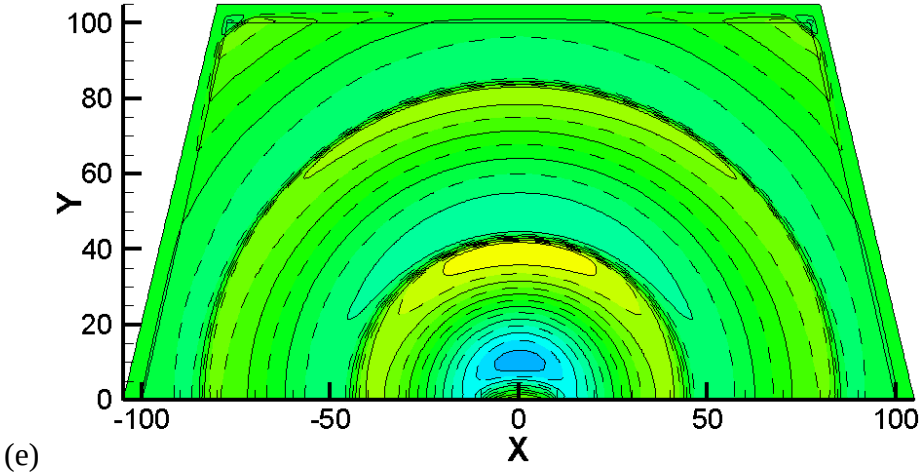

(e)

Figure 5.32. Pressure contours over period of piston oscillation: (a) t = 200, (b) t =210, (c) t = 220, (d) t = 230, and (e) t = 240 with levels from 0.5 to 0.95 in steps of 0.02 for u = 0.0.

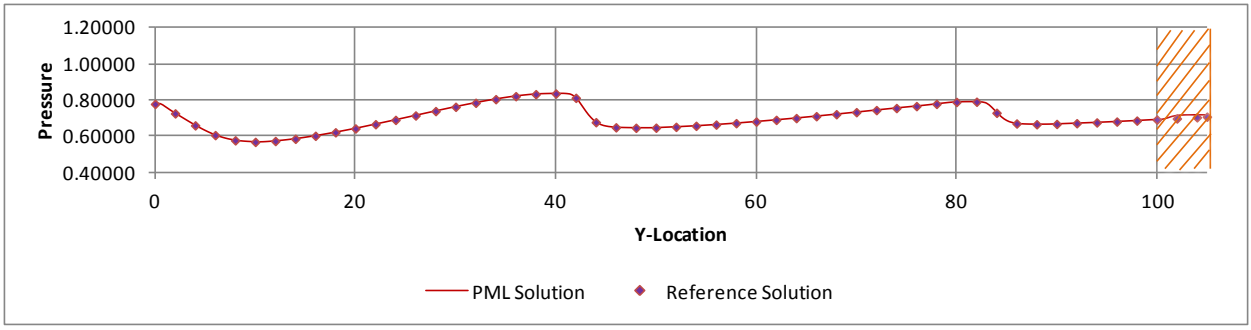
1.20000
1.00000
0.80000
0.60000
0.40000
Pressure
0
20
40
60
80
100
Y-Location
PML Solution
Reference Solution

(a)

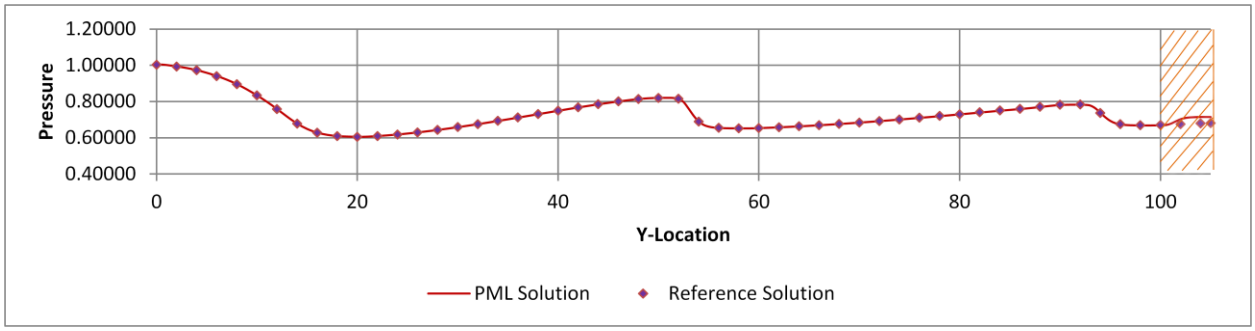
1.20000
1.00000
0.80000
0.60000
0.40000
Pressure
0
20
40
60
80
100
Y-Location
PML Solution
Reference Solution

(b)

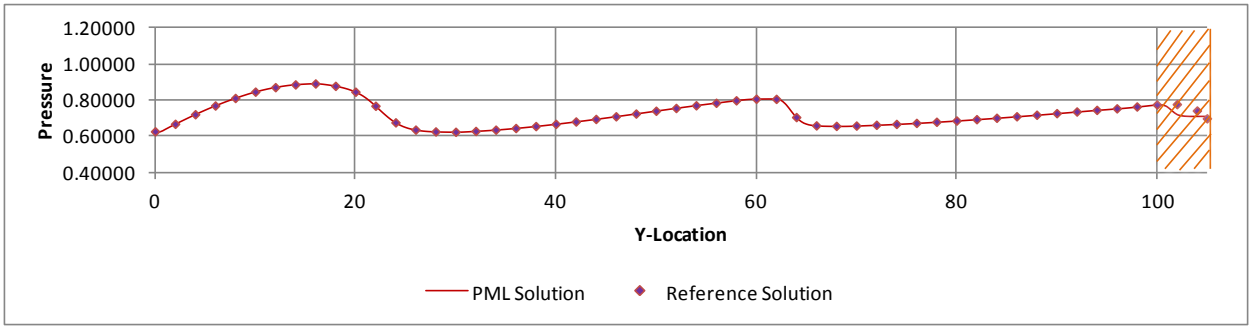
1.20000
1.00000
0.80000
0.60000
0.40000
Pressure
0
20
40
60
80
100
Y-Location
PML Solution
Reference Solution

(c)

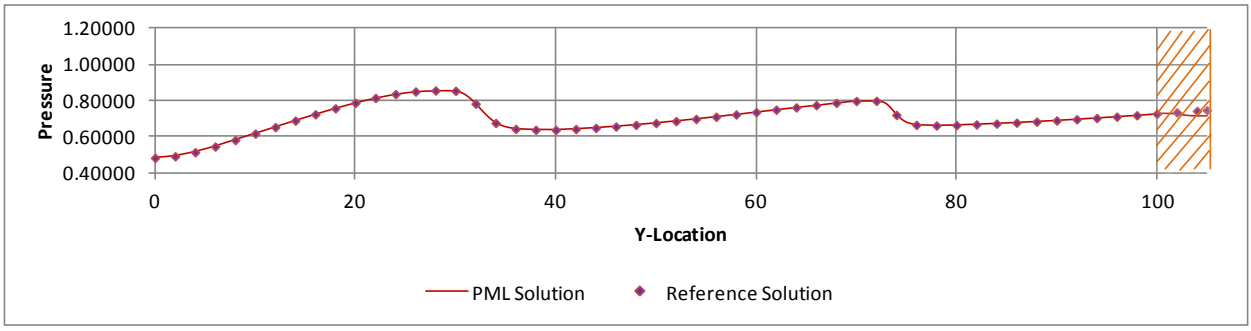
1.20000
1.00000
0.80000
0.60000
0.40000
Pressure
0
20
40
60
80
100
Y-Location
PML Solution
Reference Solution

(d)

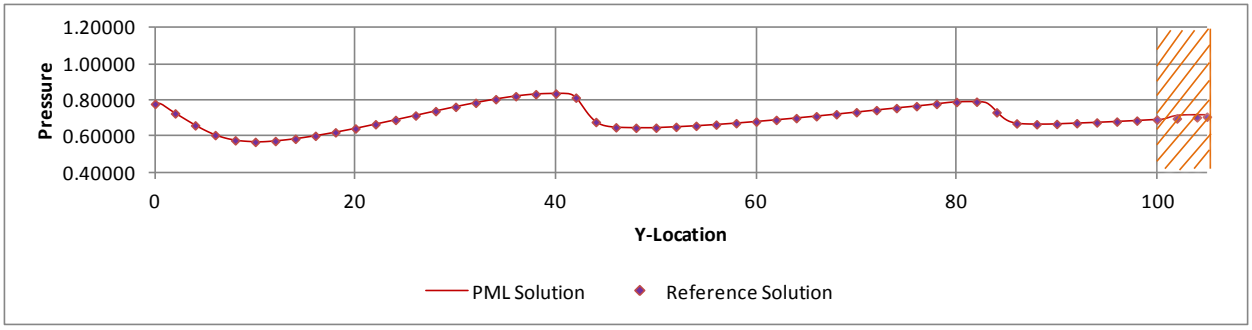

(e)

Figure 5.33. Pressure along x = 0 over period of piston oscillation: (a) t = 200, (b) t = 210, (c) t = 220, (d) t = 230, and (e) t = 240 for u = 0.0.

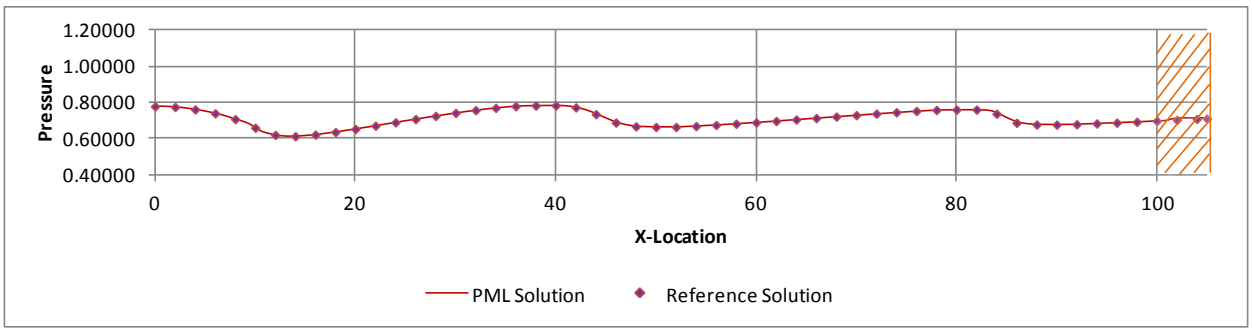

(a)

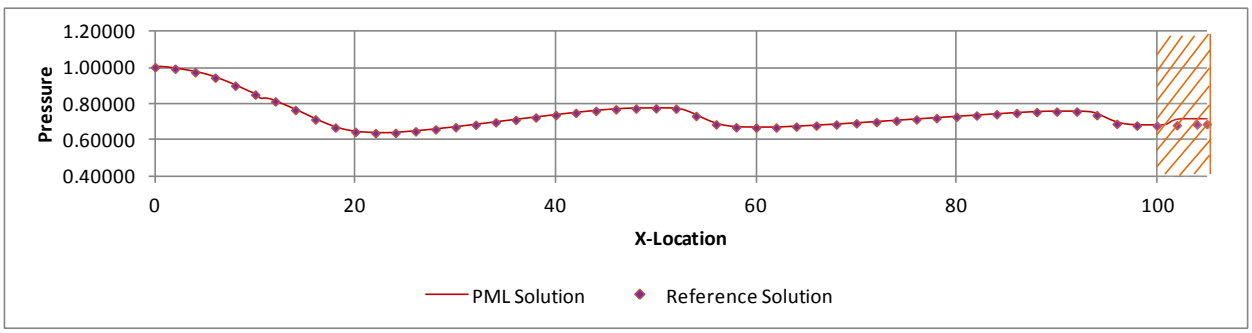

(b)

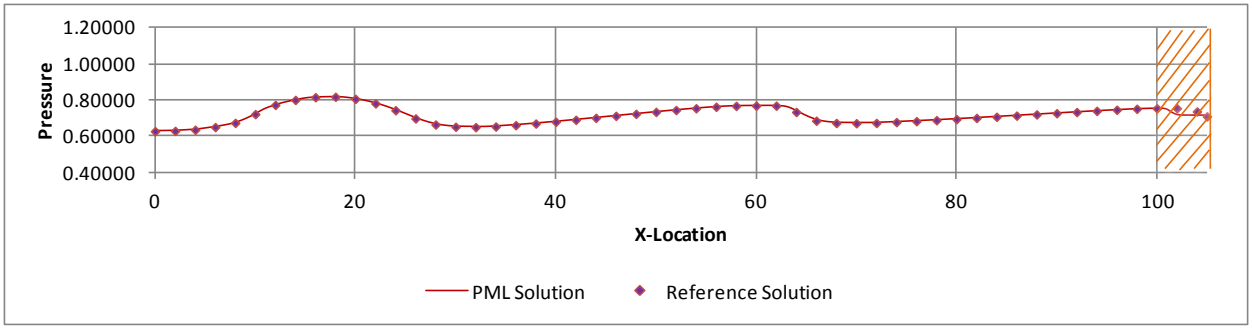

(c)

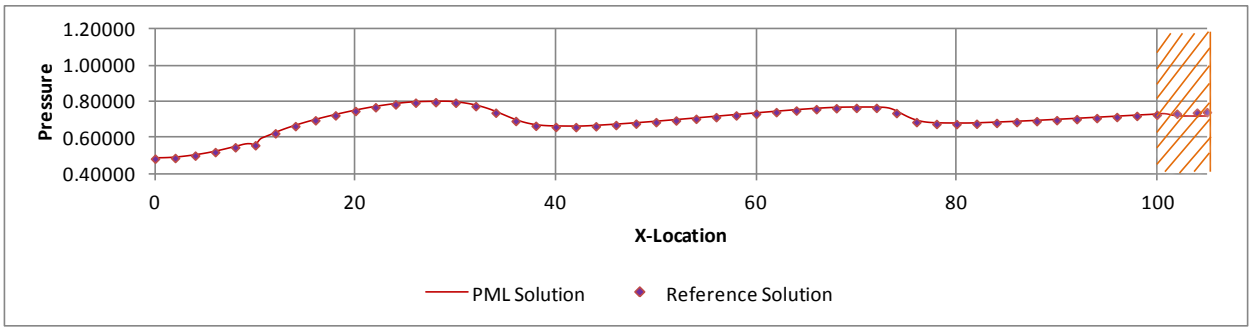

(d)

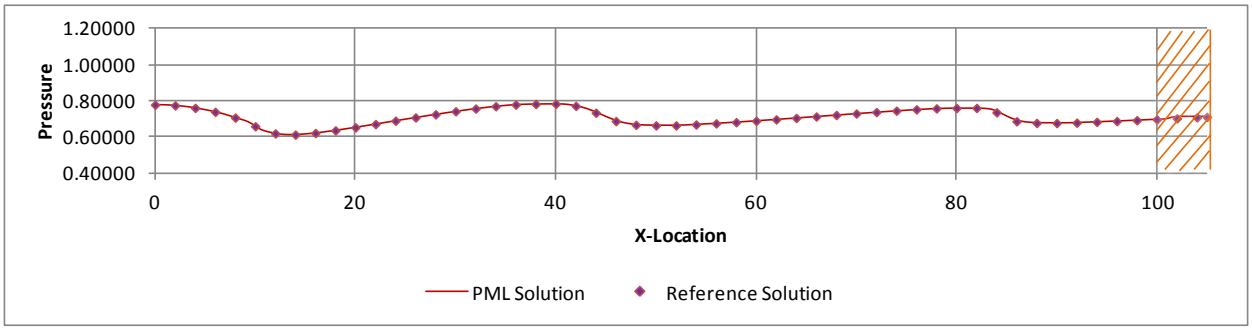

(e)

Figure 5.34. Pressure along y = 0 over period of piston oscillation: (a) t = 200, (b) t = 210, (c) t = 220, (d) t = 230, and (e) t = 240 for u = 0.0.

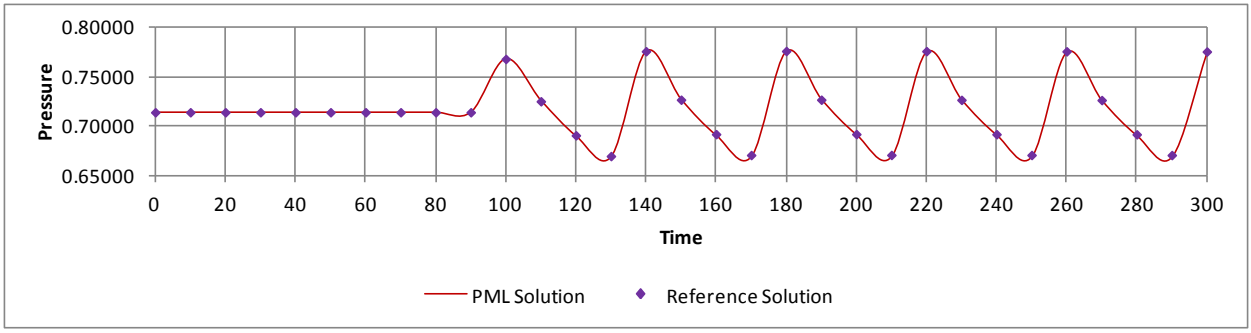

(a)

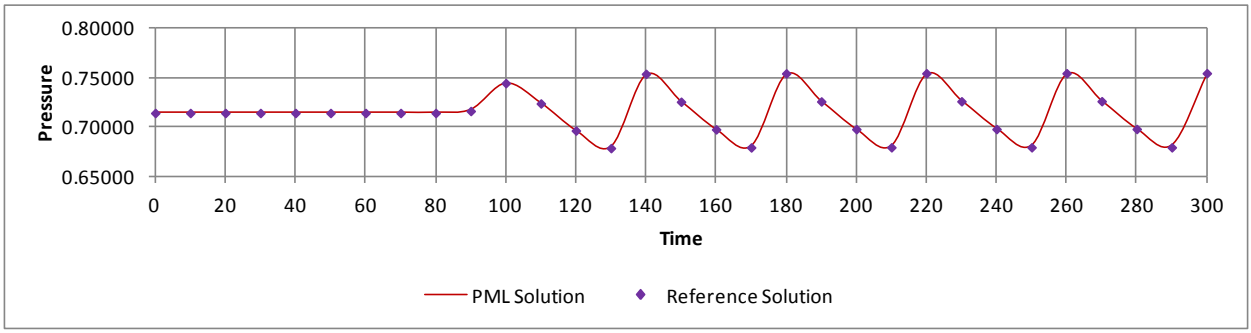

(b)

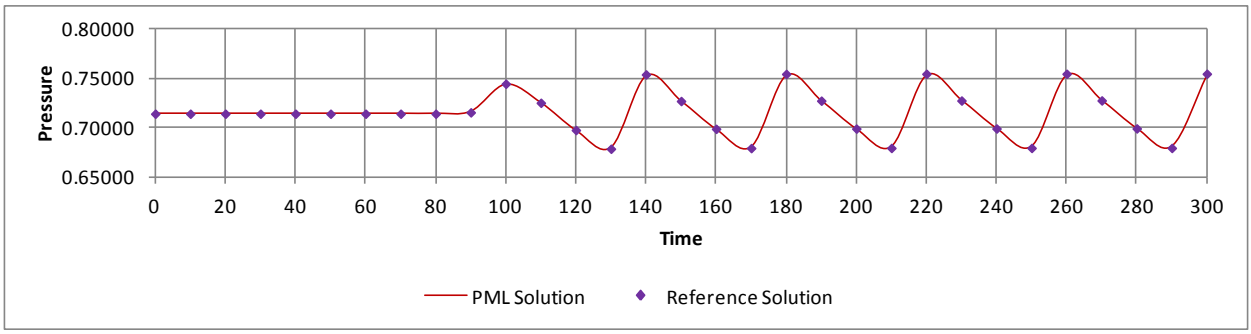

(c)

Figure 5.35. Pressure as function of time at Euler-PML interface at locations: (a) (0, 100), (b) (100, 0), and (c) (-100, 0) for u = 0.0.

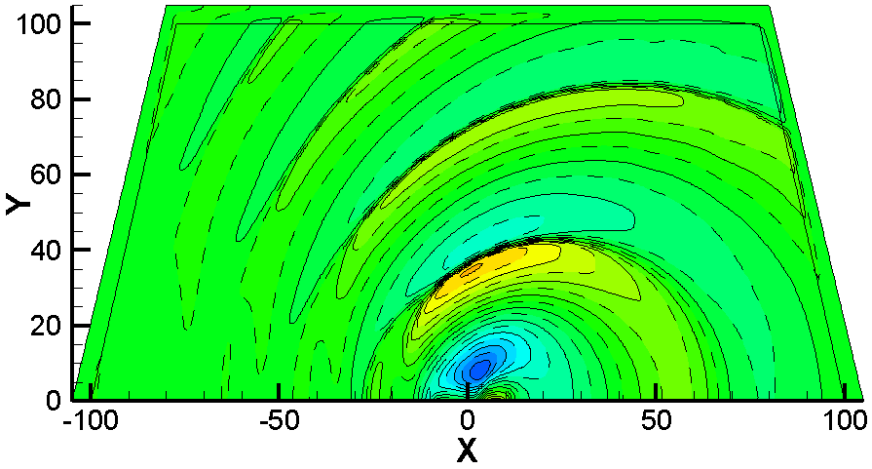
100
80
60
40
20
0
Y
-100
-50
0
50
100
X

(a)

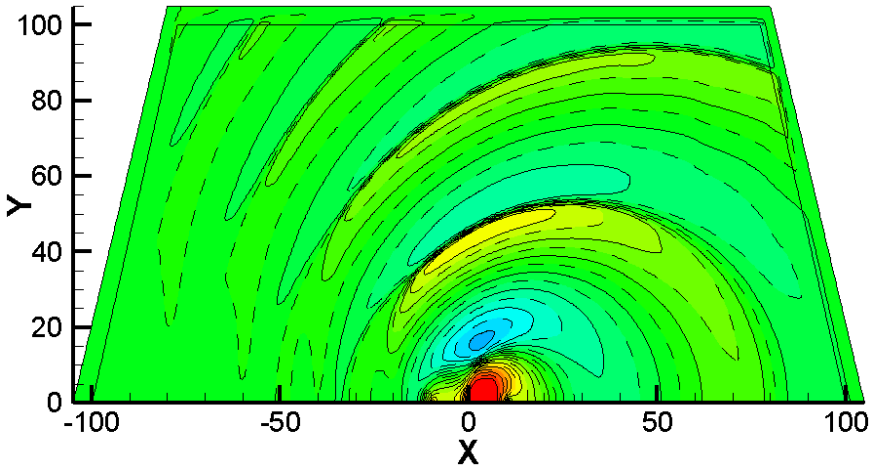
100
80
60
40
20
0
Y
-100
-50
0
50
100
X

(b)

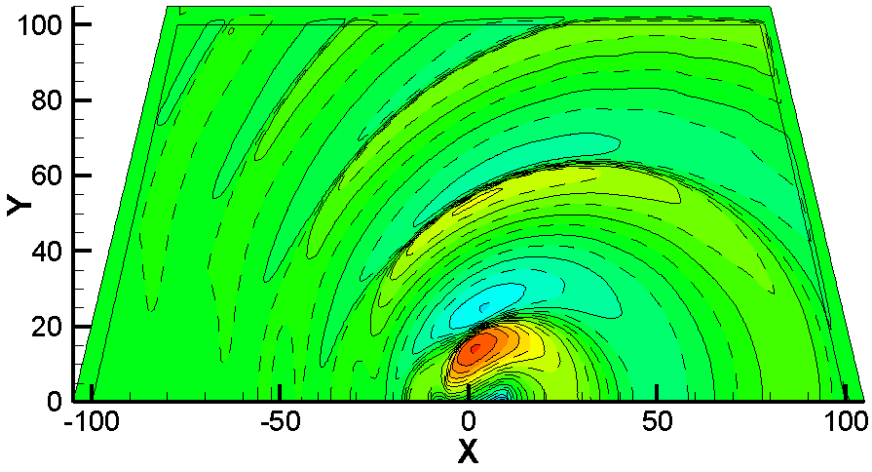
100
80
60
40
20
0
Y
-100
-50
0
50
100
X

(c)

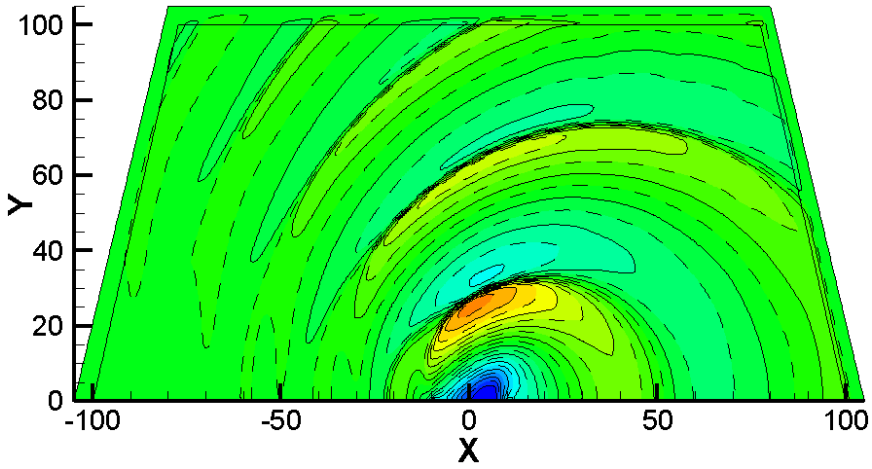

(d)

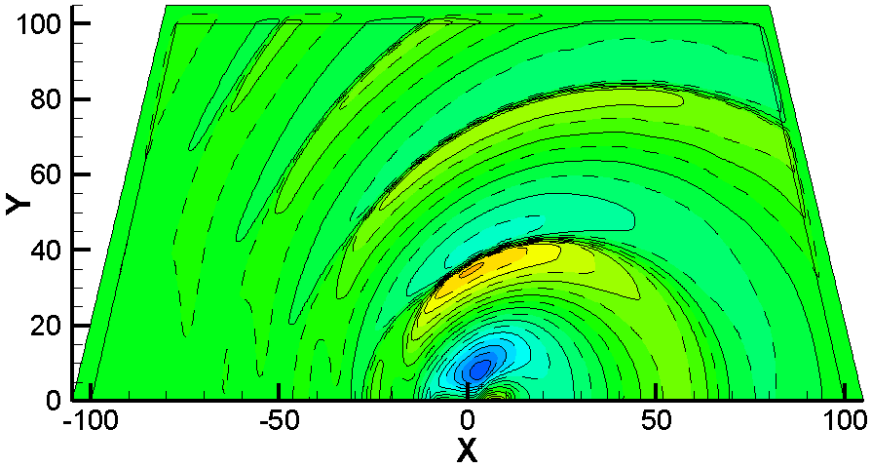

(e)

Figure 5.36. Pressure contours over a period of piston oscillation (a) t = 200, (b) t = 210, (c) t = 220, (d) t = 230, and (e) t = 240 with levels from 0.5 to 0.95 in steps of 0.02 for u = 0.5.

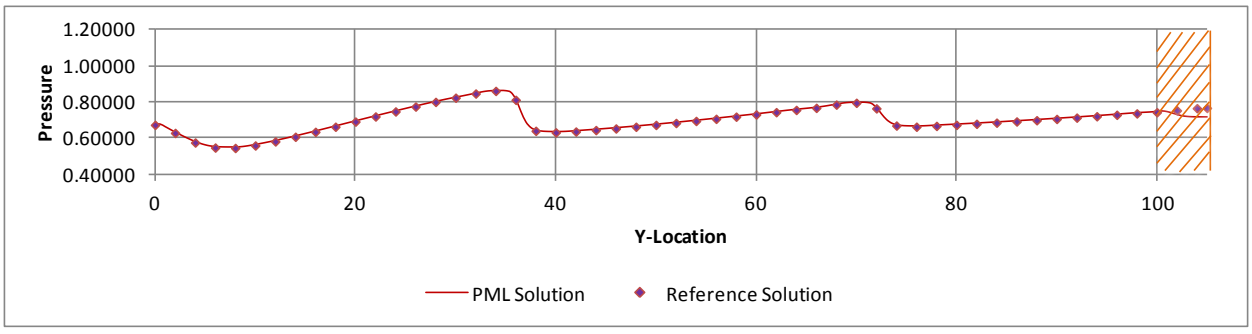

(a)

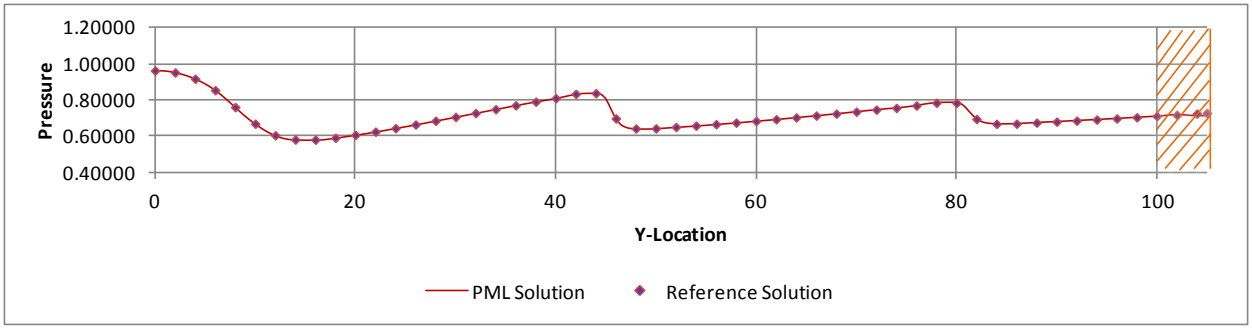

(b)

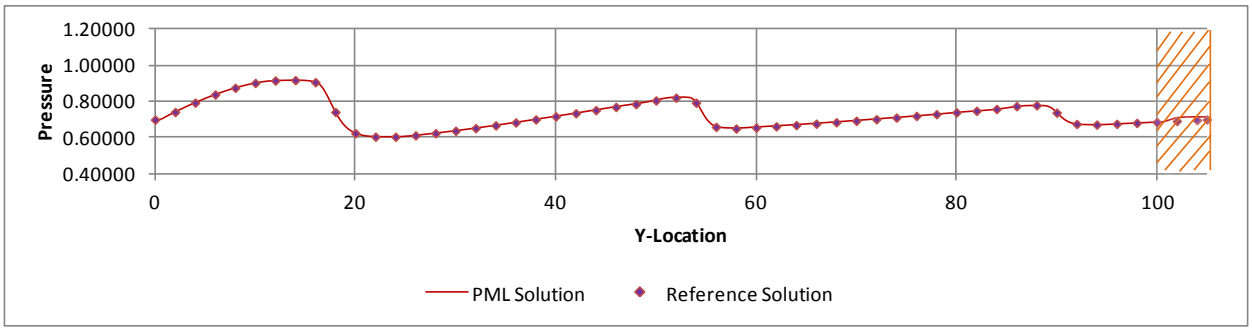

(c)

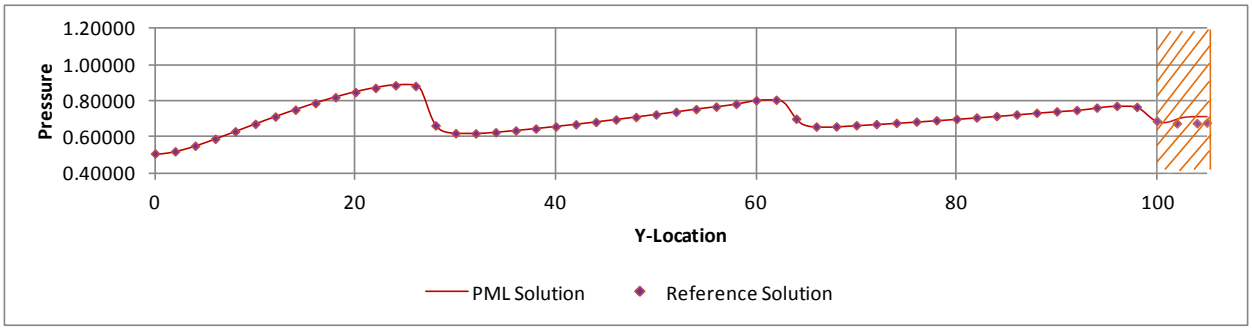

(d)

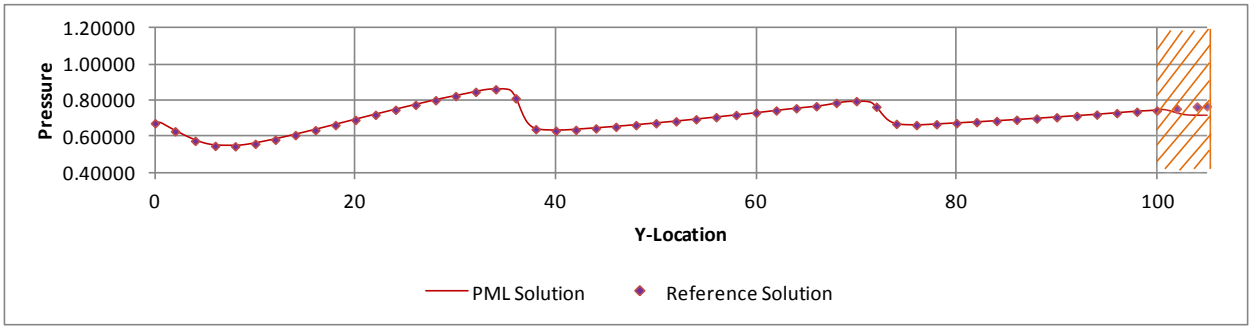

(e)

Figure 5.37. Pressure along x = 0 over period of piston oscillation: (a) t = 200, (b) t = 210, (c) t = 220, (d) t = 230, and (e) t = 240 for u = 0.5.

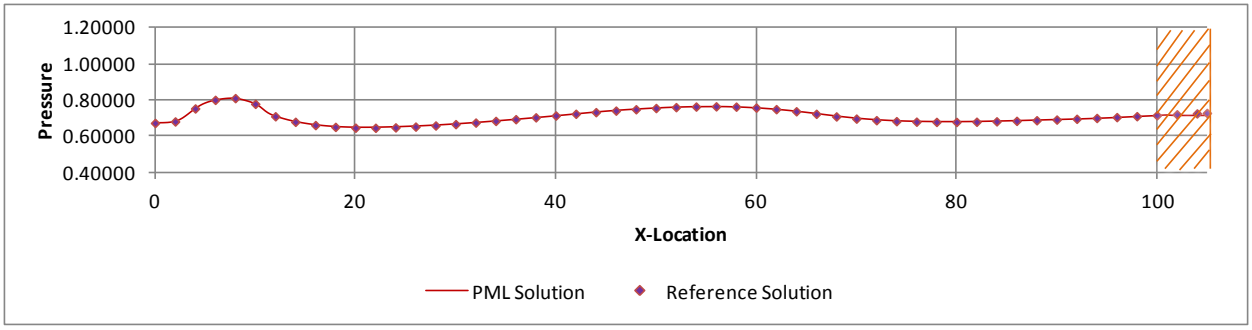
1.20000
1.00000
0.80000
0.60000
0.40000
Pressure
0
20
40
60
80
100
X-Location
PML Solution
Reference Solution

(a)

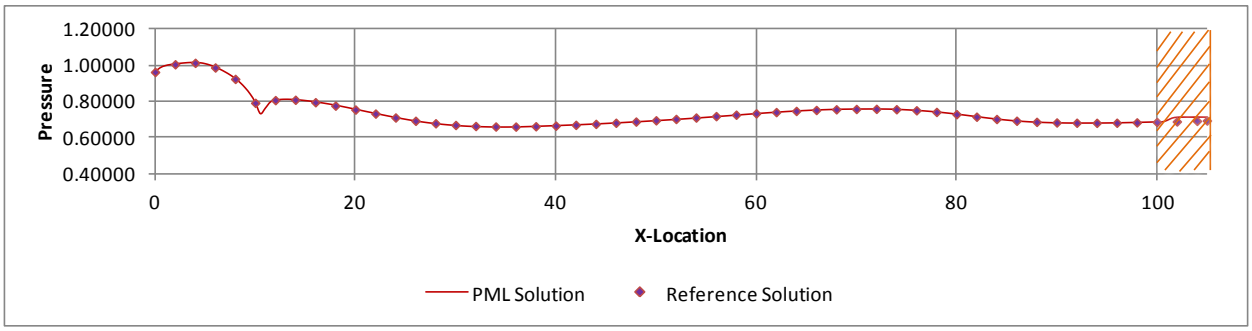
1.20000
1.00000
0.80000
0.60000
0.40000
Pressure
0
20
40
60
80
100
X-Location
PML Solution
Reference Solution

(b)

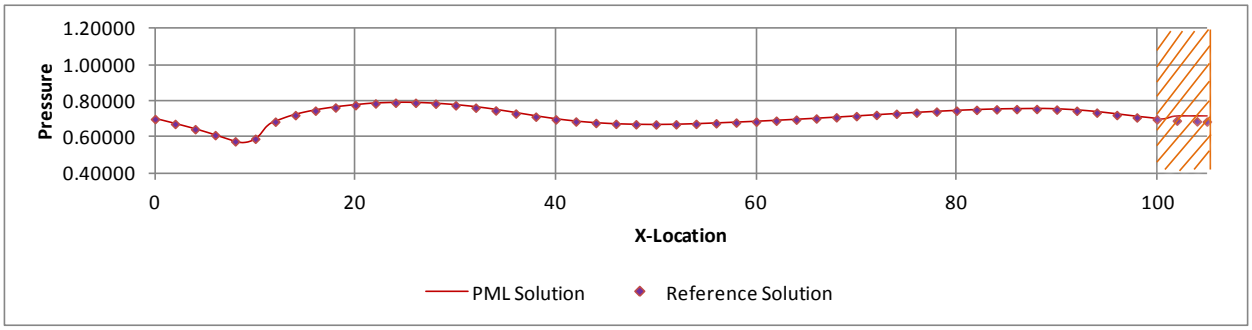
1.20000
1.00000
0.80000
0.60000
0.40000
Pressure
0
20
40
60
80
100
X-Location
PML Solution
Reference Solution

(c)

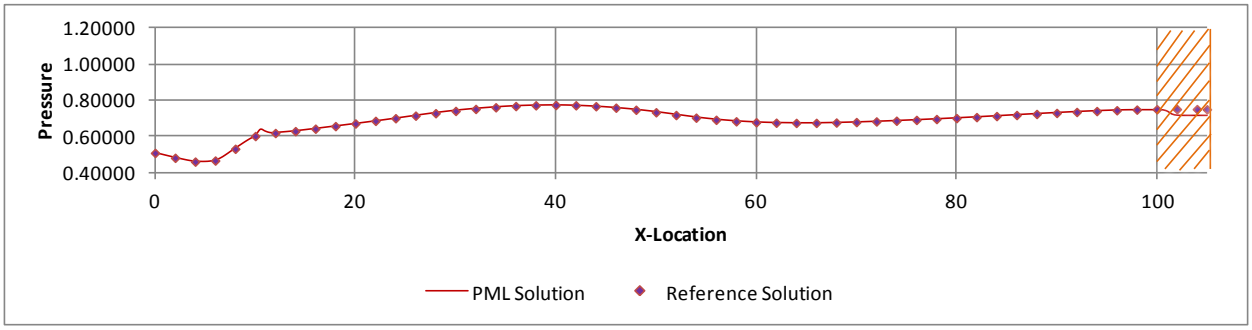
1.20000
1.00000
0.80000
0.60000
0.40000
Pressure
0
20
40
60
80
100
X-Location
PML Solution
Reference Solution

(d)

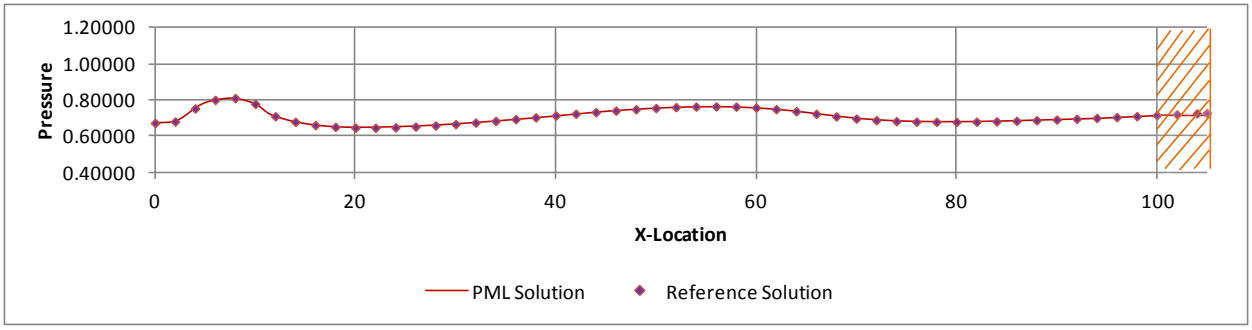

(e)

Figure 5.38. Pressure along y = 0 over period of piston oscillation: (a) t = 200, (b) t = 210, (c) t = 220, (d) t = 230, and (e) t = 240 for u = 0.5.

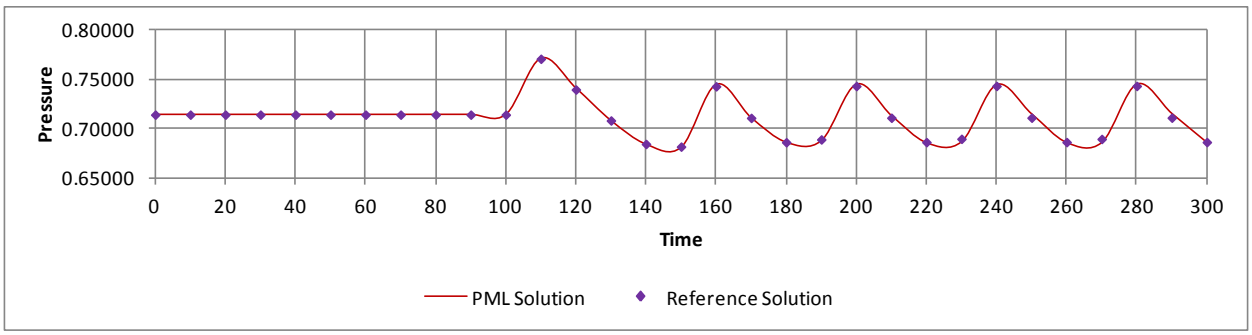

(a)

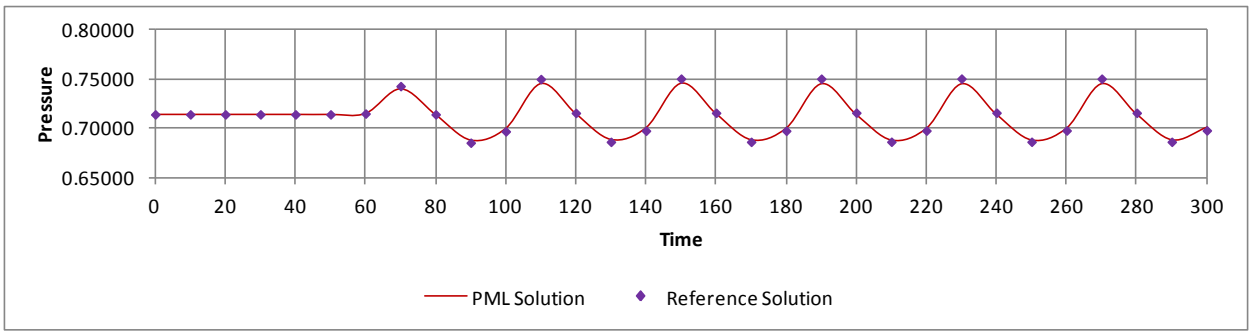

(b)

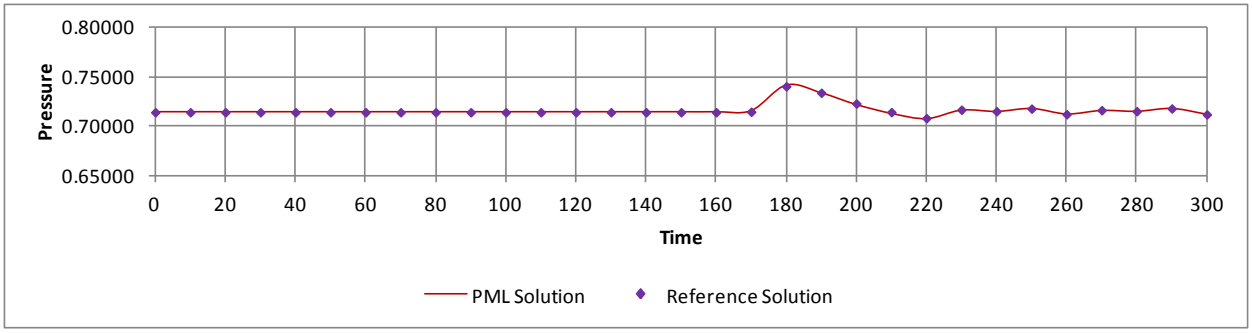

(c)

Figure 5.39. Pressure as function of time at Euler-PML interface at locations: (a) (0, 100), (b) (100, 0), and (c) (-100, 0) for u = 0.5.

5.4.5 Roll-Up Vortices

In this case, a source term in a mixing layer is simulated with a PML boundary condition. The rectangular physical domain used in this simulation is of the size [-1.5, 9.5] x [-1.1, 1.1] with a spatial-step size of $\Delta x = 0.05$ and $\Delta y = 0.01$. In the computational space, i.e., generalized coordinates, the grid spacing is $\Delta\xi = \Delta\eta = 1.0$. The physical domain includes a PML domain with ten layers, the region shaded in olive green in Figure 5.40, appended to all four sides of the physical space. A fairly large rectangular domain of size [-18, 26] x [-4.4, 4.4] is used for the reference case. A nondimensional global time-step size of 0.001 is used.

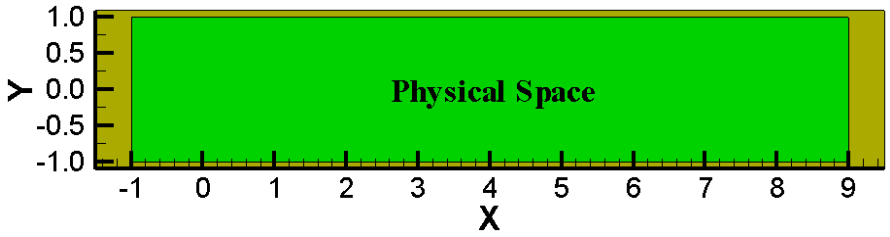

Figure 5.40. Rectangular domain showing physical space and PML domain (shaded region in olive green). Number of layers in PML domain = 10.

The initial conditions in primitive variables are given by equation (5.54):

$$\begin{pmatrix} \rho \\ u \\ v \\ p \end{pmatrix} = \begin{pmatrix} \overline{\rho}(y) \\ \overline{U}(y) \\ 0 \\ 1/\gamma \end{pmatrix} \tag{5.54}$$

where the mean velocity profile is obtained by equation (5.55). Figure 5.41 shows the velocity profile along x = 0 as defined by equation (5.55).

$$\overline{U}(y) = \frac{1}{2}\left[(U_1 + U_2) + (U_1 - U_2)\tanh\left(\frac{2y}{\delta}\right)\right] \tag{5.55}$$

The mean density, equation (5.56), is obtained from the mean temperature, equation (5.57), determined by the Crocco relation for compressible flows [17] as

$$\overline{\rho}(y) = \frac{1}{\overline{T}(y)} \tag{5.56}$$

where

$$\overline{T}(y) = T_1 \frac{\overline{U}(y) - U_2}{U_1 - U_2} + T_2 \frac{U_1 - \overline{U}(y)}{U_1 - U_2} + \frac{\gamma - 1}{2}\left(U_1 - \overline{U}(y)\right)\left(\overline{U}(y) - U_2\right) \tag{5.57}$$

The parameters that appear in equations (5.55)–(5.57) are given by equations (5.58)

$$U_1 = 0.8,\ U_2 = 0.2,\ \ \delta = 0.4,\ \ T_1 = 0.8,\ \ T_2 = 0.8,\ \ \gamma = 1.4 \tag{5.58}$$

A source term of the form, equation (5.59), is added to the equation of energy.

$$S(x, y, t) = 5\sin(\omega t)\, e^{-(\ln 2)\left[(x - x_0)^2 + (y - y_0)^2\right]/r_0^2} \tag{5.59}$$

where

$$\omega = \pi/2,\ (x_0, y_0) = (-0.5, 0) \ \text{ and } \ r_0 = 0.03 \tag{5.60}$$

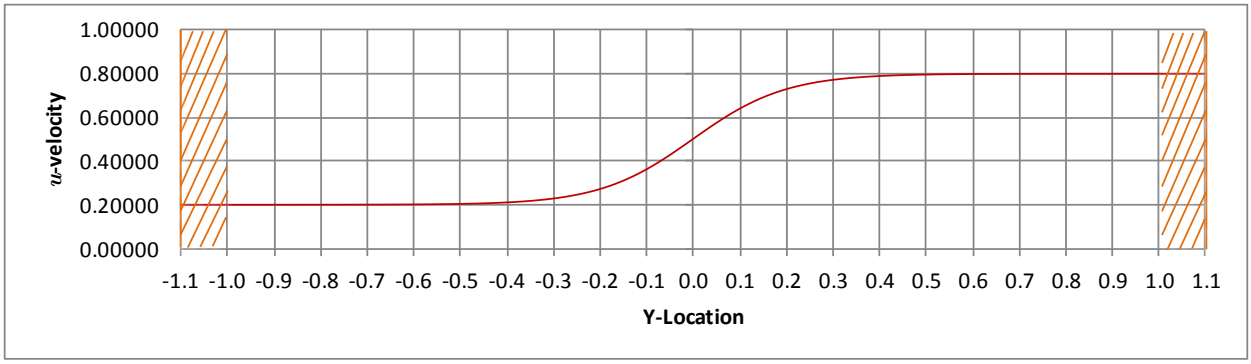

Figure 5.41 Initial velocity profile, along line x = 0, defining the mixing layer.

This source term will induce an exponentially growing Kelvin-Helmholtz instability wave which will result in roll-up vortices [17, 18]. The PML boundary condition is used on the four sides to absorb the vortices at the outflow boundary as they convect with the mean flow and the acoustic waves at all four artificial boundaries as they travel in all directions at the speed of sound. The pseudo mean-flow inside the PML domain is assumed to be the parallel flow as given by equation (5.54), and for this shear flow, the parameter β is found to be approximately 1/1.4 as per the linear wave analysis [17, 18, 21]. The values of σ_m = 200.0 and α = 2.5 are used for the PML parameters in the computational domain.

The vorticity contours at progressive time levels are presented in Figure 5.42. The vortices convecting downstream along with the flow and their absorption as they enter the PML domain are clearly seen in the contour plots.

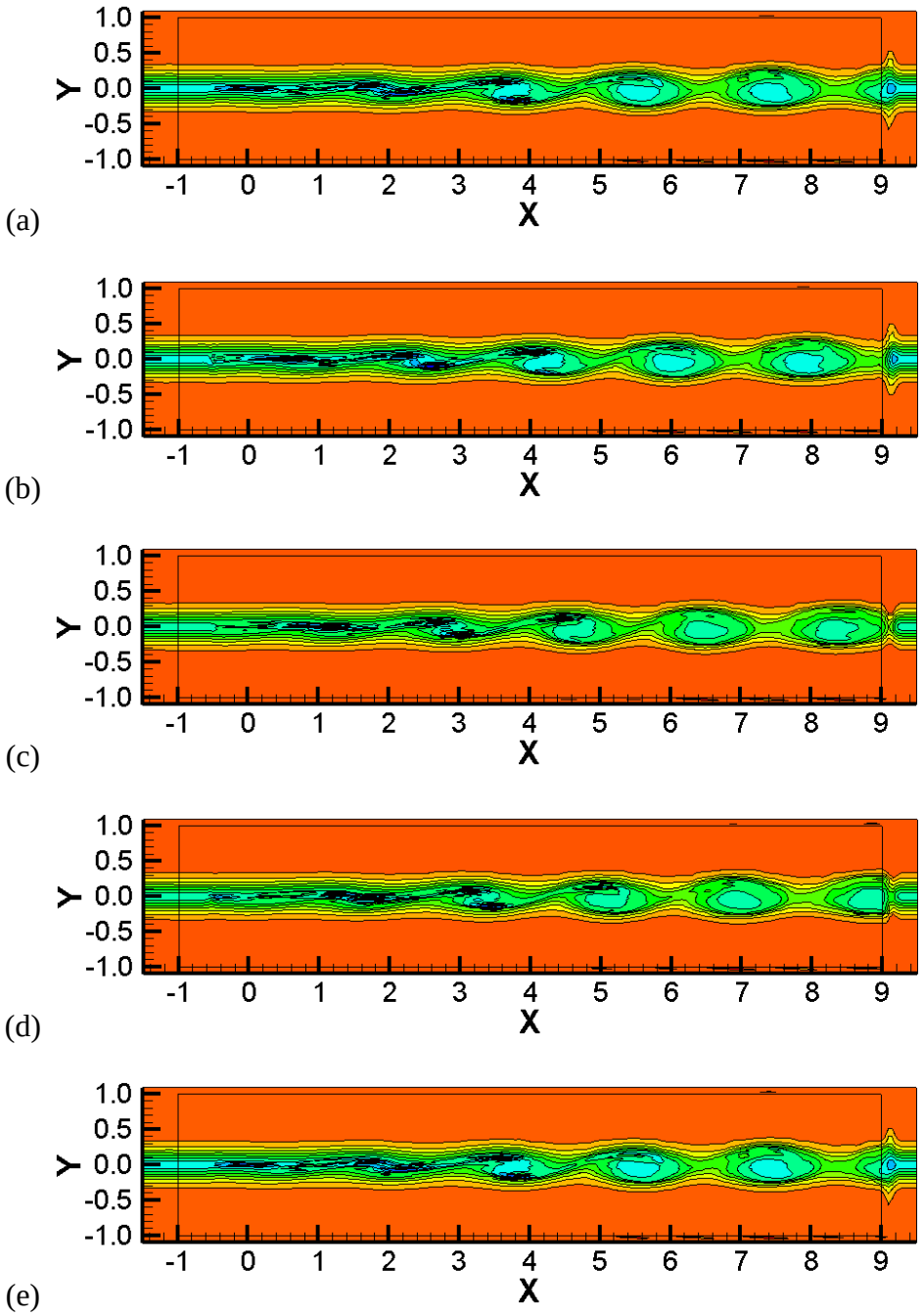

Figure 5.42. Vorticity contours at progressive times: (a) t = 40, (b) t = 45, (c) t = 50, (d) t = 55, and (e) t = 60 with levels from –2.2 to –0.2 in steps of 0.2 and at level +0.2.

The comparison of pressure, fluctuating pressure, and v-velocity obtained from the PML -based solution and a reference case at a selected point close to the outflow boundary, $(x, y) = (8.75, 0)$, is provided in Figures 5.43, 5.44, and 5.45, respectively. A good agreement in

these two solutions reveal that PML boundary condition can be effectively used for flows involving shear layers and instability waves.

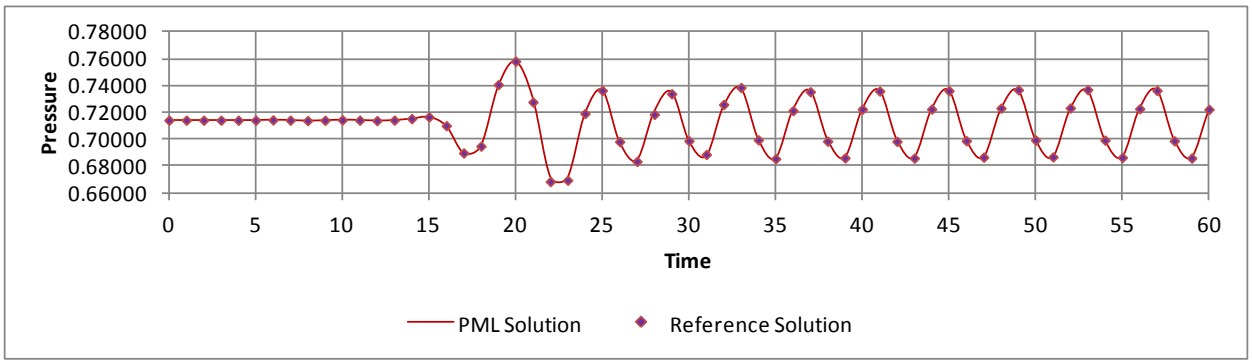

Figure 5.43 Pressure as function of time at selected point (8.75, 0).

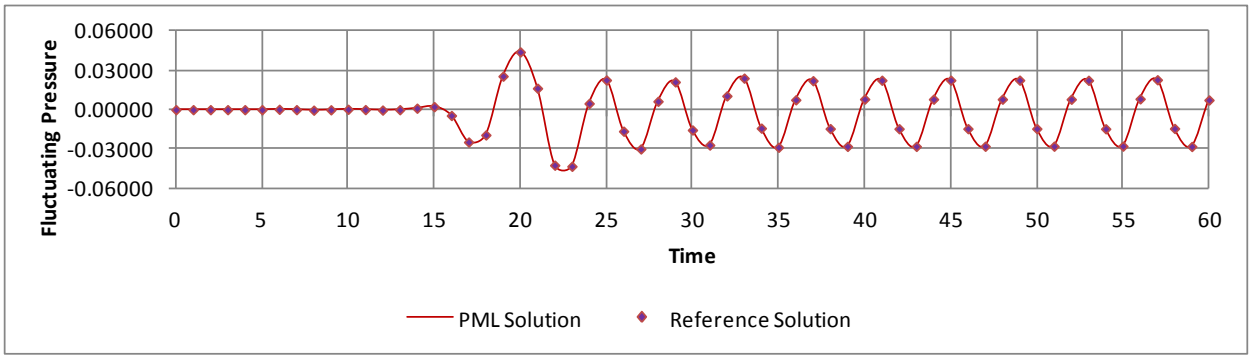

Figure 5.44 Fluctuating pressure as function of time at selected point (8.75, 0).

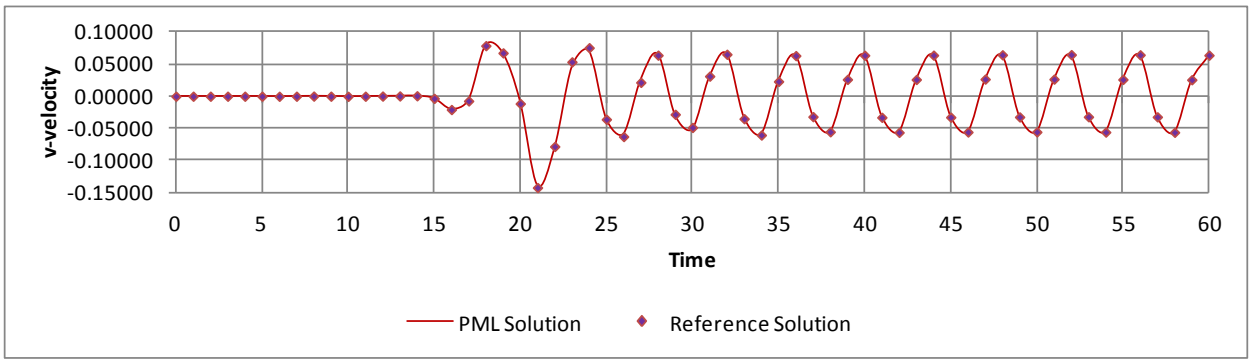

Figure 5.45 v-velocity as function of time at selected point (8.75, 0).

CHAPTER 6

CONCLUSIONS AND FUTURE WORK

A rigorous literature survey on the boundary conditions of unbounded problems of computational fluid dynamics revealed that there is an emerging concept of a nonreflecting boundary condition known as perfectly matched layer. The evolution of PML was studied carefully, especially the instability of the PML for high subsonic flows. On that basis, PML equations were constructed for linearized Euler equations, with and without the application of space-time transformation and a complex change of variables. Investigation was carried out on the stability aspect of the PML formulation for LEEs in terms of long-time integration and a combination of PML parameters that affect the absorption capability of the PML. Furthermore, analysis on the dispersion relation of the acoustic waves governed by LEEs was carried out numerically to demonstrate the benefits of space-time transformation to the stability of the PML.

Following a similar procedure, PML equations for nonlinear Euler equations were constructed and demonstrated for their effectiveness as an absorbing boundary condition. The concept of pseudo mean-flow and its associated advantages in the performance of the PML boundary condition were also demonstrated. The main objective of this research effort was to enable these equations to be applied in a generalized coordinate system so that nonrectangular physical domains and domains with nonuniform grid spacing could be handled by a single numerical solver. This was accomplished by constructing appropriate equations of transformation from physical space to computational space. Also, the idea of developing a numerical solver with generic/conventional numerical schemes without employing numerical filtering or artificial dissipation was accomplished, and numerical examples were shown to demonstrate the effectiveness of the solver and the PML formulation.

It is also found that the space-time transformation used in the construction of perfectly matched layer equations was exclusively meant for flows with mainstream direction parallel to the horizontal axis in Cartesian coordinates. The space-time transformation must be modified in such a way that it supports flows in an arbitrary direction which is an essential criterion for an effective boundary condition in generalized coordinates.

There is no doubt that the perfectly matched layer could be used as an effective nonreflecting boundary condition. But a great deal of research is needed for those cases involving high subsonic flows, transient flows, and supersonic flows governed by Navier-Stokes equations. Also, a complete mathematical stability analysis of the PML formulation must be carried out.

REFERENCES

REFERENCES

[1] Lele, S. K., "Computational Aeroacoustics—A Review," *AIAA 97-0018,* 1997.

[2] Givoli, D., "Review Article—Non-Reflecting Boundary Conditions," *Journal of Computational Physics* Vol. 94, 1991, pp 1–29.

[3] Tam, C. K. W., "Advances in Numerical Boundary Conditions for Computational Aeroacoustics," *AIAA*-2005-4716, 2005.

[4] Hu, F. Q., "Absorbing Boundary Conditions," *Journal of Computational Physics*, Vol. 18, Iss. 6, 2004, pp. 513–522.

[5] Hoffmann, K. A., and Chiang, S. T., *Computational Fluid Dynamics—Volume II*, Engineering Education System, 2000.

[6] Nizampatnam, L. S., "Investigation of Boundary Conditions for Computational Aeroacoustics," Master of Science Thesis, Department of Aerospace Engineering, Wichita State University, Wichita, KS, 1999.

[7] Velu, S. P., "Development and Application of Perfectly Matched Layer for Numerical Boundary Treatment," Master of Science Thesis, Department of Aerospace Engineering, Wichita State University, Wichita, KS, 2010.

[8] Nizampatnam, L. S., Wong, J., Hoffmann, K. A., Papadakis, M., and Agarwal, R. K., "Development of Perfectly Matched Layer Boundary Conditions for Aeroacoustic Applications," *AIAA*-2005-0223, 2000.

[9] Berenger, J. P., "A Perfectly Matched Layer for the Absorption of Electromagnetic Waves," *Journal of Computational Physics*, Vol. 114, 1994, pp. 185–200.

[10] Hu, F. Q., "On Absorbing Boundary Conditions for Linearized Euler Equations by a Perfectly Matched Layer," *Journal of Computational Physics*, Vol. 129, 1996, pp. 201–219.

[11] Hu, F. Q., "On Perfectly Matched Layer as an Absorbing Boundary Condition," *AIAA*-96-1664, 1996.

[12] Abarbanel, S., and Gottlieb, D., "A Mathematical Analysis of the PML Method," *Journal of Computational Physics,* Vol. 134, Iss. 2, 1997, pp. 357–363.

[13] Hesthaven, J. S., "On the Analysis and Construction of Perfectly Matched Layers for the Linearized Euler Equations," *Journal of Computational Physics*, Vol. 142, Iss. 1, 1998, pp. 129–147.

[14] Tam, C. K. W., and Auriault, L., "Perfectly Matched Layer as Absorbing Boundary Condition for the Linearized Euler Equations in Open and Ducted Domains," *Journal of Computational Physics*, Vol. 144, 1998, pp. 213–234.

[15] Abarbanel, S., Gottlieb, D., and Hesthaven, J. S., "Well-Posed Perfectly Matched Layers for Advective Acoustics," *Journal of Computational Physics*, Vol. 154, Iss. 2, 1999, pp. 266–283.

[16] Hu, F. Q., "A Stable, Perfectly Matched Layer for Linearized Euler Equations in Unsplit Physical Variables," *Journal of Computational Physics*, Vol. 173, 2001, pp. 455–480.

[17] Hu, F. Q., "On the Construction of PML Absorbing Boundary Condition for the Nonlinear Euler Equations," *AIAA*-2006-798, 2006.

[18] Hu, F. Q., Li, X. D., and Lin, D. K., "Absorbing Boundary Conditions for Nonlinear Euler and Navier-Stokes Equations Based on the Perfectly Matched Layer Technique," *Journal of Computational Physics*, Vol. 227, 2008, pp. 4398–4424.

[19] Hoffmann, K. A., and Chiang, S. T., *Computational Fluid Dynamics—Volume I*, Engineering Education System, 2000.

[20] Velu, S. P., and Hoffmann, K. A., "Development and Application of Perfectly Matched Layer for Numerical Boundary Treatment," *AIAA*-2012-1099.

[21] Hu, F. Q., "A Perfectly Matched Layer Absorbing Boundary Condition for Linearized Euler Equations with a Nonuniform Mean Flow," *Journal of Computational Physics*, Vol. 208, 2005, pp. 469–492.

[22] Hardin, J. C., Ristorcelli, J. R., and Tam, C. K. W., "ICASE/LaRC Workshop on Benchmark Problems in Computational Aeroacoustics (CAA)," NASA Conference Publication 3300, May 1995.

[23] Pierce, A. D., *Acoustics: An Introduction to Its Physical Principles and Applications*, McGraw-Hill Book Company, 1981.

[24] Whitham, G. B., *Linear and Nonlinear Waves*, John Wiley & Sons, 1974.

[25] Morse, P. M., and Ingrad, K. U., *Theoretical Acoustics*, McGraw-Hill Book Company, 1968.

[26] Edgar, N. B., and Visbal, M. R., "A General Buffer Zone-Type Non-Reflecting Boundary Condition for Computational Aeroacoustics," *AIAA*-2003-3300, May 2003.

[27] Whitney, J. P., "A Perfectly Matched Layer Method for the Navier-Stokes Equations," Master of Science Thesis, Department of Aeronautics and Astronautics, Massachusetts Institute of Technology, Cambridge, MA, 2006.

[28] Tam, C. K. W., and Webb, J. C., "Dispersion-Relation-Preserving Finite Difference Schemes for Computational Acoustics," *Journal of Computational Physics,* Vol. 107, 1993, pp. 262–281.